Cancellation of Arbitrary Tone Interference for All-Digital High Definition Television Transmitted Over Coaxial Cable Networks

by

Ian D. Marsland
B.Sc.Eng. (Honours), Queen's University, 1987

A THESIS SUBMITTED IN PARTIAL FULFILLMENT OF

THE REQUIREMENTS FOR THE DEGREE OF

MASTER OF APPLIED SCIENCE

in

THE FACULTY OF GRADUATE STUDIES

(Department of Electrical Engineering)

We accept this thesis as conforming
to the required standard

THE UNIVERSITY OF BRITISH COLUMBIA

April 1994

In presenting this thesis in partial fulfilment of the requirements for an advanced degree at the University of British Columbia, I agree that the Library shall make it freely available for reference and study. I further agree that permission for extensive copying of this thesis for scholarly purposes may be granted by the head of my department or by his or her representatives. It is understood that copying or publication of this thesis for financial gain shall not be allowed without my written permission.

Department of Electrical Engineering

The University of British Columbia
Vancouver, Canada

Date 28 APRIL 1994

DE-6 (2/88)

Abstract

In this thesis a novel canceller of a completely unknown tone which is interfering with a digital quadrature amplitude modulation (QAM) signal operating in an additive white Gaussian noise (AWGN) environment is proposed, analysed and evaluated. This canceller can be applied to protect all-digital high definition television (HDTV) signals from tone interference, which arises from intermodulation products, a common source of distortion in cable television networks.

Expressions for the optimal weights for the linear minimum mean-square error (MMSE) filter, consisting of L delay elements, for cancelling the tone interference are derived, under the condition that the tone's frequency and power are known to the canceller. It is shown that the MMSE is directly proportional to the combined power of the QAM signal and the Gaussian noise, and inversely proportional to L. Furthermore, as the characteristics of the tone are assumed to be completely unknown, novel fast Fourier transform (FFT) based methods for estimating the frequency and power of the tone are proposed and analysed. By using these estimates in place of the true values for the optimal weights, a suboptimal filter is derived. Performance evaluation results have shown that the performance of the suboptimal canceller is, for all practical purposes, identical to the optimal one.

To improve the performance further, without increasing the number of the filter's delay elements, a decision feedback mechanism is employed to reduce the power of the data signal. Through a combination of analytical and computer simulated performance evaluation it is found that for all practical purposes the proposed decision feedback tone canceller removes the tone interference completely.

Table of Contents

List of Figures

Notation

Data Signal

$v_c(t)$	$\leftrightarrow$	Transmitted bandpass signal
$v(t)$	$\leftrightarrow$	Data component of received lowpass signal
I_a	$\leftrightarrow$	Transmitted symbols
σ_s^2	$\leftrightarrow$	Variance of transmitted symbols

Additive White Gaussian Noise

$n_c(t)$	$\leftrightarrow$	Received bandpass noise
$n(t)$	$\leftrightarrow$	Noise component of received lowpass signal
N_0	$\leftrightarrow$	Single-sided noise PSD

Tone Interference

$z_c(t)$	$\leftrightarrow$	Bandpass tone
$z(t)$	$\leftrightarrow$	Tone component of received lowpass signal
f_{ci}	$\leftrightarrow$	Bandpass frequency of tone
f_i	$\leftrightarrow$	Baseband frequency of tone
K_{ci}	$\leftrightarrow$	Magnitude of bandpass tone
K_i	$\leftrightarrow$	Magnitude of baseband tone
ϕ_i	$\leftrightarrow$	Initial phase of tone

Modulation

T_s	$\leftrightarrow$	Symbol duration
f_c	$\leftrightarrow$	Carrier frequency
$h_T(t)$	$\leftrightarrow$	Impulse response of transmit filter
$H_T(f)$	$\leftrightarrow$	Frequency response of transmit filter
$h_R(t)$	$\leftrightarrow$	Impulse response of receive filter
$H_R(f)$	$\leftrightarrow$	Frequency response of receive filter
$h(t)$	$\leftrightarrow$	Combined impulse response of Tx and Rx filters
$H(f)$	$\leftrightarrow$	Combined frequency response of Tx and Rx filters

Received Signal

$r_c(t)$	$\leftrightarrow$	Received bandpass signal
$r(t)$	$\leftrightarrow$	Received lowpass signal
R_a	$\leftrightarrow$	Sample of received lowpass signal
N_a	$\leftrightarrow$	Noise component of received sample
Z_a	$\leftrightarrow$	Tone component of received sample
$\widehat{I}_a$	$\leftrightarrow$	Detected Symbol

Tone Interference Cancellation

L	$\leftrightarrow$	Number of samples on which tone estimates are based
ω_i	$\leftrightarrow$	Normalized tone frequency (in radians)
C	$\leftrightarrow$	Power ratio
N	$\leftrightarrow$	Periodogram block length
D	$\leftrightarrow$	Number of blocks in average periodogram
$X_d(k)$	$\leftrightarrow$	Periodogram of block d
$X_D(k)$	$\leftrightarrow$	Average periodogram over D blocks
$Z_0(k)$	$\leftrightarrow$	Shape of tone in periodogram
δ_i	$\leftrightarrow$	Displacement of actual frequency from tone spike
$G_M(\delta_i)$	$\leftrightarrow$	Fraction of tone power in tone spike
θ_1	$\leftrightarrow$	Estimate of signal plus noise power
θ_2	$\leftrightarrow$	Estimate of tone power

Acknowledgments

I would like to express my sincere gratitude to my supervisor, Dr. P. Takis Mathiopoulos, for all the support and encouragement he provided during the course of my M.A.Sc. thesis research. His excellent suggestions and continual optimism were instrumental in transforming a stack of equations into a coherent document.

For providing financial support, I would like to thank the Science Council of B.C. and Roger's Cable. Funding for this thesis was also provided through NSERC operating grant 44312 and a B.C. Advanced Systems Institute (ASI) Fellowship.

Thanks are also due to Dr. John Madden of the Canadian Cable Lab Fund and Dr. Alexander Futro of Cable Television Laboratories, Inc. for supporting and arranging my trip to Boulder, CO, to visit CableLabs facilities. I would also like to thank Tom Williams of CableLabs for providing technical advice on CTB.

I wish to thank my parents for convincing me that graduate studies are a good idea. Once again, they were right. Furthermore, I am deeply indebted to them for encouraging me to think independently, beginning in my early childhood. I would also like to thank my father and my brother for taking the time to proofread this thesis and providing much-needed constructive criticism.

Finally, I wish to thank Kelly, my wife and dearest friend, who's support and remarkable patience made this entire endeavor possible.

Chapter One

Introduction

With the recent advancements in all-digital high definition television (HDTV) [1–7], the cable industry must prepare itself for the distribution of digital signals over existing cable networks. In such cable networks, it is well known that several forms of interference exist. It is therefore important for reliable transmission that the effects of these distortions on the transmission of all-digital HDTV signals be understood. Perhaps even more importantly, whenever appropriate, these distortions must be compensated for, or even eliminated.

In this thesis distortion in the form of an additive deterministic but completely unknown interfering tone is considered, along with additive white Gaussian noise (AWGN). In the first two sections of this introductory chapter the various distortions encountered in cable TV systems are discussed, and recent developments of HDTV systems are reviewed. In Section 1.3 a brief description of known techniques for tone interference cancellation is presented. In Section 1.4 the research contributions of the thesis are stated. Finally, in Section 1.5 the organization of the thesis is presented.

1.1 Interference Encountered in Community Antenna Television (CATV) Systems

Since the beginning of regular television broadcasting in the 1930's, the popularity of television as a communication medium has grown enormously [8]. In the 1950's, community antenna television (often referred to as cable TV) systems were first installed to allow viewers in remote areas access to television signals broadcast from distant cities [9]. In these early systems, war surplus coaxial cables were used to carry TV signals to viewer's homes from a *head end*, usually an antenna situated on a nearby hill. Broadband amplifiers, constructed from vacuum tubes, were used to maintain signal power. Over the years, the popularity of CATV systems grew to the point where most viewers in North America are connected to a cable network [10]. This growth stemmed primarily from the wide range of programming that cable TV offers, and the superior image quality available. As a result of the increased popularity, the individual networks have expanded from serving only a few customers in a small town to delivering programming to hundreds of thousands of viewers in large urban areas. Accompanying this growth, many technological improvements to the cable systems have been made. Instead of consisting of a single antenna, modern *head ends* combine signals from a variety of sources, including local studios, satellites, and terrestrial broadcasts, and transmit them together over the cable network.

One important advantage cable TV has over terrestrial broadcasting is in signal quality. When signals are transmitted over the air, serious distortion may be introduced. If the receiver is a long way from the transmitter, or the transmission path is blocked by a large object such as a hill or building, the signal strength is weakened, so external interference will appear like a snow storm on the screen. If the transmitted signal is reflected off surrounding objects, the signal may be received more than once, at slightly different times. This appears as a "ghosting" effect, and is known as multipath reception. Depending on atmospheric conditions, co-channel

interference can occur if a signal from a distant broadcaster, using the same channel as the desired signal, manages to reach the receiver [9].

Because of the shielding provided by the coaxial cable, CATV networks are less susceptible to these types of distortion. In general, CATV provides a much cleaner transmission environment than terrestrial broadcasting. Nonetheless, it is still far from perfect. Various forms of other types of interference may be introduced from external sources through cracks in the cable or improperly fitted connectors, and transmission line reflections may arise in improperly terminated cables [9]. The most serious problem with coaxial cable, however, is its relatively high signal attenuation [10]. To balance the loss of signal power, broadband amplifiers must be inserted into the cable network, generally at intervals of about 2000 feet, depending on cable thickness. The required use of amplifiers is the primary limitation on CATV system performance [11].

Thermal noise generated by components in the amplifiers reduce the signal carrier-to-noise (C/N) ratio. When the signal is passed through a cascade of amplifiers, the noise is compounded. Doubling the number of amplifiers leads to a 3 dB degradation of the C/N ratio [11]. If the C/N ratio falls too low (below about 43 dB [12]), "snow" begins to appear on the picture tube. This impairment is common at receivers a long way from the *head end*, as the signal must pass through a long cascade of amplifiers [11].

In addition to introducing thermal noise, the amplifiers also distort the waveform of the transmitted signal. Although amplifiers are intended to provide linear gain with respect to input amplitude, in practice the response is non-linear. To study the non-linear distortion, it is convenient to model the relationship between the input voltage of the amplifier (V_{in}) with its output (V_{out}) by the non-linear equation

$$V_{\text{out}} = A_1 V_{\text{in}} + A_2 V_{\text{in}}^2 + A_3 V_{\text{in}}^3 + A_4 V_{\text{in}}^4 + \dots , \tag{1.1}$$

where A_1, A_2, A_3, A_4, ... are constants [9, 11, 13, 14]. The first term in the above equation represents the linear gain of the amplifier, the second term reflects the second-order distortion, the third term represents the third-order distortion, and so on. With the use of balanced push-pull amplifiers, non-linear distortion of even-order has been effectively eliminated in modern CATV networks [15]. In addition, most research into the effects of non-linear distortion in CATV networks ignores the higher-order distortion [9, 11, 13, 14]. High order distortion is not considered in this thesis, either. As a result, the response of the non-linear amplifiers can be modelled by

$$V_{\text{out}} = A_1 V_{\text{in}} + A_3 V_{\text{in}}^3 \,. \tag{1.2}$$

In practical CATV systems, many video signals are multiplexed together by modulating carriers at different frequencies. As the broadband signal is passed through a non-linear device, the modulated carriers are mixed together in a variety of ways, resulting in the creation of numerous spurious signals. To illustrate the impact of the undesired signals, it is useful to consider the simplified model of the broadband signal represented in Fig. 1, where each 6 MHz channel consists of only the carrier and video signal. Suppose a total of N different video signals, denoted by $s_n(t)$ for all $n \in [1, N]$, modulate the amplitude of N different carriers at frequencies given by f_n for $n \in [1, N]$. The combined broadband signal, $v(t)$, can be expressed as

$$v(t) = \sum_{n=1}^{N} s_n(t) \cos(2\pi f_n t) \,. \tag{1.3}$$

The spectrum of the broadband signal is shown in Fig. 1.

The third-order non-linear distortion is related to the cube of the broadband signal, which is, using this model,

$$v^3(t) = \left[\sum_{n=1}^{N} s_n(t) \cos(2\pi f_n t) \right]^3$$

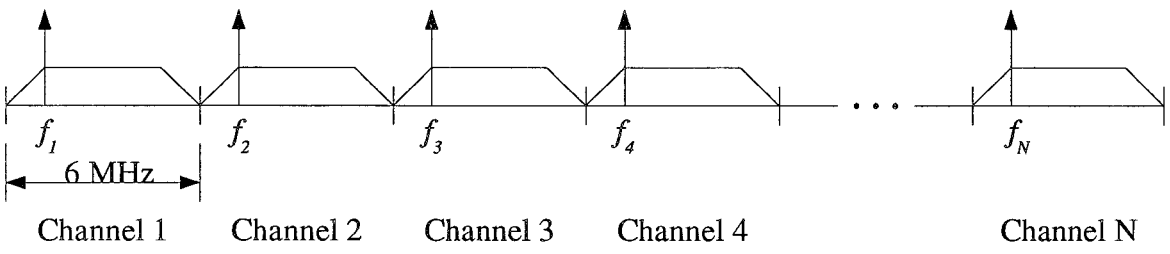

Figure 1. Simplified Spectrum of Broadband CATV Signal.

$$= \sum_{a=1}^{N}\sum_{b=1}^{N}\sum_{c=1}^{N} s_a(t)s_b(t)s_c(t)\cos(2\pi f_a t)\cos(2\pi f_b t)\cos(2\pi f_c t)$$

$$= \frac{1}{8}\sum_{a=1}^{N}\sum_{b=1}^{N}\sum_{c=1}^{N} s_a(t)s_b(t)s_c(t)\cos[2\pi(f_a \pm f_b \pm f_c)t]\,. \tag{1.4}$$

Third-order distortion products arise in relationship to the set of frequencies $\{f_a \pm f_b \pm f_c | \; \forall\, a,b,c \in [1,N]\}$. The different ways that the frequencies can be combined produce different forms of interference. This point is best illustrated by rearranging the summations in Eq. (1.4) to group together the terms where the indices are the same. After some straightforward but cumbersome algebraic manipulation, Eq. (1.4) can be rewritten as

$$v^3(t) = \frac{3}{8}\sum_{a=1}^{N} s_a^3(t)\cos(2\pi f_a t) + \frac{4}{8}\sum_{a=1}^{N}\sum_{\substack{b=1\\ b\neq a}}^{N} s_a^2(t)s_b(t)\cos(2\pi f_a t)$$

$$+ \frac{1}{8}\sum_{a=1}^{N} s_a^3(t)\cos[2\pi(3f_a)t] + \frac{2}{8}\sum_{a=1}^{N}\sum_{\substack{b=1\\ b\neq a}}^{N} s_a^2(t)s_b(t)\cos[2\pi(2f_a \pm f_b)t]$$

$$+ \frac{1}{8}\sum_{a=1}^{N}\sum_{\substack{b=1\\ b\neq a}}^{N}\sum_{\substack{c=1\\ c\neq a}}^{N} s_a(t)s_b(t)s_c(t)\cos[2\pi(f_a \pm f_b \pm f_c)t]\,. \tag{1.5}$$

The presence of the first term in Eq. (1.5) implies that each carrier will carry the modulation of the cube of desired signal in addition to the desired signal. This effect is known as self-modulation [14]. From the second term it is clear that each carrier also carries the modulation of the other signals, resulting in an effect known as cross-modulation. Visually, this results

in other signals appearing in the background of the desired one. The remaining three terms generate products that are spread throughout the frequency spectrum. They are significant because there are so many of them. In fact, there are N third-order harmonics, $2N(N-1)$ beats of the form $2f_a \pm f_b$, and $\frac{2}{3}N(N-1)(N-2)$ distinct beats of the form $f_a \pm f_b \pm f_c$. For a typical fully loaded 35 channel cable system, a total of 28,595 third-order (or triple) beats occur. Since NTSC systems use a large carrier amplitude modulation (LC-AM) system [16], the carriers are the dominant part of the transmitted signals. As such, each of the intermodulation products discussed above can be considered to be a single sinusoidal tone [9, 11].

In summary, only these two types of interference are considered in this thesis. Because of the random nature and relatively white spectrum associated with thermal noise, it can accurately be modelled as an additive white Gaussian random process. For the purposes of this thesis, only a single intermodulation product is assumed. It is modelled as a single tone that is characterized by its magnitude, K_{ci}, its bandpass frequency, f_{ci}, and its phase, ϕ_i. It is assumed that none of these parameters vary with time, in that they each maintain a constant albeit completely unknown value. As such, this distortion is not random, but deterministic, and mathematically it can be represented as

$$z_c(t) \triangleq K_{ci}\cos(2\pi f_{ci}t + \phi_i) \,, \tag{1.6}$$

with $0 \leq K_{ci} < \infty$, $f_{ci} > 0$, and $0 \leq \phi_i < 2\pi$. This model provides a good base from which analysis of the effect of the distortion can begin. Further investigation can be carried out on a more elaborate model, such as multiple tones and nonstationary tones for example, although this will not be reported in this thesis.

1.2 A Brief Review of High Definition Television (HDTV)

In North America, colour television signals are transmitted using a system recommended by the National Television Systems Committee (NTSC) of the American Federal Communications Commission (FCC) in 1953 [16]. Although the NTSC system was very innovative at that time, it possesses some limitations. It does not provide enough spatial resolution for adequate display on the large screens that are presently available, and it displays images too narrow for the wide aspect ratio of many motion pictures. Another drawback of current television standards is that there is no single worldwide standard. In fact, according to the CCIR (Comité Consultatif International Radio), an international body which attempts to coordinate broadcasting standards, there are eleven different television standards in common use [8]. In the "global village" of the 1990's, this barrier to international communication is unacceptable.

In 1987, the FCC decided to consider the development of a new standard for terrestrial television broadcasting. It established the FCC Advisory Committee on Advanced Television Service to investigate issues regarding the new standard [1]. Referred to as advanced television (ATV), or high definition television (HDTV), this standard was expected to incorporate greater spatial resolution and a wider aspect ratio. Furthermore, it was hoped that it could be accepted internationally [2]. The Advisory Committee began studying twenty-three proposed systems in its quest for a practical HDTV standard. Some proposals were deemed infeasible and other were discounted as they possessed serious disadvantages. In 1990 it was decided that only five warranted further investigation. It is interesting to note that at the time of this decision, only one of these five proposals was all-digital.

Beginning in 1991, the Advisory Committee supervised a number of tests of the remaining systems to determine their relative merits [3]. The Advanced Television Test Centre (ATTC) performed laboratory and field testing of the systems from a terrestrial broadcasting

perspective. At Cable Television Laboratories, Inc. (CableLabs), similar cable television related testing was performed. The Advanced Television Evaluation Laboratory (ATEL) was established in Ottawa to provide subjective evaluation of the image quality of the proposals [3]. In February 1993, the Advisory Committed published its ATV system recommendations [3]. Although no standard was in sight, significant decisions had been made. Perhaps the most import decisions were that HDTV signals will be allocated channels no wider that the 6 MHz ones used by NTSC-compatible broadcasters, and digital compression and modulation schemes will be employed exclusively. Four of the five proposals were modified to incorporate a digital design, and the fifth dropped out of consideration. The proponents of all-digital HDTV transmission are currently implementing modifications to their systems to rectify some of the minor problems identified during the testing procedure. The remaining systems currently being considered for HDTV transmission are: 1) the DigiCipher system proposed by the American Television Alliance (ATVA), a collaboration of General Instrument Corp. and Massachusetts Institute of Technology; 2) the Digital Spectrum-Compatible HDTV (DSC-HDTV) system proposed by Zenith Electronics Corp. and AT&T Bell Laboratories; 3) the Advanced Digital Television (ADTV) system proposed by the Advanced Television Research Consortium (ATRC), consisting of Thomson Consumer Electronics, Inc., Phillips Consumer Electronics Co., NBC, and the David Sarnoff Research Centre; and 4) the ATVA-Progressive System proposed by the American Television Alliance. All these systems are all-digital, and in general it appears that they have more similarities than differences. Although a detailed description of each of the systems is beyond the scope of this thesis, their main similarities will be described in Chapter 2.

To conclude this very brief review of HDTV, it is worth mentioning that research into all-digital HDTV transmission has resulted in some major technological breakthroughs. For example, advanced image compression algorithms have successfully been developed, allowing

the enormous quantity of information associated with the high resolution, wide aspect ratio HDTV signals to be reduced sufficiently to allow transmission in 6 MHz channels [3]. Due to this success, other applications of digital television are being considered. Telephone companies are very much interested in using the new image compression technology to provide high quality video telephone communication. Also, cable television networks plan to apply digital compression to NTSC signals to reduce bandwidth, greatly increasing the number of channels available to cable TV subscribers. Since the cable industry will be transmitting both HDTV and compressed digital NTSC signals, it will certainly be a major user of digital television technology.

1.3 Tone Cancellation Techniques

As will be shown in Section 2.6 of this thesis, a single tone of sufficient magnitude can impede the ability of CATV networks to distribute all-digital HDTV signals, to the point where video transmission almost completely fails. To maintain acceptable image quality, some means of removing the tone is required. The issue of removing sinusoidal interference is a classical communication problem. A wide variety of solutions have been proposed, each possessing their own advantages and limitations. In general, these solutions fall into three broad categories: *i*) fixed notch filters, *iii*) transform domain processing, and *iii*) adaptive noise cancellation.

Early attempts at tone removal employed fixed notch filters. If the frequency of the tone is known, these filters perform adequately. However, practical implementations of these filters have nulls with non-zero bandwidth, leading to some distortion of the desired signal. Furthermore, since the frequency of the tone must be known *a priori*, these filters are unacceptable for removing tones arising from CTB.

Transform domain processing techniques employ discrete Fourier transforms (DFTs) to convert the signal to the transform domain, where the signal is processed. One technique uses conditional median filtering to reduce the power of the tone without significantly altering the DFT coefficients of the desired signal [17]. Another applies a set of non-uniform weights to the coefficients in an attempt to maximize the signal-to-noise ratio [18]. After processing, the signal is transformed back to the time domain with an inverse DFT. In general, these techniques work well only for sufficiently strong tones.

The most robust and popular techniques for removing tone interference involve the use of adaptive noise cancellation, as described by Widrow *et al.* [19]. Fig. 2 shows a typical adaptive noise canceller. The adaptive filter processes the delayed input to produce an estimate of the interfering tone. This estimate is subtracted from the primary input to effectively cancel the tone. As shown in Fig. 3, the adaptive filter is implemented with a tapped delay line. The adaptive algorithm heuristically adjusts the weights in an effort to minimize the mean square error between the actual tone and the filter output. Numerous different techniques for determining the weights have been proposed (see, for example, [19–21]), all providing different trade-offs between simplicity and accuracy. In general, adaptive noise cancellation techniques are the most versatile and efficient methods for removing tones, even when the tone is relatively weak. Furthermore, no *a priori* knowledge of the tone is required.

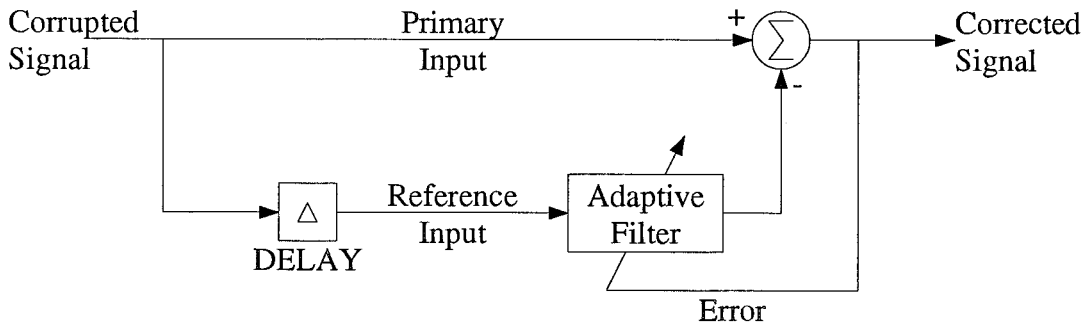

Figure 2. Adaptive Noise Canceller.

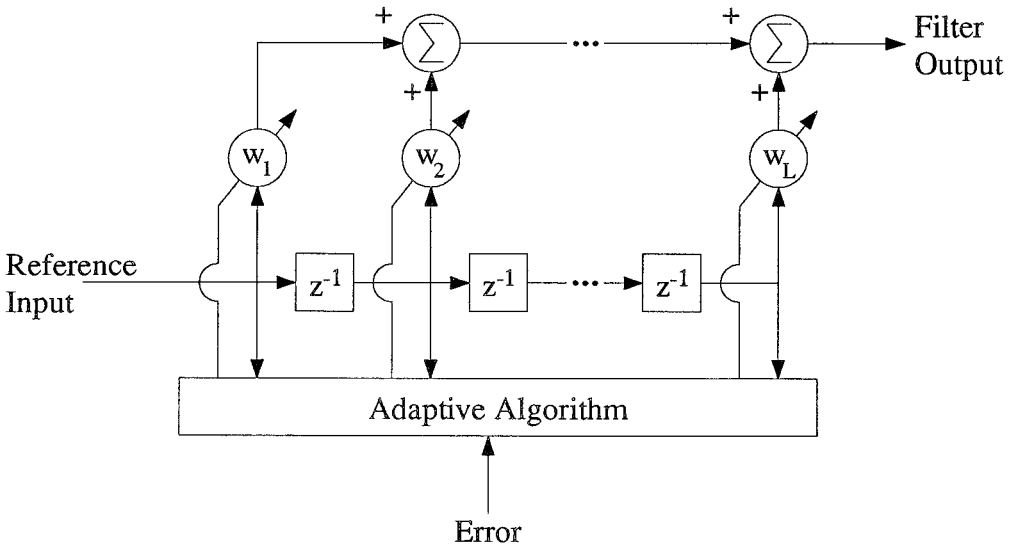

Figure 3. Adaptive Filter.

1.4 Research Contributions of Thesis

In this thesis, a novel technique for removing a completely unknown tone which is interfering with a digital QAM signal is proposed, analysed and evaluated in an AWGN environment. The optimal weights for the linear minimum mean-square error (MMSE) filter for cancelling the tone interference are determined, under the condition that the tone's frequency and power are known to the canceller. Novel methods for estimating the frequency and power of the tone are developed, which are based on the finite-length discrete Fourier transform (FFT). Using these estimates in place of the actual frequency and power yields a suboptimal filter that performs practically identically to the optimal one under normal distortion conditions. In addition, a decision feedback mechanism is employed to further improve the performance of the tone interference canceller by reducing the effect the data signal has on the cancellation process. Through a combination of analytical and computer simulated performance evaluation it is found that for all practical purposes the proposed decision feedback tone canceller removes the tone interference completely.

1.5 Organization of Thesis

Including this introductory chapter, this thesis consists of five chapters and four appendices, and is organized as follows.

Chapter 2 contains an overview of all-digital HDTV transmission, with analysis of errors arising from AWGN and tone interference. In Section 2.2 the HDTV compression algorithms are described in general terms, and the implications of transmission errors on the decoding process are discussed. Section 2.3 contains a descriptions of the error protection that is provided in the form of channel coding. Quadrature amplitude modulation (QAM) is discussed in Section 2.4, with emphasis on the symbol encoder, transmit filter, and carrier modulation. Mathematical models for the AWGN and tone interference are given in Section 2.5. In Section 2.6 the demodulation process is described and the propagation of distortion from the channel through the demodulator and receive filter to the symbol detector is analysed. The effect of the distortion on the probability of transmission error is studied.

In Chapter 3 a novel tone interference canceller is proposed. A method of estimating tone interference is present in Section 3.2 that is based on the linear minimum mean-square error (MMSE) family of estimators. In Section 3.3 a method for estimating the frequency and power of the tone as well as the Gaussian noise power is presented. These quantities are required by the proposed tone interference canceller. Section 3.4 contains a detailed summary of the canceller, including block diagrams of potential implementations.

The results of extensive testing of the proposed canceller by means of computer simulation is presented in Chapter 4. Performance is analysed over a wide range of distortion conditions and compared with theoretical bounds. Different implementations are compared and contrasted to provide an understanding of the relevance of certain design parameters.

Chapter 5 summarizes the contributions of this thesis and suggests future research topics

that could be carried out to extend the effective performance of the proposed tone interference canceller.

Appendix A provides a proof that the filer weights for linear MMSE tone interference cancellation are optimal. Appendices B and C contain derivations of the means and variances of some of the other estimators used in Chapter 3 of this thesis. Finally, Appendix D provides listings of all the computer source code written for the research of this thesis.

Chapter Two

System Model Description and Analysis

2.1 Introduction

This chapter contains an overview of the components employed in all-digital HDTV transmission. Since the FCC has yet to approve a standard for HDTV transmission, a generic model is presented here. Although this model differs slightly from the proposals, it embodies all their primary ideas. To illustrate some specific points, emphasis will be given to the DigiCipher system, which was the first all-digital HDTV proposal. A simplified model for an all-digital HDTV transmission system that is satisfactory for the purpose of this thesis is presented in Fig. 4.

The four data sources supply digital data to be transmitted, and their formats differ slightly among the proposed systems. For the DigiCipher system, the digital video data is used to transmit frames consisting of 960 lines with 1408 pixels per line at a frame rate of 29.97 Hz

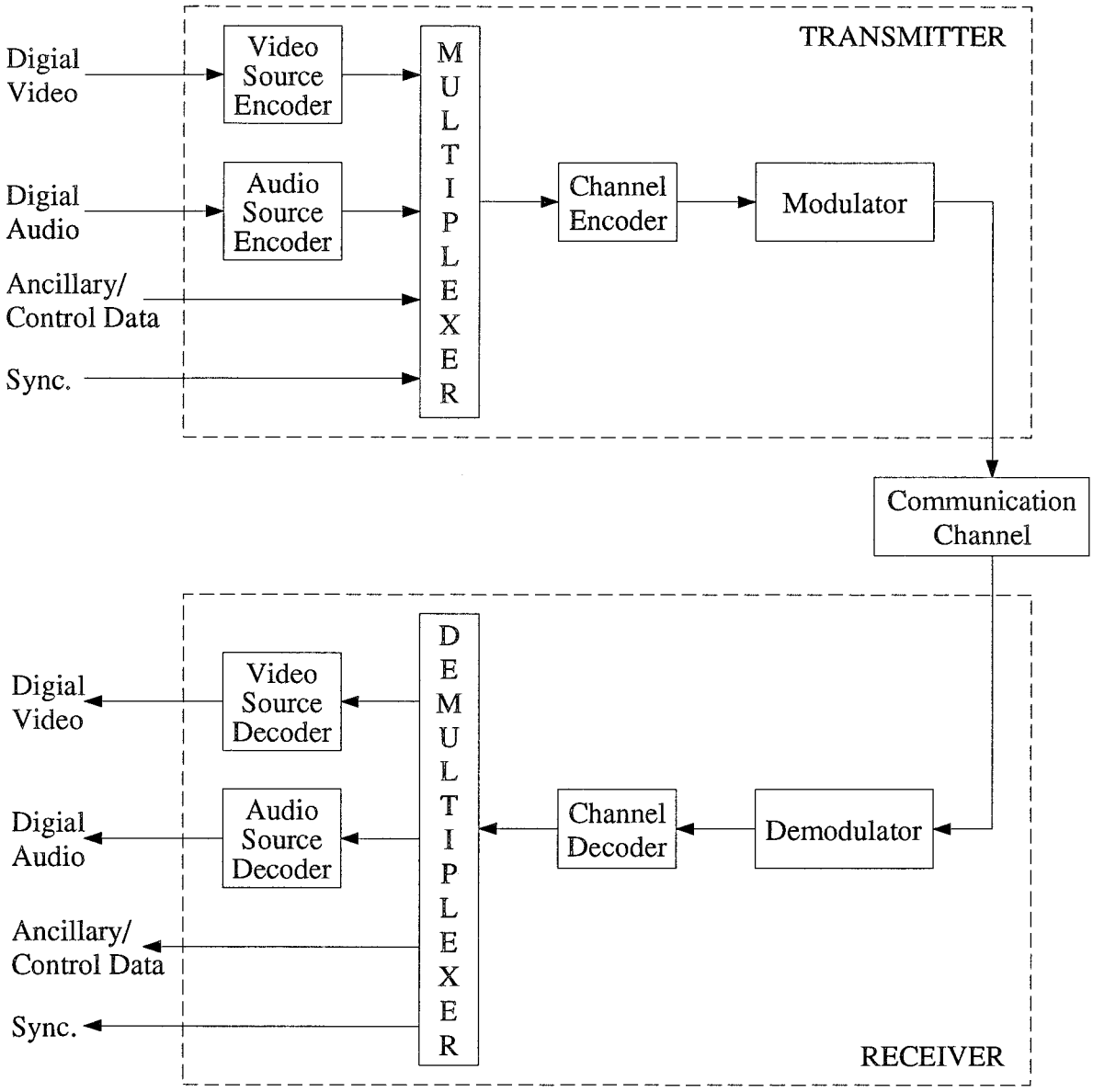

Figure 4. All-digital HDTV Transmission System [4].

[3]. It is derived from sampling an analogue composite red-green-blue (RGB) signal which has 1050 lines per frame scanned in a 2:1 interleaved format. The two fields per frame are scanned with a field rate of 59.94 Hz, and have 16:9 width-to-height aspect ratio. The DigiCipher digital audio signal is produced from four separate audio channels sampled at 48 kHz with 16–bit precision in the A/D conversion. The ancillary/control data is reserved for purposes such as the transmission of TeleText and subscriber access control [3]. Additional data may also be included for the purpose of system synchronization. To allow all this data

to be transmitted over a single channel band-limited to 6 MHz, source coding is used to implement compression schemes in the source encoder, with corresponding decompression in the source decoder. Channel coding is used to protect the compressed data from any errors that may arise during transmission. Also, bandwidth efficient modulation schemes are used to represent the digital data in a format suitable for transmission over the communication channel. A HDTV receiver reverses the transmission process by demodulating the received signal, correcting transmission errors, and decompressing the digital signals. It is expected that any transmission errors will be controlled successfully, allowing the reception of high quality video and audio, free from serious impairments.

To study the performance of HDTV transmission, the processes of source coding, channel coding, and modulation are discussed in this chapter. As this covers an extremely large field, only a very short description is presented. The organization of this chapter is as follows: in Section 2.2 an overview of the source coding process employed in compressing HDTV signals is presented; in Section 2.3 the techniques used for channel coding to protect the transmitted HDTV signal from errors are discussed; in Section 2.4 a bandwidth efficient modulation scheme is presented that allows the HDTV signal to be transmitted over the coaxial cable TV network; in Section 2.5 the modelling of the coaxial cable TV channel is discussed in detail, with a description of the distortion it introduces; in Section 2.6 the demodulation process is discussed, and the propagation of distortion arising in the communication channel through the demodulator is studied.

2.2 Source Coding

The purpose of the source encoders is to reduce the number of bits required to represent the video and audio signals. This compression must be carried out in a manner that allows

the source decoder to recreate reliable replicas of the original signals. This is accomplished by two means: noiseless compression, which removes redundant information that can be reproduced exactly by the decoder, and noisy compression, which removes information that has little visible impact on the human eye or audible impact on the human ear. Because of the different natures of video and audio signals, different source coding procedures are used.

A typical video source encoder is shown in Fig. 5. Both temporal and spatial compression are applied to provide superior compression rates. The individual components of the source encoder must be considered separately to gain an understanding of the coding process.

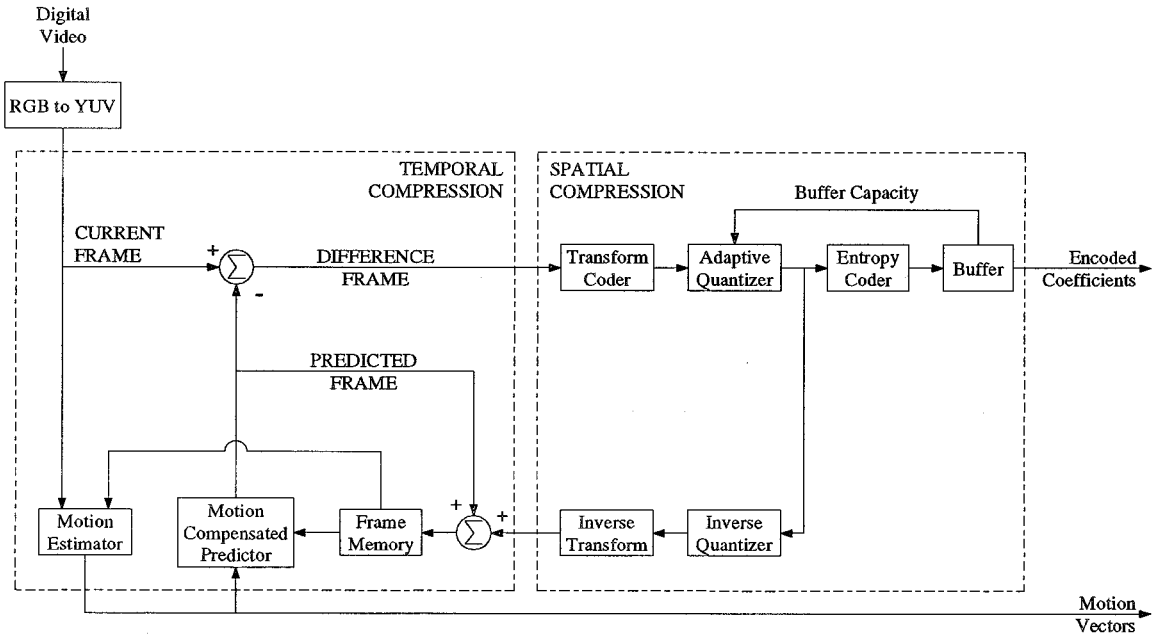

Figure 5. Typical Digital Video Source Encoder [4].

The digital RGB video signal is first converted into its luminance and chrominance components (the YUV signal space). Since the human eye is less sensitive to fine detail in chrominance than in luminance [22], the chrominance signals are subsampled horizontally by a factor of four, and alternate lines are discarded [5]. This is one source of image degradation introduced in the compression process.

Temporal compression is achieved through motion compensated predictive coding. By analysing the relative displacement of small segments of the image between the current frame and the previous frame, the motion estimator produces a set of motion vectors. The motion compensated predictor applies the motion vectors to the previous frame to produce a prediction of the current frame. Since it is expected that the predicted frame will closely resemble the current frame, the difference of these two images typically contains less information that the actual frame. The motion estimation is based only on the luminance component, and the same motion vectors are applied to the chrominance components.

Spatial compression is applied to the difference frame to further reduce the amount of information to transmit. The difference frame is divided into blocks containing 8x8 pixels each. A two-dimensional discrete cosine transform (DCT) is applied to each block, providing spatial frequency representations of the blocks. The adaptive quantizer converts the DCT coefficients into binary data. Since the human eye is less sensitive to intensity variations at high spatial frequencies [22], fewer bits are required to represent these coefficients than the low frequency ones. The quantization process is the second source of image degradation introduced from compression. To achieve additional compression, redundancy is removed from the quantized DCT coefficients by run-length and Huffman entropy coding.

Since the compression algorithms produce data at a variable rate depending on the amount of redundancy in the video signal, a buffer is used to store the data and emit it at a constant rate. If the buffer fills to near capacity, the adaptive quantizer is signalled to allocate fewer bits to the DCT coefficients. This increases the compression rate at the expense of image quality. As the amount of data in the buffer decreases, the quantizer can return to allocating more bits.

Fig. 6 shows a typical digital video source decoder. Essentially, it reverses the operation of the decoder. The encoded coefficients are decoded to produce the quantized DCT coefficients. These are identical to the ones produced by the adaptive quantizer in the transmitter. The

inverse quantizer provides the inverse function of the adaptive quantizer. Quantization rounding errors cause a slight difference between the output of the inverse quantizer in the receiver and the input of the adaptive quantizer in the transmitter. The inverse transform converts the rounded DCT coefficients back into the spatial domain, creating the *update information.* This information is the same as the transmitter's *difference frame*, expect for the effects of quantization rounding errors. The received motion vectors are applied to the stored previous frame, producing the *predicted frame.* The update information is added, resulting in the received *current frame*, which differs from the transmitted frame only in quantization error. Finally, the frame is converted to the RGB domain for display on the receiver's screen.

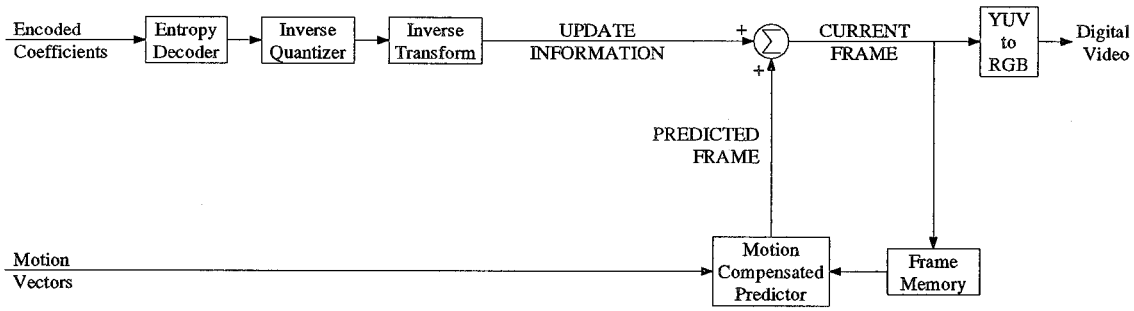

Figure 6. Typical Digital Video Source Decoder [4].

To prevent the propagation of quantization error from frame to frame, some extra work must be done by the transmitter. Since the *previous frame* used by the receiver differs from the true *previous frame*, any quantization errors it contains will be carried into the current frame as well. To prevent this problem, the encoder does not use the true *previous frame* for motion estimation, but produces its own copy of the *update information* that the receiver will use by applying inverse quantization and an inverse transform. This is added to the encoder's *predicted frame* and stored for use as the *previous frame* for the basis of the next frame transmitted. As a result, the transmitted motion vectors define a mapping from the receiver's *previous frame* to the current frame, and interframe quantization error propagation no longer occurs.

Although compression errors do not propagate from frame to frame, the loss of information associated with the chrominance sub-sampling and adaptive quantization does imply that the receiver is unable to exactly reproduce the original video signal. Nonetheless, these impairments should not significantly affect the image quality since they primarily affect information imperceptible to normal human eyesight [22]. Image distortion is greatest when there is little intraframe and interframe redundancy in the video signal, since coarser quantization must be employed to compensate for the additional information. This usually occurs immediately following a scene change, and during scenes involving rapid motion.

Although compression errors slightly distort the video signal, transmission errors can be much more serious. However, the source coding process also involves some inherent protection against these errors. Because of the compression algorithms employed, a single bit error can affect the video signal in a variety of ways. An error in the encoded coefficients will affect the amplitude of only one DCT coefficient. This would cause a slight alteration of the all the amplitudes in one 8x8 pixel block. This effect will be more noticeable if a low frequency DCT coefficient is in error [7]. Although having distortion in one block may not be too severe, this distortion also propagates to succeeding frames. A much more serious problem occurs when the error causes the entropy decoder to lose synchronization, causing all the coefficients in the remainder of the block to be scrambled. Furthermore, this loss of synchronization may be carried into subsequent blocks, destroying a large area of the image. To help maintain synchronization, end-of-block markers are inserted into the encoded coefficients. Errors in the motion vectors also have a serious effect on the received image. Not only do objects in the image appear distorted, they also appear in the wrong position. This distortion also propagates to succeeding frames.

To limit the effects of error propagation, frames without motion compensation are periodically transmitted. These frames are referred to as intra-frames, or I-frames. Although

the use of I-frames results in a significant reduction the image compression rate, it prevents errors from propagating indefinitely. The source coder also employs some error concealment techniques to reduce the visual impact transmission errors may incur.

The source coding process described in this section is only a simplification of the actual process. A number of details, such as channel acquisition, have been omitted for the sake of brevity. Source coding is also applied to the audio signals. Although the proposals use different compression systems, they are all capable of compressing the audio data to about 0.5 Mbit/s [3]. The audio data is multiplexed with the video data along with ancillary and synchronization data to produce a single binary data stream.

Although the video compression rates vary slightly between the proposals, they all allow for an enormous reduction in the amount of data that needs to be transmitted. For example, the DigiCipher system compresses the 121 million samples per second of its analog RGB signal into a 12.59 Mbit/s binary data signal [5]. Usually there is a trade-off between image quality and image compression. Although some care has been taken to minimize the impact of transmission errors on image quality, the compressed data remains quite sensitive to errors. A single bit can have a substantial impact on image quality for a noticeably long duration. To provide additional protection against errors occurring in the channel, channel coding is applied.

2.3 Channel Coding

To protect the compressed binary data stream from transmission errors, a HDTV system must use channel coding. Proposed techniques include error detection, forward error correction, and data interleaving [6]. A combination of some or all of these techniques are incorporated in all the HDTV proposals, ensuring reliable data communication. Through the

use of cyclic redundancy check codes, transmission errors can usually be detected. When an error is detected, the source decoder is informed of the corrupt data so that error concealment techniques can be initiated. Although most errors can be detected, the error concealment techniques can not perfectly hide the resulting image defects, so they are used only as a last line of defence. Most error protection comes from the use of forward error correction (FEC). Reed-Solomon codes are used to correct most transmission errors. These block codes are known for their superior ability to correct multiple bursts of errors [23]. For example, a (127, 117) Reed-Solomon code transmits 117 seven-bit symbols in blocks containing 127 symbols, and can correct up to five symbol errors per block, or one error burst of up to 35 bits per 889 bit block [7]. Additional protection against error bursts is achieved in some proposals with data interleaving.

Clearly, channel coding is capable of providing very adequate protection of the compressed digital data. Occasional random errors and even short error bursts are controlled successfully, causing absolutely no degradation of image quality. Errors that occur more frequently may defeat the error correction, but their impact is minimized by error concealment. As the error frequency increases, however, all proposals exhibit rapid degradation from the point where errors are noticeable but tolerable, to the point of unusability, where the image is far too severely impaired to be viewed [3].

To study the likelihood of transmission errors, the modulation and demodulation of the data signal must be analysed, including the effect of the channel distortion.

2.4 Modulation

To transmit HDTV signals over a coaxial cable television network, a modulation scheme must be employed. Modulation allows many different TV signals to be transmitted simul-

taneously over a single cable. The two modulation schemes being considered for HDTV are quadrature amplitude modulation (QAM), and vestigial sideband modulation (VSB). Only QAM is considered in this thesis, and results will be different if a different modulation scheme is used. A block diagram of a typical QAM transmitter is shown in Fig. 7. A symbol encoder combines bits from the data source (the output of the channel encoder) into multi-bit symbols. By transmitting several bits at once in a symbol, a higher data transmission rate can be attained. The digital symbol stream is passed through a pulse shaping transmit filter which limits the bandwidth of the transmitted signal. The filtered signal is then used to modulate the amplitude of a carrier wave. A more detailed description of the QAM transmission process follows.

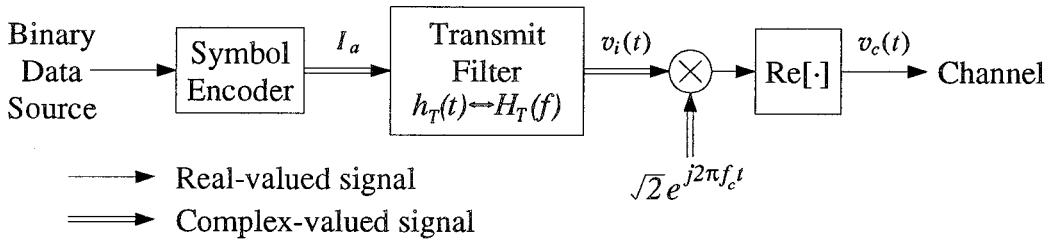

Figure 7. Typical QAM Transmitter [24].

2.4.1 Symbol Encoder

To increase the data transmission rate without increasing the required bandwidth, a symbol encoder combines groups of binary digits from the channel encoder into multi-amplitude, complex-valued symbols. During each symbol interval, an M-QAM symbol encoder collects $\log_2 M$ bits from the data source, and based on the value of the bits, selects one of M possible symbols from a finite set of allowable symbols known as the signal constellation, which shall be denoted by $\mathcal{S}$. The points in the signal constellation describe the in-phase and quadrature-phase amplitudes to be transmitted for each symbol. These amplitudes take on values from the alphabet $\left\{\pm A, \pm 3A, \ldots, \pm\left(\sqrt{M}-1\right)A\right\}$.

For all the examples presented in this thesis, a 16–QAM system is assumed. This system groups bits into 4–bit symbols for transmission. The FCC standard for HDTV may require the use of a higher order modulation scheme, such as 32–QAM or 64–QAM. The theoretical analysis in this thesis can readily be extended to these higher order schemes. The symbol constellation for a 16–QAM scheme is depicted in Fig. 8. For example, the group of bits 1001 is mapped to the symbol $S_9 = (-3A, A) = -3A + jA$.

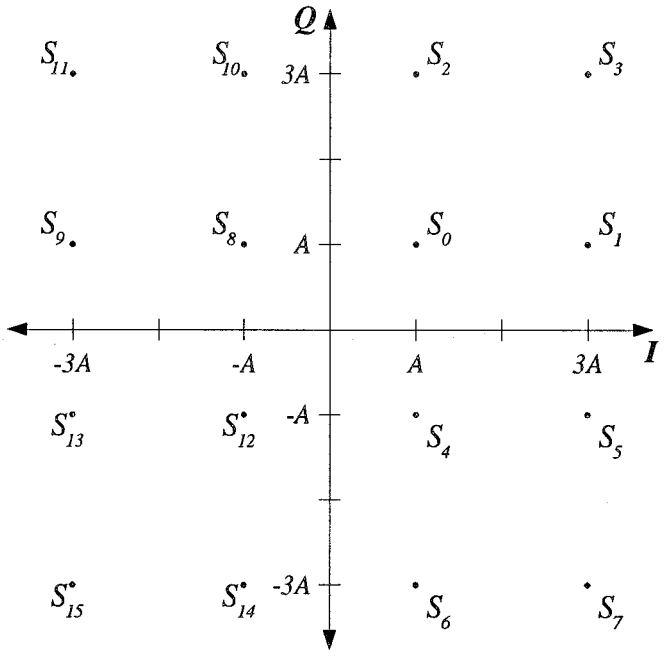

Figure 8. 16–QAM Signal Constellation.

The selected symbols are emitted at a rate of $1/T_s$ symbols per second, where T_s is the duration of the symbol interval. The resulting symbol stream will be denoted by $\{I_a | I_a \in \mathcal{S},\ -\infty \leq a \leq \infty\}$, where I_a is the symbol emitted at time $t = aT_s$. To develop a theoretical analysis of the performance of the transmission system it is convenient to model the transmitted symbol stream by a discrete random process. Under this model, each transmitted symbol is randomly selected from $\mathcal{S}$, with each point in $\mathcal{S}$ being selected with equal probability. In addition, it is assumed that each symbol is selected independently of the

others in the stream. As a result, the mean (denoted by $\mathbf{E}[\cdot]$) of the random process is

$$\mathbf{E}[I_a] = 0 \ , \tag{2.1}$$

and the autocorrelation is

$$\mathbf{E}[I_a^* I_b] = \sigma_s^2 \delta(b-a) = \begin{cases} \sigma_s^2 & \text{iff } a = b \\ 0 & \text{otherwise} \end{cases} , \tag{2.2}$$

where $*$ denotes complex conjugate, $\delta(\cdot)$ is the Kronecker delta function, and σ_s^2 is the average energy per symbol. For 16–QAM, this is $\sigma_s^2 = 10A^2$.

2.4.2 Transmit Filter

Filters are used in the transmitter and receiver to limit the bandwidth of the transmitted signal and minimize the effect of noise introduced in the communication channel. In addition to serving these two purposes, the filters are customarily designed so that they introduce no intersymbol interference (ISI) [24]. Let $H_T(f)$ and $h_T(t)$ denote the frequency and impulse response of the transmit filter, and let $H_R(f)$ and $h_R(t)$ denote the frequency and impulse response of the receive filter. The combined frequency response of the two filters is $H(f) = H_T(f)H_R(f)$, and the combined impulse response is $h(t) = h_T(t) \circledast h_R(t)$, where $\circledast$ denotes the convolution operation.

To maintain compatibility with existing television spectral usage, it is necessary to limit the bandwidth required to transmit HDTV signals to 6 MHz. This is achieved by requiring that $H_T(f) \equiv 0$ for all $|f| \geq 3$ MHz. To maximize the received signal-to-noise ratio, the receive filter must be matched to the transmit filter [24], so that $H_R^*(f) = H_T(f)$. To prevent the introduction of ISI, it is necessary that the combined impulse response has the property $h(cT_s) = 0$ for all integers $c \neq 0$.

One filter meeting these three requirements is the root-raised cosine filter. Because of its simplicity of implementation, it is commonly used in communication systems. This filter

has a frequency response of

$$H_T(f) = \begin{cases} \sqrt{T_s}\,, & |f| \le \frac{1-\alpha}{2T_s} \\ \sqrt{T_s}\cos\left[\frac{\pi T_s}{2\alpha}|f| - \frac{\pi}{4\alpha}(1-\alpha)\right]\,, & \frac{1-\alpha}{2T_s} < |f| < \frac{1+\alpha}{2T_s} \\ 0\,, & |f| \ge \frac{1+\alpha}{2T_s} \end{cases}\,, \tag{2.3}$$

where α is referred to as the rolloff factor and denotes the excess bandwidth used as compared to the minimum Nyquist bandwidth which is given by $\alpha = 0$. A plot of the frequency response for various values of α is shown in Fig. 9. When $\alpha = 0.2$, the symbol rate must be chosen so that $T_s > 0.2 \times 10^{-6}$ seconds to limit the bandwidth to 6 MHz. The impulse response of the root-raised cosine filter can be derived as[1]

$$h_T(t) = \frac{1/\sqrt{T_s}}{1 - \left(\frac{4\alpha t}{T_s}\right)^2}\left[\frac{\sin\left(2\pi\frac{1-\alpha}{2T_s}t\right)}{\frac{\pi t}{T_s}} + \frac{\cos\left(2\pi\frac{1+\alpha}{2T_s}t\right)}{\frac{\pi}{4\alpha}}\right]\,. \tag{2.4}$$

Note that this filter is non-causal, so in practical hardware implementations a truncated version of the impulse response must be used. A truncated version was also used in the software simulations that were executed to produce the results in Chapter 4.

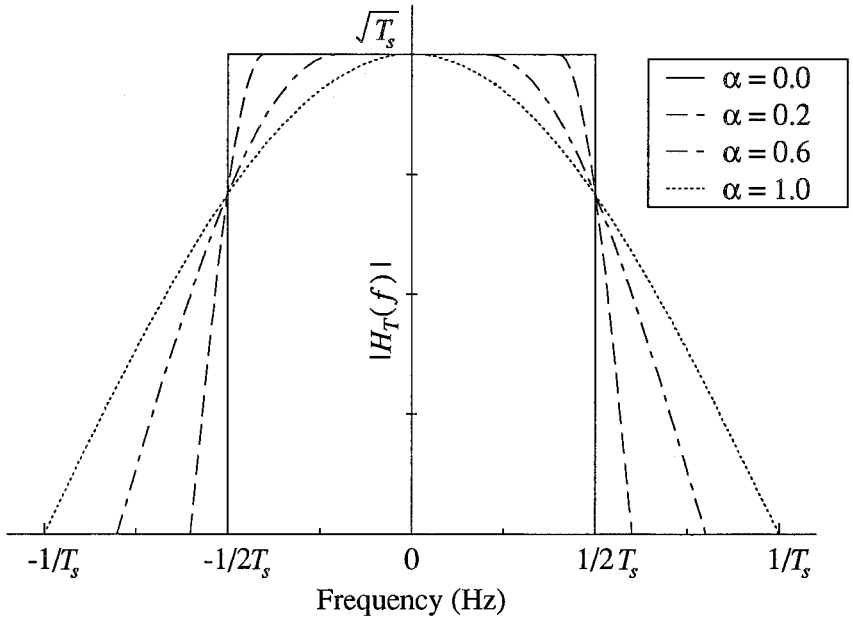

Figure 9. Frequency Response of Root-Raised Cosine Filter.

[1] This follows from the straightforward but tedious inverse Fourier transform of Eq. (2.3). This result is not usually included in textbooks.

The corresponding receive filter is identical to the transmit filter, and the combined impulse response is

$$h(t) = \frac{\sin\frac{\pi t}{T_s}}{\frac{\pi t}{T_s}} \frac{\cos\frac{\pi t\alpha}{T_s}}{1 - \frac{4\alpha^2 t^2}{T_s^2}} . \tag{2.5}$$

Note that for any integer, c,

$$\begin{aligned} h(cT_s) &= \frac{\sin \pi c}{\pi c} \frac{\cos \pi c\alpha}{1 - 4\alpha^2 c^2} \\ &= \delta(c) = \begin{cases} 1 & \text{iff } c = 0 \\ 0 & \text{otherwise} \end{cases} , \end{aligned} \tag{2.6}$$

so no ISI is caused by the filters.

In this thesis it is assumed that ideal root-raised cosine filters are used in the transmitter and receiver. Furthermore, it is assumed that the rolloff factor is strictly less that one. For all examples, a rolloff factor of $\alpha = 0.2$ is used to limit the bandwidth to 6 MHz.

The output of the transmit filter, $v_i(t)$, can be expressed in the time domain as

$$v_i(t) = \sum_{a=-\infty}^{\infty} I_a h_T(t - aT_s) . \tag{2.7}$$

For theoretical analysis, it is useful to model $v_i(t)$ as a random process. It has a mean of

$$\mathbf{E}[v_i(t)] = \sum_{a=-\infty}^{\infty} \mathbf{E}[I_a] h_T(t - aT_s) = 0 , \tag{2.8}$$

and an autocorrelation function given by

$$\begin{aligned} \phi_{v_i}(t;\tau) &\triangleq \mathbf{E}[v_i^*(t) v_i(t+\tau)] \\ &= \sum_{a=-\infty}^{\infty} \sum_{b=-\infty}^{\infty} \mathbf{E}[I_a^* I_b] h_T^*(t - aT_s) h_T(t + \tau - bT_s) . \end{aligned} \tag{2.9}$$

Substituting Eq. (2.2) for $\mathbf{E}[I_a^* I_b]$ yields

$$\phi_{v_i}(t;\tau) = \sum_{a=-\infty}^{\infty} \sum_{b=-\infty}^{\infty} \sigma_s^2 \delta(b-a) h_T^*(t-aT_s) h_T(t+\tau-bT_s)$$
$$= \sigma_s^2 \sum_{a=-\infty}^{\infty} h_T^*(t-aT_s) h_T(t+\tau-aT_s) \; . \tag{2.10}$$

Since this is a function of t as well as τ, and $\phi_{v_i}(t+T_s;\tau) = \phi_{v_i}(t;\tau)$, $v_i(t)$ is a cyclostationary random process, with a period of T_s.

2.4.3 Modulation

The purpose of modulation is to shift the spectrum of the data signal from the baseband into a higher frequency range. In a QAM system, the data signal modulates the amplitude of a carrier wave. More specifically, the real component of the data signal is used to modulate an in-phase carrier, while the imaginary component modulates a quadrature carrier. Mathematically, the modulated signal can be expressed as

$$v_c(t) = \mathbf{Re}\left[v_i(t) \sqrt{2} e^{j2\pi f_c t} \right] \; , \tag{2.11}$$

where $\mathbf{Re}[\cdot]$ denotes the real part of $[\cdot]$ and f_c is the carrier frequency. Note that the average transmitted signal power is

$$P_{v_c} = \frac{1}{T_s} \sigma_s^2 \; . \tag{2.12}$$

The resulting signal can be multiplexed with other TV signals that modulate carriers at different frequencies, allowing several different TV signals to be transmitted simultaneously over a single cable.

2.5 Communication Channel

As the modulated signal passes through the cable television network, distortion is introduced. As mentioned earlier, only two types of distortion are considered in this thesis. It

is assumed that the transmitted signal passes through the channel unaffected except for the addition of noise and a single interfering tone. To gain a theoretical understanding of the impact these distortions have, it is necessary to employ mathematical models describing them.

The white noise, denoted by $n_c(t)$, is modelled as a Gaussian random process that has a mean of zero and a flat double-sided noise spectral density of $N_0/2$. This implies that its autocorrelation function is

$$\phi_{n_c}(\tau) \triangleq \mathrm{E}[n_c(t)n_c(t+\tau)] = \frac{N_0}{2}\delta(\tau) \,, \tag{2.13}$$

where $\delta(\cdot)$ is the Dirac delta. Throughout this thesis this type of distortion is referred to as additive white Gaussian noise (AWGN), or merely as noise. It is useful to describe the strength of the noise in terms of the signal-to-noise ratio (SNR). For a M-QAM system with $\log_2 M$ bits per symbol, the SNR per bit is defined as

$$\mathrm{SNR} \triangleq \frac{\sigma_s^2}{N_0 \log_2 M} \,. \tag{2.14}$$

As discussed in the introduction, a single additive sinusoidal tone interferer is characterized by its magnitude, K_{ci}, its bandpass frequency, f_{ci}, and its phase, ϕ_i. It is assumed that none of these parameters vary with time, in that they each maintain a constant albeit unknown value. This distortion is not random, but deterministic. Mathematically, the value of the tone at any time is given by

$$z_c(t) \triangleq K_{ci}\cos(2\pi f_{ci}t + \phi_i) \,, \tag{2.15}$$

where $0 \leq K_{ci} < \infty$, $f_{ci} > 0$, and $0 \leq \phi_i < 2\pi$. The average power of this tone is $P_{z_c} = \frac{1}{2}K_{ci}^2$. A practical measure of the tone's strength is the signal-to-interference ratio (SIR) per bit, which is defined as

$$\mathrm{SIR} \triangleq \frac{P_{v_c}}{P_{z_c}} \cdot \frac{1}{\log_2 M} = \frac{\frac{1}{T_s}\sigma_s^2}{\frac{1}{2}K_{ci}^2} \cdot \frac{1}{\log_2 M} = \frac{2\sigma_s^2}{T_s K_{ci}^2 \log_2 M} \,. \tag{2.16}$$

When the transmitted signal, $v_c(t)$, passes through the cable television network, the two types of distortion are added to it. The signal observed at the received, $r_c(t)$, is the sum of the three independent signals, so

$$r_c(t) = v_c(t) + n_c(t) + z_c(t) \, . \tag{2.17}$$

From $r_c(t)$, the QAM receiver must reproduce the transmitted symbol sequence.

2.6 Demodulation

A block diagram of a typical QAM receiver is shown in Fig. 10. It is composed of three main units: a demodulator, a filter, and a symbol detector. The demodulator converts the received bandpass signal into a baseband one, the filter removes out-of-band noise and further filters the signal, and the symbol detector attempts to determine the transmitted symbol sequence from samples of the filtered signal.

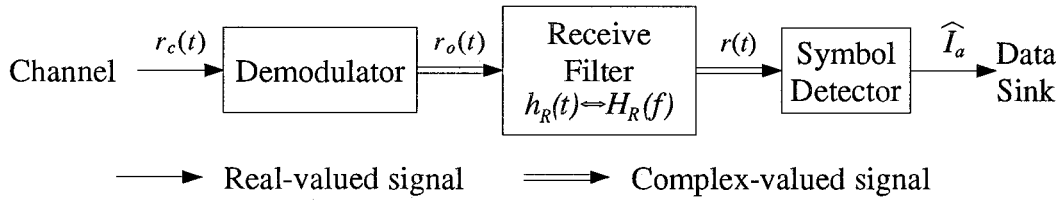

Figure 10. Typical QAM Receiver [24].

2.6.1 Demodulation

The demodulation process shifts the frequency spectrum of the received signal from around the carrier frequency into the baseband. Mathematically, this is accomplished by the operation

$$r_o(t) \triangleq r_c(t) \cdot \sqrt{2} e^{-j2\pi f_c t} \, , \tag{2.18}$$

where $r_c(t)$ is the received bandpass signal and $r_o(t)$ is the resulting baseband signal. The carrier frequency is f_c, and, as signal synchronization is beyond the scope of this thesis, it is assumed that f_c is known at the receiver[2]. This is a requirement for a coherent demodulator.

Since the demodulation operation is linear and the received signal consists of three independent components (the data signal, the noise, and the tone), the demodulated signal also has three independent components. By defining

$$v_o(t) \triangleq v_c(t) \cdot \sqrt{2} e^{-j2\pi f_c t} , \tag{2.19}$$

$$n_o(t) \triangleq n_c(t) \cdot \sqrt{2} e^{-j2\pi f_c t} , \tag{2.20}$$

and

$$z_o(t) \triangleq z_c(t) \cdot \sqrt{2} e^{-j2\pi f_c t} , \tag{2.21}$$

the demodulated signal can be expressed as

$$\begin{aligned} r_o(t) &\triangleq r_c(t) \cdot \sqrt{2} e^{-j2\pi f_c t} \\ &= [v_c(t) + n_c(t) + z_c(t)] \cdot \sqrt{2} e^{-j2\pi f_c t} \\ &= v_o(t) + n_o(t) + z_o(t) , \end{aligned} \tag{2.22}$$

where Eq. (2.17) has been used to substitute for $r_c(t)$. Further analysis of the demodulated components is useful.

Eq. (2.19), the expression for the demodulated data signal component, can be simplified by substituting Eq. (2.11) for $v_c(t)$, yielding

$$\begin{aligned} v_o(t) &\triangleq v_c(t) \cdot \sqrt{2} e^{-j2\pi f_c t} \\ &= \sqrt{2} \mathbf{Re}\left[v_i(t) \sqrt{2} e^{j2\pi f_c t} \right] e^{-j2\pi f_c t} \\ &= v_i(t) + v_i^*(t) e^{-j4\pi f_c t} . \end{aligned} \tag{2.23}$$

[2] There are several suitable methods available for achieving synchronization for the AWGN channel. See, for example, [24, 25].

The effect of demodulation on the noise component of the received signal is best analysed in terms of the mean and the autocorrelation function of $n_o(t)$. The mean is given by

$$\mathbf{E}[n_o(t)] = \mathbf{E}[n_c(t)] \cdot \sqrt{2}e^{-j2\pi f_c t} = 0 \,, \tag{2.24}$$

since $n_c(t)$ is a zero-mean random process, and the autocorrelation function is

$$\begin{aligned}
\phi_{n_o}(\tau) &= \mathbf{E}[n_o^*(t)n_o(t+\tau)] \\
&= \mathbf{E}\left[n_c(t)\sqrt{2}e^{j2\pi f_c t} \cdot n_c(t+\tau)\sqrt{2}e^{-j2\pi f_c(t+\tau)}\right] \\
&= 2\mathbf{E}[n_c(t)n_c(t+\tau)]e^{-j2\pi f_c \tau} \\
&= 2\phi_{n_c}(\tau)e^{-j2\pi f_c \tau} \,.
\end{aligned} \tag{2.25}$$

Substitution Eq. (2.13) for $\phi_{n_c}(\tau)$ yields

$$\begin{aligned}
\phi_{n_o}(\tau) &= 2\tfrac{N_0}{2}\delta(\tau)e^{-j2\pi f_c \tau} \\
&= N_0\delta(\tau) \,.
\end{aligned} \tag{2.26}$$

Since $n_o(t)$ is merely a scalar multiple of $n_c(t)$, it is also a Gaussian random process [26].

By substitution Eq. (2.15) for $z_c(t)$, the demodulated tone component can be expressed as

$$\begin{aligned}
z_o(t) &\triangleq z_c(t) \cdot \sqrt{2}e^{-j2\pi f_c t} \\
&= \sqrt{2}K_{ci}\cos(2\pi f_{ci}t + \phi_i)e^{-j2\pi f_c t} \\
&= \tfrac{\sqrt{2}}{2}K_{ci}\left[e^{j(2\pi f_{ci}t+\phi_i)} + e^{-j(2\pi f_{ci}t+\phi_i)}\right]e^{-j2\pi f_c t} \\
&= \tfrac{\sqrt{2}}{2}K_{ci}e^{j2\pi(f_{ci}-f_c)t}e^{j\phi_i} + \tfrac{\sqrt{2}}{2}K_{ci}e^{-j2\pi(f_{ci}+f_c)t}e^{-j\phi_i} \\
&= \tfrac{\sqrt{2}}{2}K_{ci}e^{j2\pi f_i t}e^{j\phi_i} + \tfrac{\sqrt{2}}{2}K_{ci}e^{-j2\pi(2f_c+f_i)t}e^{-j\phi_i} \,,
\end{aligned} \tag{2.27}$$

where $f_i \triangleq f_{ci} - f_c$ is the relative frequency of the tone in relationship to the carrier.

2.6.2 Receive Filter

After the received signal has been demodulated, it is passed through the receive filter, which has an impulse response of $h_R(t)$. The purpose of this filter is to remove signals falling outside the bandwidth of the transmitted signal, to remove the high frequency components of $v_o(t)$ and $z_o(t)$, and to reduce the power of the noise signal, without introducing ISI. The output of the filter is defined as

$$\begin{aligned} r(t) &\triangleq r_o(t) \circledast h_R(t) \\ &= [v_o(t) + n_o(t) + z_o(t)] \circledast h_R(t) \\ &= v_o(t) \circledast h_R(t) + n_o(t) \circledast h_R(t) + z_o(t) \circledast h_R(t) \\ &= v(t) + n(t) + z(t) \,. \end{aligned} \tag{2.28}$$

Clearly, the lowpass received signal consists of three components: $v(t) \triangleq v_o(t) \circledast h_R(t)$, the filtered data signal; $n(t) \triangleq n_o(t) \circledast h_R(t)$, the filtered noise signal; and $z(t) \triangleq z_o(t) \circledast h_R(t)$, the filtered tone. Analysis of these three signal components is straightforward.

The filtered data signal can be expressed in terms of the transmitted symbol sequence by substituting Eq. (2.23) for $v_o(t)$, so that

$$\begin{aligned} v(t) &= v_o(t) \circledast h_R(t) \\ &= \left[v_i(t) + v_i^*(t)e^{-j4\pi f_c t}\right] \circledast h_R(t) \\ &= v_i(t) \circledast h_R(t) + \left[v_i^*(t)e^{-j4\pi f_c t}\right] \circledast h_R(t) \,. \end{aligned} \tag{2.29}$$

Converting this to the frequency domain with the use of a Fourier transform yields

$$V(f) = V_i(f)H_R(f) + V_i^*(-f - 2f_c)H_R(f) \,. \tag{2.30}$$

where $H_R(f)$ is the frequency response of the receive filter, and $V_i(f)$ is given by

$$V_i(f) = \int_{-\infty}^{\infty} v_i(t)e^{-j2\pi ft}dt$$

$$= \int_{-\infty}^{\infty} \sum_{a=-\infty}^{\infty} I_a h_T(t - aT_s) e^{-j2\pi ft} dt$$
$$= \sum_{a=-\infty}^{\infty} I_a \int_{-\infty}^{\infty} h_T(t) e^{-j2\pi f(t+aT_s)} dt$$
$$= \sum_{a=-\infty}^{\infty} I_a H_T(f) e^{-j2\pi faT_s} . \tag{2.31}$$

Since one of the requirements of the transmit filter is that it is band limited, $H_T(f) \equiv 0$ for $f \geq 1/T_s$ (given $\alpha < 1$). Therefore $V_i(f) \equiv 0$ for $f \geq 1/T_s$. Furthermore, since the receive filter is matched to the transmit filter, $H_R(f)$ is also equal to zero for $f \geq 1/T_s$. Since $2f_c \gg 1/T_s$, the range of f for which $V_i^*(-f - f_c)$ is non-zero does not coincide with the range of f for which $H_R(f)$ is non-zero. As a result, the second term in Eq. (2.30) can be discarded, leaving

$$V(f) = V_i(f) H_R(f)$$
$$= \sum_{a=-\infty}^{\infty} I_a H_T(f) H_R(f) e^{-j2\pi faT_s} . \tag{2.32}$$

By substituting $H(f) = H_T(f) H_R(f)$ as the combined frequency response of the two filters, this becomes

$$V(f) = \sum_{a=-\infty}^{\infty} I_a H(f) e^{-j2\pi faT_s} , \tag{2.33}$$

and the inverse Fourier transform is

$$v(t) = \int_{-\infty}^{\infty} V(f) e^{j2\pi ft} dt$$
$$= \sum_{a=-\infty}^{\infty} I_a \int_{-\infty}^{\infty} H(f) e^{j2\pi f(t-aT_s)} df$$
$$= \sum_{a=-\infty}^{\infty} I_a h(t - aT_s) , \tag{2.34}$$

where $h(t)$ is the combined impulse response of the two filters.

Since the demodulated noise signal is Gaussian and the operation of the receiver filter is linear, the filtered noise signal is also Gaussian. Its mean is

$$\begin{aligned}\mathbf{E}[n(t)] &= \mathbf{E}[n_o(t)] \circledast h_R(t) \\ &= 0 \,, \end{aligned} \tag{2.35}$$

and its autocorrelation function is

$$\begin{aligned}\phi_N(\tau) &\triangleq \mathbf{E}[n^*(t)n(t+\tau)] \\ &= \mathbf{E}[\{n_o^*(t) \circledast h_R^*(t)\} \cdot \{n_o(t+\tau) \circledast h_R(t+\tau)\}] \\ &= \mathbf{E}\left[\int_{-\infty}^{\infty} n_o^*(\alpha)h_R^*(t-\alpha)d\alpha \cdot \int_{-\infty}^{\infty} n_o(\beta)h_R(t+\tau-\beta)d\beta\right] \\ &= \int_{-\infty}^{\infty}\int_{-\infty}^{\infty} \mathbf{E}[n_o^*(\alpha)n_o(\beta)]h_R^*(t-\alpha)h_R(t+\tau-\beta)d\beta d\alpha \\ &= \int_{-\infty}^{\infty}\int_{-\infty}^{\infty} \phi_{n_o}(\beta-\alpha)h_R^*(t-\alpha)h_R(t+\tau-\beta)d\beta d\alpha \,. \end{aligned} \tag{2.36}$$

Substituting Eq. (2.26) for $\phi_{n_o}(\tau)$ yields

$$\begin{aligned}\phi_N(\tau) &= \int_{-\infty}^{\infty}\int_{-\infty}^{\infty} N_0\delta(\beta-\alpha)h_R^*(t-\alpha)h_R(t+\tau-\beta)d\beta d\alpha \\ &= N_0\int_{-\infty}^{\infty} h_R^*(t-\alpha)h_R(t+\tau-\alpha)d\alpha \\ &= N_0\int_{-\infty}^{\infty} h_R^*(-\beta)h_R(\tau-\beta)d\beta \\ &= N_0\int_{-\infty}^{\infty} h_T(\beta)h_R(\tau-\beta)d\beta \\ &= N_0 h(\tau) \,. \end{aligned} \tag{2.37}$$

In summary, $n(t)$ is a complex-valued Gaussian random process, with a mean of zero and an autocorrelation of $N_0h(\tau)$.

The final term to analyse is for the filtered tone interference. By following a procedure similar to the one used in the analysis of the data signal, a simple expression for $z(t)$ can

be found. Clearly, from Eq. (2.27),

$$\begin{aligned} z(t) &\triangleq z_o(t) \circledast h_R(t) \\ &= \left[\frac{\sqrt{2}}{2}K_{ci}e^{j2\pi f_i t}e^{j\phi_i} + \frac{\sqrt{2}}{2}K_{ci}e^{-j2\pi(2f_c+f_i)t}e^{-j\phi_i}\right] \circledast h_R(t) \,. \end{aligned} \tag{2.38}$$

Its Fourier transform is

$$\begin{aligned} Z(f) &= \left[\frac{\sqrt{2}}{2}K_{ci}\delta(f-f_i)e^{j\phi_i} + \frac{\sqrt{2}}{2}K_{ci}\delta(f+2f_c+f_i)e^{-j\phi_i}\right] H_R(f) \\ &= \frac{\sqrt{2}}{2}K_{ci}H_R(f_i)\delta(f-f_i)e^{j\phi_i} + \frac{\sqrt{2}}{2}K_{ci}H_R(-2f_c-f_i)\delta(f+2f_c+f_i)e^{-j\phi_i} \,. \end{aligned} \tag{2.39}$$

Note that

$$2f_c + f_i = 2f_c + f_{ci} - f_c = f_c + f_{ci} \,. \tag{2.40}$$

Because f_{ci} is defined to be positive, $f_c + f_{ci} \gg 1/T_s$, so $H_R(-2f_c - f_i) = 0$ since the receive filter is band limited. As a result, the second term in Eq. (2.39) is equal to zero. The inverse Fourier transform yields

$$\begin{aligned} z(t) &= \int_{-\infty}^{\infty} \frac{\sqrt{2}}{2}K_{ci}H_R(f_i)\delta(f-f_i)e^{j\phi_i}e^{j2\pi ft}df \\ &= \frac{\sqrt{2}}{2}K_{ci}H_R(f_i)e^{j2\pi f_i t}e^{j\phi_i} \,. \end{aligned} \tag{2.41}$$

It is convenient to define $K_i = \frac{\sqrt{2}}{2}K_{ci}H_R(f_i)$ as the magnitude of the filtered tone, so that

$$z(t) = K_i e^{j2\pi f_i t}e^{j\phi_i} \,. \tag{2.42}$$

The signal-to-interference ratio, expressed in terms of K_i, is (from Eq. 2.16)

$$\begin{aligned} \text{SIR} &= \frac{2\sigma_s^2}{T_s K_{ci}^2 \log_2 M} \\ &= \frac{2\sigma_s^2}{T_s 2K_i^2/H_R^2(f_i)\log_2 M} \\ &= \frac{\sigma_s^2 H_R^2(f_i)}{K_i^2 T_s \log_2 M} \,. \end{aligned} \tag{2.43}$$

Eq. (2.42) is the mathematical model that shall be used to represent the tone interference throughout the remainder of this thesis. When the tone signal falls within the bandwidth of the data signal (that is, $|f_i| < (1+\alpha)/2T_s$), it distorts the transmitted data signal, possibly introducing errors when an attempt is made to determine the transmitted symbol sequence.

2.6.3 Signal Power Spectral Density

A useful means of describing the received signal is its power spectral density (PSD). This can be found by considering the components of $r(t)$ separately, and then combining the results.

For the data component, it is useful to model $v(t)$ by a random process. It has a mean of

$$\mathbf{E}[v(t)] = \sum_{a=-\infty}^{\infty} \mathbf{E}[I_a] h(t - aT_s) = 0 \,, \tag{2.44}$$

and an autocorrelation function given by

$$\begin{aligned} \phi_V(t;\tau) &\triangleq \mathbf{E}[v^*(t)v(t+\tau)] \\ &= \sum_{a=-\infty}^{\infty} \sum_{b=-\infty}^{\infty} \mathbf{E}[I_a^* I_b] h^*(t - aT_s) h(t + \tau - bT_s) \,. \end{aligned} \tag{2.45}$$

Substituting Eq. (2.2) for $\mathbf{E}[I_a^* I_b]$ yields

$$\begin{aligned} \phi_V(t;\tau) &= \sum_{a=-\infty}^{\infty} \sum_{b=-\infty}^{\infty} \sigma_s^2 \delta(b-a) h^*(t - aT_s) h(t + \tau - bT_s) \\ &= \sigma_s^2 \sum_{a=-\infty}^{\infty} h^*(t - aT_s) h(t + \tau - aT_s) \\ &= \sigma_s^2 \sum_{a=-\infty}^{\infty} \int_{-\infty}^{\infty} H^*(\alpha) e^{-j2\pi\alpha(t-aT_s)} d\alpha \int_{-\infty}^{\infty} H(\beta) e^{j2\pi\beta(t+\tau-aT_s)} d\beta \\ &= \sigma_s^2 \int_{-\infty}^{\infty} \int_{-\infty}^{\infty} H^*(\alpha) H(\beta) e^{-j2\pi\alpha t} e^{j2\pi\beta(t+\tau)} \sum_{a=-\infty}^{\infty} e^{-j2\pi(\beta-\alpha)aT_s} d\beta d\alpha \\ &= \sigma_s^2 \int_{-\infty}^{\infty} \int_{-\infty}^{\infty} H^*(\alpha) H(\beta) e^{j2\pi(\beta-\alpha)t} e^{j2\pi\beta\tau} \frac{1}{T_s} \sum_{a=-\infty}^{\infty} \delta\left(\beta - \alpha - \frac{a}{T_s}\right) d\beta d\alpha \\ &= \sigma_s^2 \frac{1}{T_s} \sum_{a=-\infty}^{\infty} \int_{-\infty}^{\infty} H^*(\alpha) H\left(\alpha + \frac{a}{T_s}\right) e^{j2\pi\frac{at}{T_s}} e^{j2\pi\left(\alpha+\frac{a}{T_s}\right)\tau} d\alpha \,. \end{aligned} \tag{2.46}$$

Since this function is periodic with respect to t, $v(t)$ is a cyclostationary random process, with a period of T_s. To remove the time dependence, it is convenient to compute the time-average autocorrelation function by integrating over a single period. Thus

$$\begin{aligned}
\overline{\phi}_V(\tau) &\triangleq \frac{1}{T_s}\int_{-\frac{T_s}{2}}^{\frac{T_s}{2}} \phi_V(t;\tau)dt \\
&= \sigma_s^2 \frac{1}{T_s}\sum_{a=-\infty}^{\infty}\int_{-\infty}^{\infty} H^*(\alpha)H\left(\alpha+\frac{a}{T_s}\right)\frac{1}{T_s}\int_{-\frac{T_s}{2}}^{\frac{T_s}{2}} e^{j2\pi\frac{at}{T_s}}dt e^{j2\pi\left(\alpha+\frac{a}{T_s}\right)\tau}d\alpha \\
&= \sigma_s^2 \frac{1}{T_s}\sum_{a=-\infty}^{\infty}\int_{-\infty}^{\infty} H^*(\alpha)H\left(\alpha+\frac{a}{T_s}\right)\frac{\sin\pi a}{\pi a}e^{j2\pi\left(\alpha+\frac{a}{T_s}\right)\tau}d\alpha \\
&= \sigma_s^2 \frac{1}{T_s}\sum_{a=-\infty}^{\infty}\int_{-\infty}^{\infty} H^*(\alpha)H\left(\alpha+\frac{a}{T_s}\right)\delta(a)e^{j2\pi\left(\alpha+\frac{a}{T_s}\right)\tau}d\alpha \\
&= \sigma_s^2 \frac{1}{T_s}\int_{-\infty}^{\infty} H^*(\alpha)H(\alpha)e^{j2\pi\alpha\tau}d\alpha\ . \qquad (2.47)
\end{aligned}$$

The average power spectral density of the data component can be found by taking the Fourier transform of $\overline{\phi}_V(\tau)$. Therefore,

$$\begin{aligned}
\bar{\Phi}_V(f) &\triangleq \int_{-\infty}^{\infty}\overline{\phi}_V(\tau)e^{-j2\pi f\tau}d\tau \\
&= \sigma_s^2\frac{1}{T_s}\int_{-\infty}^{\infty} H^*(\alpha)H(\alpha)\int_{-\infty}^{\infty} e^{j2\pi(\alpha-f)\tau}d\tau d\alpha \\
&= \sigma_s^2\frac{1}{T_s}\int_{-\infty}^{\infty} H^*(\alpha)H(\alpha)\delta(\alpha-f)d\alpha \\
&= \sigma_s^2\frac{1}{T_s}|H(f)|^2\ . \qquad (2.48)
\end{aligned}$$

The PSD of the noise component, determined directly from the autocorrelation function given by Eq. (2.37), is

$$\begin{aligned}
\Phi_N(f) &\triangleq \int_{-\infty}^{\infty}\phi_N(\tau)e^{-j2\pi f\tau}d\tau \\
&= \int_{-\infty}^{\infty} N_0 h(\tau)e^{-j2\pi f\tau}d\tau \\
&= N_0\int_{-\infty}^{\infty}\int_{-\infty}^{\infty} H(\beta)e^{j2\pi\beta\tau}d\beta e^{-j2\pi f\tau}d\tau \\
&= N_0\int_{-\infty}^{\infty} H(\beta)\int_{-\infty}^{\infty} e^{j2\pi(\beta-f)\tau}d\tau d\beta
\end{aligned}$$

$$= N_0 \int_{-\infty}^{\infty} H(\beta)\delta(\beta - f)d\beta$$
$$= N_0 |H_R(f)|^2 \,. \tag{2.49}$$

Since the interfering tone is deterministic and periodic, its PSD must be found from its Fourier series representation. Clearly

$$\Phi_Z(f) = K_i^2 \delta(f - f_i) \,. \tag{2.50}$$

Since the tone is a deterministic signal it doesn't have an autocorrelation function. Nonetheless, it is useful to define the function

$$\begin{aligned}\phi_Z(\tau) &\triangleq z^*(t)z(t+\tau) \\ &= K_i e^{-j2\pi f_i t} e^{-j\phi_i} K_i e^{j2\pi f_i (t+\tau)} e^{j\phi_i} \\ &= K_i^2 e^{j2\pi f_i \tau} \,. \end{aligned} \tag{2.51}$$

Note that the Fourier transform of this functions is

$$\begin{aligned}\mathcal{F}\{\phi_Z(\tau)\} &= \int_{-\infty}^{\infty} \phi_Z(\tau) e^{-j2\pi f\tau} d\tau \\ &= \int_{-\infty}^{\infty} K_i^2 e^{j2\pi f_i \tau} e^{-j2\pi f\tau} d\tau \\ &= K_i^2 \delta(f - f_i) \\ &= \Phi_Z(f) \,. \end{aligned} \tag{2.52}$$

Clearly $\phi_Z(\tau)$ can be used in a manner similar to the autocorrelation functions of the data and noise signals.

Since $v(t)$ and $n(t)$ have zero mean and are statistically independent, the autocorrelation function for the received signal can be expressed as

$$\phi_R(t;\tau) \triangleq \mathbf{E}[r^*(t)r(t+\tau)]$$

$$
\begin{aligned}
&= \mathbf{E}[\{v^*(t) + n^*(t) + z^*(t)\} \cdot \{v(t+\tau) + n(t+\tau) + z(t+\tau)\}] \\
&= \mathbf{E}[v^*(t)v(t+\tau)] + \mathbf{E}[v^*(t)]\mathbf{E}[n(t+\tau)] + \mathbf{E}[v^*(t)]z(t+\tau) \\
&\quad + \mathbf{E}[n^*(t)]\mathbf{E}[v(t+\tau)] + \mathbf{E}[n^*(t)n(t+\tau)] + \mathbf{E}[n^*(t)]z(t+\tau) \\
&\quad + z^*(t)\mathbf{E}[v(t+\tau)] + z^*(t)\mathbf{E}[n(t+\tau)] + z^*(t)z(t+\tau) \\
&= \mathbf{E}[v^*(t)v(t+\tau)] + \mathbf{E}[n^*(t)n(t+\tau)] + z^*(t)z(t+\tau) \\
&= \phi_V(t;\tau) + \phi_N(\tau) + \phi_Z(\tau) \, . \qquad (2.53)
\end{aligned}
$$

Since this is periodic, the average autocorrelation must be found.

$$
\begin{aligned}
\overline{\phi}_R(\tau) &\triangleq \frac{1}{T_s} \int_{-\frac{T_s}{2}}^{\frac{T_s}{2}} \phi_R(t;\tau) dt \\
&= \overline{\phi}_V(\tau) + \phi_N(\tau) + \phi_Z(\tau) \, . \qquad (2.54)
\end{aligned}
$$

The average PSD can then be computed as

$$
\begin{aligned}
\bar{\Phi}_R(f) &\triangleq \int_{-\infty}^{\infty} \overline{\phi}_R(\tau) e^{-j2\pi f\tau} d\tau \\
&= \int_{-\infty}^{\infty} \overline{\phi}_V(\tau) e^{-j2\pi f\tau} d\tau + \int_{-\infty}^{\infty} \phi_N(\tau) e^{-j2\pi f\tau} d\tau + \int_{-\infty}^{\infty} \phi_Z(\tau) e^{-j2\pi f\tau} d\tau \\
&= \bar{\Phi}_V(f) + \Phi_N(f) + \Phi_Z(f) \\
&= \sigma_s^2 \tfrac{1}{T_s} |H(f)|^2 + N_0 |H_R(f)|^2 + K_i^2 \delta(f - f_i) \, . \qquad (2.55)
\end{aligned}
$$

As expected, the PSD of the received signal is characterized by an impulse occurring at the frequency of the interfering tone. This property is exploited in the next chapter, where a method for removing the tone from the received signal is presented.

2.6.4 Symbol Detection

Once the received signal has been filtered, the symbol detector attempts to determine the transmitted data symbols. This is accomplished with the use of samples of the received signal. As with the carrier synchronization in Section 2.6.1, it is assumed in this thesis that

perfect symbol synchronization is achieved, so that samples can be collected at the symbol rate, $1/T_s$, and at the precise symbol sampling instants. Let R_a denote the value of the equivalent lowpass received signal at time $t = aT_s$ so that

$$\begin{aligned} R_a &\triangleq r(aT_s) \\ &= v(aT_s) + z(aT_s) + n(aT_s) \ . \end{aligned} \tag{2.56}$$

Therefore R_a is the value of sample a, and is a result of the addition of three independent terms.

The first term, $v(aT_s)$, is due to the transmitted signal and can be evaluated with Eq. (2.34) as

$$v(aT_s) = \sum_{c=-\infty}^{\infty} I_c h(aT_s - cT_s) \ . \tag{2.57}$$

Since the root-raised cosine transmit and receive filters are designed to cause no intersymbol interference (see Eq. (2.6)), $h(nT_s) = \delta(n)$. As a result,

$$v(aT_s) = \sum_{c=-\infty}^{\infty} I_c \delta(a - c) = I_a \ , \tag{2.58}$$

the value of the symbol transmitted at $t = aT_s$.

The second term in Eq. (2.56) is caused by the additive noise introduced in the communication channel. By defining

$$N_a \triangleq n(aT_s) \tag{2.59}$$

and noting that

$$\mathbf{E}[N_a] = \mathbf{E}[n(aT_s)] = 0, \tag{2.60}$$

and

$$\begin{aligned} \mathbf{E}[N_a^* N_b] &= \mathbf{E}[n^*(aT_s)n(bT_s)] = \phi_N(bT_s - aT_s) \\ &= N_0 \delta(b - a) \ , \end{aligned} \tag{2.61}$$

it is possible to describe this term as a complex-valued discrete-time Gaussian random process with a mean of zero and a variance of N_0. Note that different samples are uncorrelated.

The third term in Eq. (2.56) is results from the presence of the tone interference added in the channel, and can be expressed as

$$\begin{aligned} Z_a &\triangleq z(aT_s) \\ &= K_i e^{j2\pi f_i a T_s} e^{j\phi_i} . \end{aligned} \tag{2.62}$$

This is dependent on three constant but unknown parameters, K_i, f_i, and ϕ_i, which completely describe the tone interference.

Each received sample can be expressed as $R_a = I_a + N_a + Z_a$, where I_a is the transmitted symbol, N_a reflects distortion due to additive white Gaussian noise, and Z_a is the distortion due to the interfering tone. The set of samples $\{R_a\}$ is all that is available to the decision device. From these decision variables the decision device attempts to determine the transmitted symbol sequence, $\{I_a\}$. For each sample, the detected symbol, $\widehat{I}_a$, is the point in the QAM signal constellation, $\mathcal{S}$, that is closest to R_a. That is, the decision device selects $\widehat{I}_a = S_i$ if and only if

$$|S_i - R_a| < |S_j - R_a| \tag{2.63}$$

for all $S_i, S_j \in \mathcal{S}$. This selection is the symbol most likely to have been transmitted at $t = aT_s$, given R_a.

If the noise and interference terms are sufficiently small, $\widehat{I}_a = I_a$ and no detection error occurs. On the other hand, if either of these terms is large, an incorrect decision may be made, resulting in a detection error. The probability of a detection error depends on the separation between adjacent symbols in the signal constellation, the magnitude of the tone interference, and the average power of the noise samples. Since the additive noise is random, a high noise

power implies a high likelihood that the noise term will be large for each sample, resulting in a correspondingly high probability of detection error. This differs slightly from the effect the tone has. A strong tone implies that the tone term is large for all samples, so its effect on the probability of error is much more drastic.

Fig. 11 shows a state-space diagram for the received signal when a 16–QAM system is used. Each point represents the received in-phase and quadrature values for a single sample. A total of 8192 samples were used to generate this plot, when noise with a SNR of 35 dB and a tone with a SIR of 35 dB corrupt the transmitted symbols. By comparing this diagram with the signal constellation shown in Fig. 8, it is evident that the received samples tend to fall in clusters around the symbol points in the signal constellation. Because both the noise and tone are weak, transmission errors are unlikely to occur. When the noise is stronger, however, the points in the state-space diagram become more dispersed. This is shown in Fig. 12 when the SNR is 10 dB. Although the samples still occur in clusters, the clusters are much wider, resulting in a greater likelihood of detection error. The effect of a large tone is significantly different, as indicated in Fig. 13, when the SIR = 10 dB and the SNR = 35 dB. Note that the samples fall in rings around the symbol points. When the noise is weak, as in this example, it is still possible to determine the transmitted symbols with a high likelihood of success. However, if the noise is also large, detection errors become very probable. Fig. 14 shows the state-space diagram when SNR = 10 dB and SIR = 10 dB. The samples no longer appear in clusters or rings, but are spread throughout the state-space.

Although a convenient closed form expression for the probability of a symbol detection error in terms of the noise power and tone parameters is not readily available, the probability of error can be calculated numerically by using the computer program listed in Appendix D. Fig. 15 contains a plot of the probability of symbol detection error (P_ϵ) vs. SNR for various

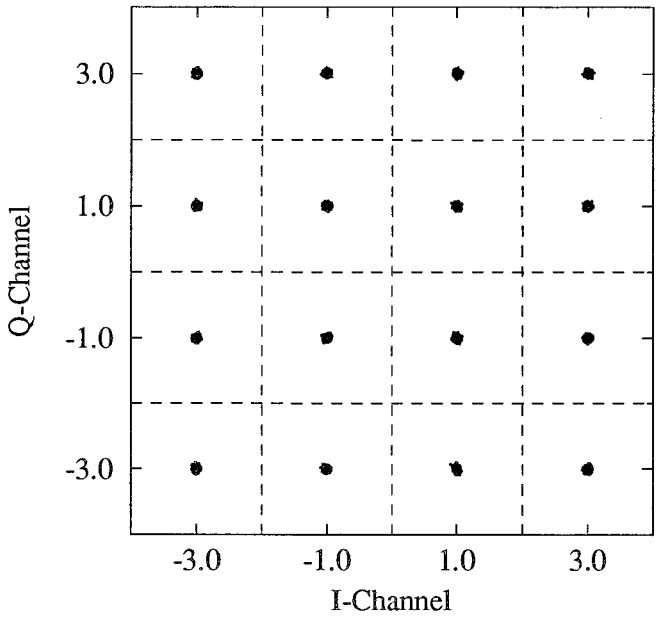

Figure 11. 16–QAM State-space Diagram. SNR = 35 dB, SIR = 35 dB.

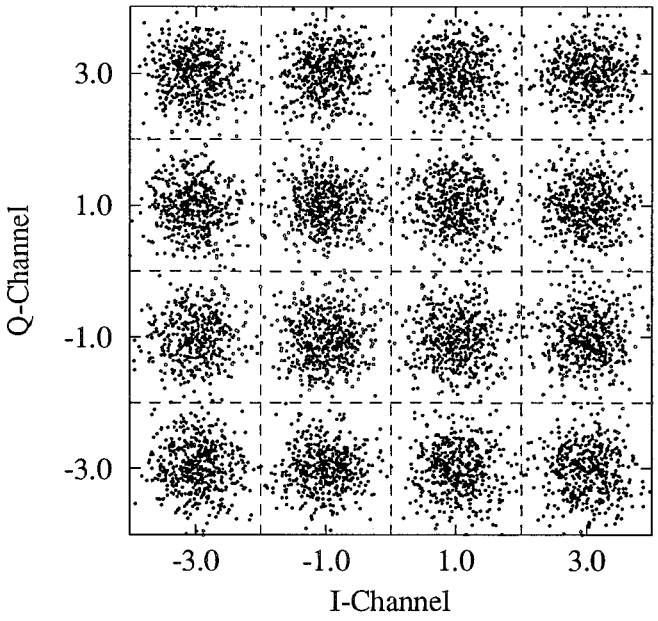

Figure 12. 16–QAM State-space Diagram. SNR = 10 dB, SIR = 35 dB.

SIRs when 16–QAM is used. In general, increasing the SNR decreases P_ϵ[3]. The exception to this occurs when the SIR is very small. In this case the SNR has no effect, and almost

[3] Note that these results are only exact for the cases in which the frequency of the tone is an irrational number. When the frequency is rational, the results will vary slightly, but not signficantly for the purposes of the graph.

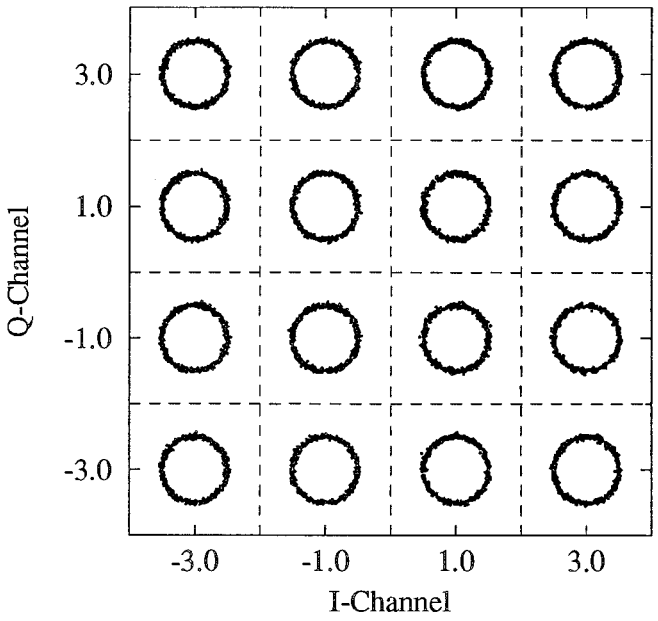

Figure 13. 16–QAM State-space Diagram. SNR = 35 dB, SIR = 10 dB.

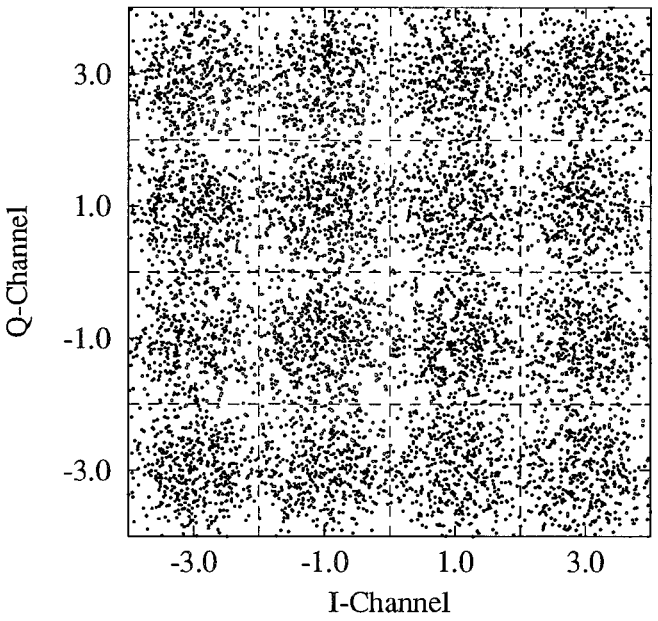

Figure 14. 16–QAM State-space Diagram. SNR = 10 dB, SIR = 10 dB.

all symbols are detected incorrectly. The serious effect the tone has on the probability of error is obvious.

Referring back to Fig. 10, after selecting $\widehat{I}_a$ as the detected symbol, the M-QAM receiver converts it into the $\log_2 M$ bit pattern associated with the symbol. These bits are emitted in

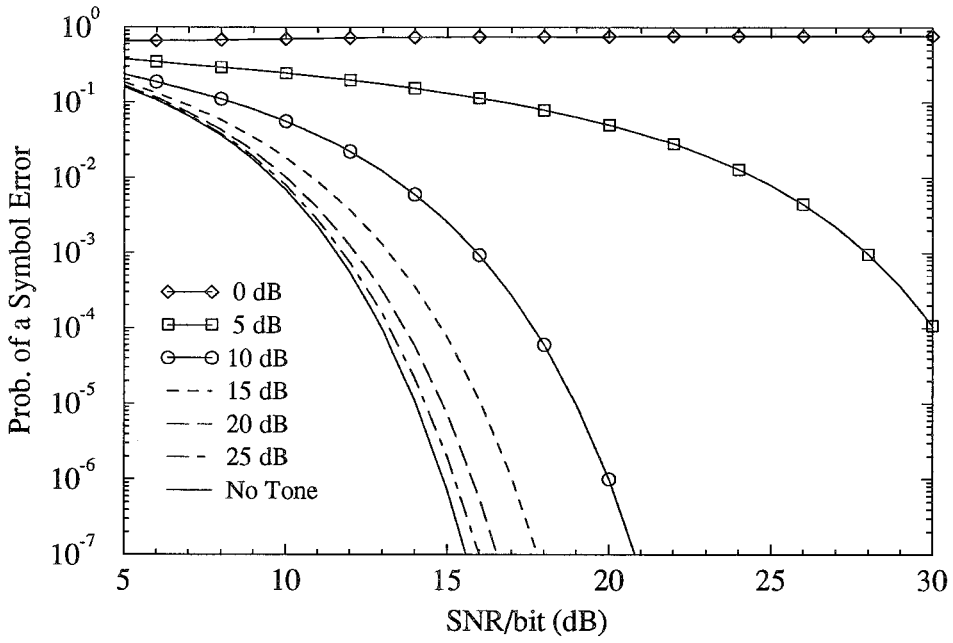

Figure 15. Probability of Symbol Detection Error.

sequence with the bits from the other detected symbols, producing a binary data stream. This data stream should be identical to the one produced by the channel encoder in the transmitter. Because errors can occur during transmission, some of the bits may be in error, so the data stream is passed to the channel decoder. If the error rate is low, the error correcting ability of the channel decoder will prevent visible distortion. Furthermore, the effect of uncorrected errors will be concealed by the source coder.

When there is no interfering tone it is known from the results of field testing performed by the FCC Advisory Committee that the DigiCipher system cannot operate reliably when the SNR is less than about 6.5 dB [3]. Performance for the other proposals is similar. Since maintaining signal levels above this point is not difficult in CATV networks, reliable digital image transmission is possible. However, if a strong interfering tone distorts the signal, image degradation may occur. For example, if a tone with a SIR of 10 dB is present, the SNR must be greater than about 9 dB for impairment-free transmission. If the SIR is 5 dB the SNR must exceed 18 dB to prevent excessive transmission errors. Clearly the increased

probability of error associated with a strong tone adversely affects performance to the point where preventative measures need to be taken.

2.7 Conclusion

In this chapter the all-digital transmission of HDTV signals was investigated. The powerful digital compression algorithms of the proposed systems are capable of reducing the large amount of information associated with the high resolution, wide aspect ratio, HDTV signals sufficiently to allow transmission over the 6 MHz channels currently used by traditional NTSC signals. To protect the fragile compressed data from the ravages of transmission errors, strong error correcting codes are employed. Provided that the transmitted signal power is sufficiently high, errors introduced from AWGN and an interfering tone arising from the communication channel can be effectively eliminated. Transmission of HDTV signals over existing cable TV networks is definitely feasible.

Unfortunately, the presence of a strong interfering tone has a dramatic effect on transmission errors, and complete collapse of the error correcting ability of the channel coder is possible. While increasing signal power will ensure the integrity of the transmitted HDTV signals, it is not an ideal solution. In the next chapter a robust method for cancelling tone interference is proposed, allowing reliable data transmission even in the presence of strong tone interference.

Chapter Three

A Novel Tone Interference Canceller

3.1 Introduction

As noted in the previous chapter, distortion introduced in the communication channel may lead to transmission errors. If too many errors occur, the channel decoder will not be able to correct them, leading to image and sound quality degradation. Under severe interference conditions, the receiver will be unable to present even a vague facsimile of the desired television signal. Distortion in the form of a strong tone falling within the band of the desired signal significantly increases the likelihood of transmission errors. In a traditional QAM receiver, samples of the received signal are used directly as decision variables to determine the transmitted symbols. Unfortunately, an interfering tone added in the communication channel will distort the samples, possibly preventing correct symbol detection. To alleviate this problem it is desirable to use a decision variable that has the effect of the tone removed or at least significantly reduced.

In this chapter a novel method is proposed for removing such a tone from the received signal. This proposed system is designed to operate in conjunction with QAM digital signals. In Section 3.2 of this chapter a method of estimating the effect of the tone on each of the received samples is developed. For successful operation, the frequency of the tone must be determined. A method for achieving this is proposed in Section 3.3. This chapter concludes with a summary of the proposed interference canceller in Section 3.4.

3.2 Tone Interference Estimation

Ideally, the frequency, magnitude and phase of the interfering tone would be known, allowing the receiver to calculate the effect of the tone on each decision variable by using Eq. (2.62). That is:

$$Z_a = K_i e^{j2\pi f_i a T_s} e^{j\phi_i} \ . \tag{3.1}$$

A new decision variable could be generated by subtracting Z_a from each received sample. The new decision variable, R'_a, would equal

$$\begin{aligned} R'_a &= R_a - Z_a \\ &= I_a + N_a + Z_a - Z_a \\ &= I_a + N_a \ , \end{aligned} \tag{3.2}$$

and would allow the decision device to determine the transmitted symbol more accurately. The interfering tone would no longer have any effect.

Unfortunately, the parameters of the interfering tone are generally not known at the receiver, so Z_a can not be calculated explicitly. Instead, an estimate, $\widehat{Z}_a$, of the effect of the tone must be used. In this case the new decision variable is

$$R'_a \triangleq R_a - \widehat{Z}_a$$

$$= I_a + N_a + Z_a - \widehat{Z}_a$$

$$= I_a + N_a + \varepsilon_a \ , \tag{3.3}$$

where $\varepsilon_a \triangleq Z_a - \widehat{Z}_a$ is the residue remaining when an imprecise estimator is used. If the residue is small, the decision device is more likely to correctly determine the transmitted symbol than if no attempt is made to remove the interference. Ideally, an estimator that minimizes the probability of error would be used, ensuring the greatest possible reliability of the data. Unfortunately, the non-linear nature of the probability of error make this type of estimator impractical [27]. In practice, estimators that minimize the mean of the square of the error (MSE) between the estimate and the desired value are used instead. This type of estimator, known as the minimum mean-square error (MMSE) estimator [27] is nonetheless capable of effective tone cancellation.

The MMSE estimator is the one that minimizes the average residual power. Clearly, the residue is an important measure of the accuracy of the estimator. It is convenient to measure the residue in a manner analogous to the SIR. The signal-to-residue ratio (SRR) is defined as the ratio of the average signal power (per bit) to the average residual power, so

$$\text{SRR} \triangleq \frac{\sigma_s^2/T_s}{\gamma \log_2 M} \ , \tag{3.4}$$

where

$$\gamma = \mathbf{E}\left[|\varepsilon_a|^2\right] \tag{3.5}$$

is the average residual power. To reduce the likelihood of a transmission error it is necessary to find an estimator for Z_a that results in a high SRR

To successfully cancel the interfering tone, accurate estimates of the tone at each sampling instant is required. These estimates must be generated only from observations of the received signal. Although there are numerous methods for finding estimates, it is important to use one that is both simple and accurate.

3.2.1 Linear MMSE Estimator

The problem with using true MMSE estimators is that they are generally infeasible. Even if the form of the MMSE estimator could be found mathematically, it would likely be extremely difficult to implement. In practice, some limitations on the estimator must be made. To maintain simplicity, a estimator should rely only on discrete samples of the received signal and not on the entire analogue continuous-time signal. In addition, it is convenient to use only samples collected at the symbol sampling instants. Therefore, an estimator of Z_a should be based only on the samples $\{R_{a-n} | \forall\, n \in \mathbf{I}\}$. For reasons to be discussed in Subsection 3.2.3, it is further required that n be greater than or equal to one. Another requirement of simplicity is that the samples be combined in a linear fashion to produce the estimates. A linear estimator of Z_a takes the form

$$\widehat{Z}_a = \sum_{n=1}^{L} \mathrm{w}_n R_{a-n} \ , \tag{3.6}$$

where L is the number of samples used and $\{\mathrm{w}_n\}$ are weight coefficients for the samples. Thus $\widehat{Z}_a$, as generated by Eq. (3.6), is essentially a weighted average of L samples of the received signal. By carefully selecting the weights it is possible to control the accuracy of the estimates.

As noted earlier, it is desirable to find an estimator that maximizes the SRR. Given that it is also necessary to stick to the simple linear estimates of the form given by Eq. (3.6), it is desirable to use the linear minimum mean-square error estimator. Thus, it is necessary to find the weights $\{\mathrm{w}_n\}$ which minimize

$$\gamma = \mathbf{E}\left[|\varepsilon_a|^2\right] = \mathbf{E}\left[\left|Z_a - \widehat{Z}_a\right|^2\right] \ , \tag{3.7}$$

to find the linear MMSE estimator. Although actually finding the optimal weights is a tedious task, it is proved in Appendix A that the mean-square error is minimized when

$$\mathrm{w}_n = \frac{1}{L+C} e^{j\omega_i n} \ , \tag{3.8}$$

where $C = (\sigma_s^2 + N_0)/K_i^2$ is the ratio of the data plus noise power to tone power, and $\omega_i = 2\pi f_i T_s$ is the normalized frequency of the tone in radians. Therefore

$$\widehat{Z}_a = \frac{1}{L+C} \sum_{n=1}^{L} R_{a-n} e^{j\omega_i n} \tag{3.9}$$

is the linear MMSE estimator of Z_a.

At this point it is useful to consider how this method provides accurate estimates. By substituting $R_{a-n} = I_{a-n} + N_{a-n} + Z_{a-n}$ into Eq. (3.9) it is clear that

$$\widehat{Z}_a = \frac{1}{L+C} \sum_{n=1}^{L} I_{a-n} e^{j\omega_i n} + \frac{1}{L+C} \sum_{n=1}^{L} N_{a-n} e^{j\omega_i n} + \frac{1}{L+C} \sum_{n=1}^{L} Z_{a-n} e^{j\omega_i n} . \tag{3.10}$$

The three components in this equation are due to the transmitted symbols, the AWGN, and the interfering tone. The first component in Eq. (3.10) is essentially a weighted average of L transmitted symbols. Since these symbols are assumed to be random with zero mean, this average tends to zero for large L. This is an application of the central limit theorem of probability theory [28]. The second component is caused by the AWGN signal, and also tends to zero for the same reason. The third component is due to the interfering tone, which has a deterministic nature. Each sample of the tone has the same magnitude but a different phase. The phase changes by ω_i radians with each successive sample, that is, $Z_{a+1} = Z_a e^{j\omega_i}$. To align the phases of each sample, they are multiplied by a the appropriate power of $e^{j\omega_i}$, so the third term is actually the sum of a constant. Mathematically, this can be shown as

$$\begin{aligned}
\frac{1}{L+C} \sum_{n=1}^{L} Z_{a-n} e^{j\omega_i n} &= \frac{1}{L+C} \sum_{n=1}^{L} K_i e^{j\omega_i (a-n)} e^{j\phi_i} e^{j\omega_i n} \\
&= \frac{1}{L+C} \sum_{n=1}^{L} K_i e^{j\omega_i a} e^{j\phi_i} \\
&= \frac{1}{L+C} \sum_{n=1}^{L} Z_a \\
&= Z_a \frac{L}{L+C} ,
\end{aligned} \tag{3.11}$$

by substituting Eq. (3.1) for Z_{a-n} and Z_a. Clearly the third component of Eq. (3.10) tends to Z_a for large L. By combining the results for these three terms for large L, it is clear that $\widehat{Z}_a \to Z_a$ as $L \to \infty$. When L is finite, however, the effect of the data symbols and noise comes into play. If the noise is strong or the tone weak, the estimates are less reliable. To compensate, the sum in Eq. (3.9) is divided by $L + (\sigma_s^2 + N_0)/K_i^2$ instead of by L alone, as might be expected.

It is worth noting that the MMSE, calculated by substituting Eq. (3.8) for w_n in Eq. (A.9), is

$$
\begin{aligned}
\gamma_{\min} &= K_i^2 \left[1 - \sum_{n=1}^{L} \mathrm{w}_n e^{-j\omega_i n} - \sum_{n=1}^{L} \mathrm{w}_n^* e^{j\omega_i n} + \sum_{n=1}^{L} \sum_{m=1}^{L} \mathrm{w}_n^* \mathrm{w}_m e^{-j\omega_i (m-n)} \right] \\
&\qquad + (\sigma_s^2 + N_0) \sum_{n=1}^{L} \mathrm{w}_n^* \mathrm{w}_n \\
&= K_i^2 \left[1 - \sum_{n=1}^{L} \frac{1}{L+C} e^{j\omega_i n} e^{-j\omega_i n} - \sum_{n=1}^{L} \frac{1}{L+C} e^{-j\omega_i n} e^{j\omega_i n} \right] \\
&\qquad + K_i^2 \sum_{n=1}^{L} \sum_{m=1}^{L} \frac{1}{L+C} e^{-j\omega_i n} \frac{1}{L+C} e^{j\omega_i m} e^{-j\omega_i (m-n)} \\
&\qquad + (\sigma_s^2 + N_0) \sum_{n=1}^{L} \frac{1}{L+C} e^{-j\omega_i n} \frac{1}{L+C} e^{j\omega_i n} \\
&= K_i^2 \left[1 - \frac{L}{L+C} - \frac{L}{L+C} + \frac{L^2}{(L+C)^2} \right] + (\sigma_s^2 + N_0) \frac{L}{(L+C)^2} \\
&= \frac{K_i^2}{(L+C)^2} \left[(L+C)^2 - 2L(L+C) + L^2 \right] + \frac{K_i^2}{(L+C)^2} \frac{(\sigma_s^2 + N_0)}{K_i^2} L \\
&= \frac{K_i^2}{(L+C)^2} \left[L^2 + 2LC + C^2 - 2L^2 - 2LC + L^2 + LC \right] \\
&= \frac{K_i^2}{(L+C)^2} \left[LC + C^2 \right] \\
&= K_i^2 \frac{C}{L+C} \\
&= \frac{\sigma_s^2 + N_0}{L + (\sigma_s^2 + N_0)/K_i^2} \, .
\end{aligned}
\tag{3.12}
$$

Eq. (3.12) represents the optimal performance of any linear estimator that attempts to minimize the MSE. Since a number of tone cancellers fall into this category it is worthwhile to explore the MMSE further. This provides a yardstick for comparing different cancellers.

To begin this analysis first consider the effect of the number of samples, L. If $L = 0$, the MMSE is K_i^2. This is intuitive because if no samples are used to estimate the tone, no estimate is available for cancellation purposes and the residual power is the same as the power in the tone. When L is small, the random nature of the transmitted symbols and Gaussian noise make the estimate of the interference unreliable, so the residual power remains large. As more samples are used, the effect of the transmitted symbols and noise diminish, allowing for increasingly accurate estimates. Finally, as $L \rightarrow \infty$ the MMSE tends to zero. By selecting L sufficiently large it is possible to generate estimates with any desirable accuracy. To compare different cancellers it is necessary to compare them for the same value of L.

As can be seen from Eq. (3.12), the MMSE depends not only on L, but on the power of the noise and tone. To simplify analysis it is more useful to study the maximum SRR, namely

$$\mathrm{SRR}_{\max} = \frac{\sigma_s^2/T_s}{\gamma_{\min} \log_2 M} , \tag{3.13}$$

instead of the MMSE. Fig. 16 contains a plot of $\mathrm{SRR}_{\max}$ vs. SIR for different SNRs and a fixed value of L = 32. It is worth noting that the maximum SRR is essentially independent of the noise power, except when the tone is strong (SIR < 10 dB), and even then the noise has little effect. In addition, note that the linear MMSE estimator can achieve cancellation to a SRR of greater than about 8 dB for all tones in SNR > 0 dB when L = 32. Clearly strong tones are attenuated, allowing for more reliable symbol detection. Of course, attenuation can be increased by using a larger value of L, if necessary.

Although the SRR is a useful measure of transmission performance, particularly in relationship to the probability of transmission error, it is not particularly useful for measuring

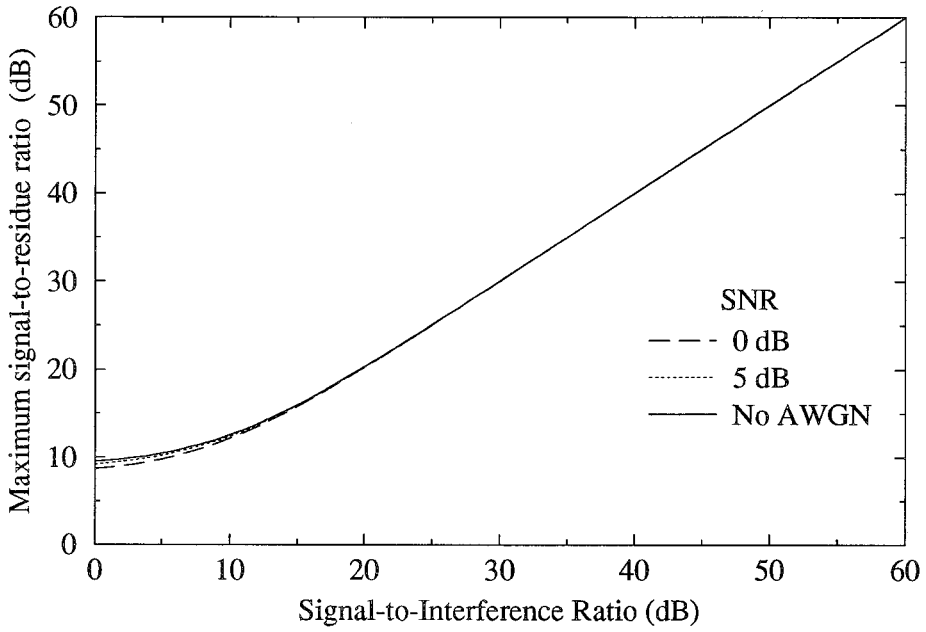

Figure 16. $\mathrm{SRR}_{\max}$ vs. SIR, $L = 32$.

the cancellation performance. A more practical measure is the ratio of the average residual power to the power of the tone, γ/K_i^2. If this quantity is less that one, some performance gain has been achieved (*i.e.*, the residual power after cancellation is less that the tone power before cancellation). Furthermore, it is useful to work with a logarithmic scale. Define the performance gain (in dB) as

$$\begin{aligned} G_{\|\mathrm{dB}} &\triangleq -10 \log \frac{\gamma}{K_i^2} \\ &= \mathrm{SRR}_{\|\mathrm{dB}} - \mathrm{SIR}_{\|\mathrm{dB}} \, . \end{aligned} \tag{3.14}$$

A positive value of G indicates a gain, while a negative value indicates system degradation.

In Fig. 17 the theoretical bound on the gain, given by

$$\begin{aligned} G_{\max} &= -10 \log \frac{\gamma_{\min}}{K_i^2} \\ &= -10 \log \frac{(\sigma_s^2 + N_0)/K_i^2}{L + (\sigma_s^2 + N_0)/K_i^2} \, , \end{aligned} \tag{3.15}$$

is plotted as a function of the SIR when $L = 32$. Curves for several different noise powers are included. From this graph it is apparent that linear estimates perform better at tone cancellation when the tone is strong. This is reassuring since the need to cancel strong tones is greater than the need to cancel weak ones. Note also that cancellation is completely ineffective for SIR > 20 dB when $L = 32$. Increasing L will allow weaker tones to be cancelled, but in Section 3.2.3 a better solution is presented.

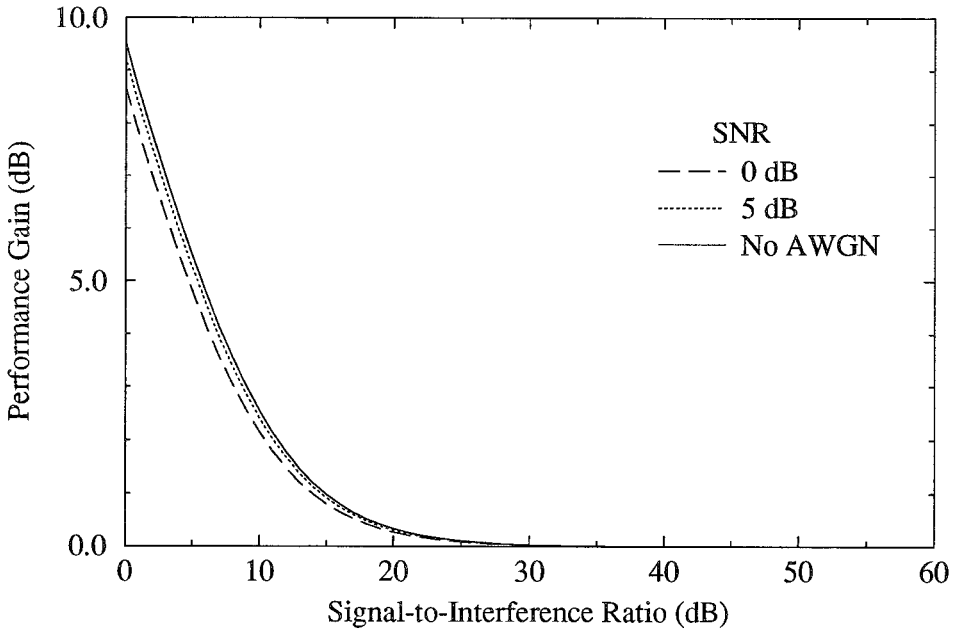

Figure 17. $G_{\max}$ vs. SIR, $L = 32$.

3.2.2 Sub-Optimal Linear Estimator

Although the estimator given by Eq. (3.9) is optimal in the linear MMSE sense, it has a drawback. It requires knowledge of the frequency (f_i) and magnitude (K_i) of the tone, along with the noise PSD (N_0). Since, in general, this information is not known at the receiver, this method is no more feasible that the ideal one presented at the beginning of this section. Fortunately, estimates for $\omega_i = 2\pi f_i T_s$ and $C = \left(\sigma_s^2 + N_0\right)/K_i^2$ can be used instead

of the actual values. By using these estimated parameters, sub-optimal estimates of Z_a with acceptable accuracy can be generated. As will be shown in the next chapter, performance nearly identical to the theoretical bound given in Fig. 17 can be achieved. In the next section a procedure for producing the intermediate estimates is presented. Before then, however, it is useful to analyse the MSE when these estimates are used.

When $\widehat{\omega}_i$ and $\widehat{C}$ are used as estimates for ω_i and C, the MSE can be found by substituting

$$\widehat{\mathrm{w}}_n = \frac{1}{L+\widehat{C}} e^{j\widehat{\omega}_i n} \tag{3.16}$$

for w_n in Eq. (A.9) yielding

$$\begin{aligned}
\gamma &= K_i^2 \left[1 - \sum_{n=1}^{L} \mathrm{w}_n e^{-j\omega_i n} - \sum_{n=1}^{L} \mathrm{w}_n^* e^{j\omega_i n} + \sum_{n=1}^{L}\sum_{m=1}^{L} \mathrm{w}_n^* \mathrm{w}_m e^{-j\omega_i (m-n)} \right] \\
&\quad + \left(\sigma_s^2 + N_0\right) \sum_{n=1}^{L} \mathrm{w}_n^* \mathrm{w}_n \\
&= K_i^2 \left[1 - \sum_{n=1}^{L} \frac{1}{L+\widehat{C}} e^{j\widehat{\omega}_i n} e^{-j\omega_i n} - \sum_{n=1}^{L} \frac{1}{L+\widehat{C}} e^{-j\widehat{\omega}_i n} e^{j\omega_i n} \right] \\
&\quad + K_i^2 \sum_{n=1}^{L}\sum_{m=1}^{L} \frac{1}{L+\widehat{C}} e^{-j\widehat{\omega}_i n} \frac{1}{L+\widehat{C}} e^{j\widehat{\omega}_i m} e^{-j\omega_i (m-n)} \\
&\quad + \left(\sigma_s^2 + N_0\right) \sum_{n=1}^{L} \frac{1}{L+\widehat{C}} e^{-j\widehat{\omega}_i n} \frac{1}{L+\widehat{C}} e^{j\widehat{\omega}_i n} \\
&= K_i^2 \left[1 - \frac{1}{L+\widehat{C}} \sum_{n=1}^{L} e^{j(\widehat{\omega}_i - \omega_i) n} - \frac{1}{L+\widehat{C}} \sum_{n=1}^{L} e^{-j(\widehat{\omega}_i - \omega_i) n} \right] \\
&\quad + K_i^2 \left(\frac{1}{L+\widehat{C}} \right)^2 \sum_{n=1}^{L}\sum_{m=1}^{L} e^{j(\widehat{\omega}_i - \omega_i)(m-n)} \\
&\quad + \left(\sigma_s^2 + N_0\right) \left(\frac{1}{L+\widehat{C}} \right)^2 \sum_{n=1}^{L} 1 \, .
\end{aligned} \tag{3.17}$$

Since the mean-square error does not depend on the actual frequency of the interference but on the accuracy of the frequency estimate, it is useful to define

$$2\pi\epsilon = \widehat{\omega}_i - \omega_i \tag{3.18}$$

as the error in the frequency estimate. Using this definition along with the property

$$\begin{aligned}\sum_{n=1}^{L} e^{j(\widehat{\omega}_i-\omega_i)n} &= \sum_{n=1}^{L} e^{j2\pi\epsilon n} = e^{j2\pi\epsilon}\sum_{n=0}^{L-1} e^{j2\pi\epsilon n} \\ &= e^{j2\pi\epsilon}\frac{\sin(\pi\epsilon L)}{\sin(\pi\epsilon)}\frac{e^{j\pi\epsilon L}}{e^{j\pi\epsilon}} \\ &= \frac{\sin(\pi\epsilon L)}{\sin(\pi\epsilon)}e^{j\pi\epsilon(L+1)}\end{aligned} \tag{3.19}$$

allows the MSE to be expressed as

$$\begin{aligned}\gamma &= K_i^2\left[1 - \frac{1}{L+\widehat{C}}\frac{\sin(\pi\epsilon L)}{\sin(\pi\epsilon)}e^{j\pi\epsilon(L+1)} - \frac{1}{L+\widehat{C}}\frac{\sin(\pi\epsilon L)}{\sin(\pi\epsilon)}e^{-j\pi\epsilon(L+1)}\right] \\ &\quad + K_i^2\left(\frac{1}{L+\widehat{C}}\right)^2\frac{\sin^2(\pi\epsilon L)}{\sin^2(\pi\epsilon)} + (\sigma_s^2+N_0)\left(\frac{1}{L+\widehat{C}}\right)^2 L \\ &= K_i^2\left[1 - \frac{2}{L+\widehat{C}}\frac{\sin(\pi\epsilon L)}{\sin(\pi\epsilon)}\cos[\pi\epsilon(L+1)] + \left(\frac{1}{L+\widehat{C}}\right)^2\frac{\sin^2(\pi\epsilon L)}{\sin^2(\pi\epsilon)}\right] \\ &\quad + K_i^2 C\left(\frac{1}{L+\widehat{C}}\right)^2 L \\ &= K_i^2\left[1 - \frac{2}{L+\widehat{C}}\frac{\sin(\pi\epsilon L)}{\sin(\pi\epsilon)}\cos[\pi\epsilon(L+1)] + \left(\frac{1}{L+\widehat{C}}\right)^2\left(\frac{\sin^2(\pi\epsilon L)}{\sin^2(\pi\epsilon)} + CL\right)\right].\end{aligned} \tag{3.20}$$

Although Eq. (3.20) seems complicated, it does provide some insight into how the accuracy of $\widehat{\omega}_i$ and $\widehat{C}$ affect the mean-square error.

To illustrate the effect of error in $\widehat{\omega}_i$, Fig. 18 contains a plot of γ versus L when SNR = 15 dB, SIR = 10 dB, and $\widehat{C} = C$, for various values of ϵ. For the sake of comparison, the curve for the minimum mean-square error, which is achieved if $\epsilon = 0.0$, is also included. For small L, the MSE when ϵ is non-zero is very close to the MMSE, but for larger L the MSE is noticeable larger than the MMSE. This discrepancy is more pronounced for larger values of ϵ. Although the slight discrepancies shown in Fig. 18 are undesirable, error in $\widehat{\omega}_i$ has a much more serious implication. For larger values of L, the MSE becomes excessive, as shown in Fig. 19. The MSE does not approach zero for large values of L like the MMSE, but instead

tends to K_i^2, as shown in Fig. 20. This situation occurs for all non-zero values of ϵ. No matter how small ϵ is, there is a point beyond which increasing L does not reduce the mean-square error. This phenomenon can be explained by recalling how $\widehat{Z}_a$ is calculated. When there is a slight error in the frequency estimate the system is unable to correctly compensate for the varying phase of the tone in each of the samples. When L is small this does not produce a serious problem. However, for large L the system completely loses track of the phase information in Z_a, causing the third term in Eq. (3.10) to tend to zero, forcing $\widehat{Z}_a$ itself to zero. As a result, there is a limit to the number of samples that can be used to generate accurate estimates of the interference.

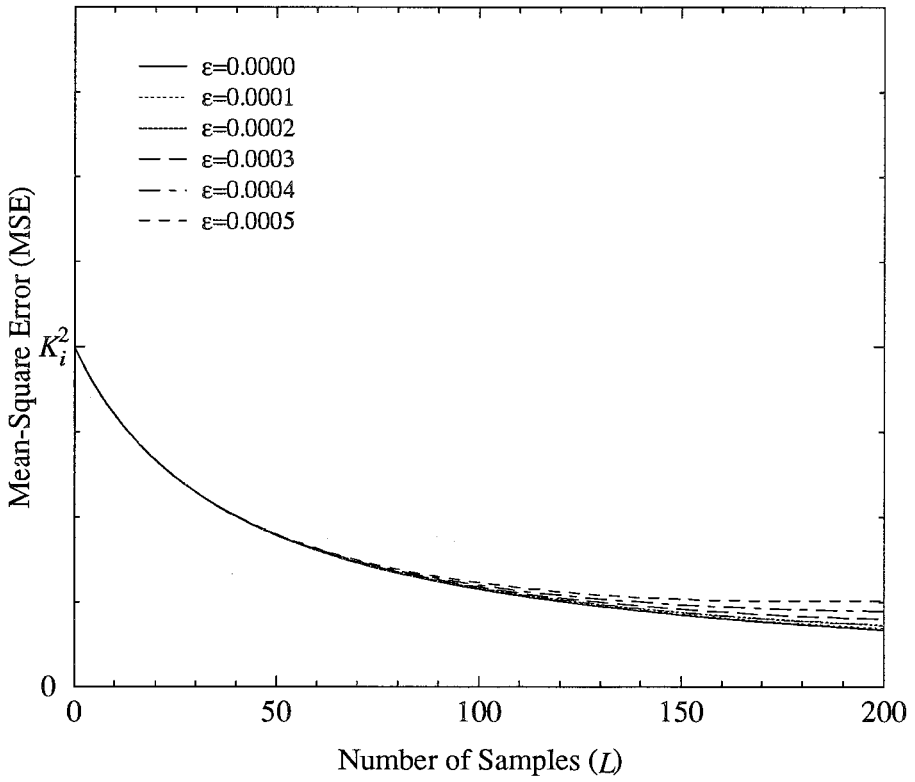

Figure 18. MSE vs. L. SNR = 15 dB, SIR = 10 dB, $\widehat{C} = C$, various ϵ.

Since there is an upper bound on L, there is a corresponding lower bound on the mean-square error that can be achieved when an imprecise estimate for ω_i is used. This implies that the interference cannot be reduced below a certain threshold. For the example in Fig. 19,

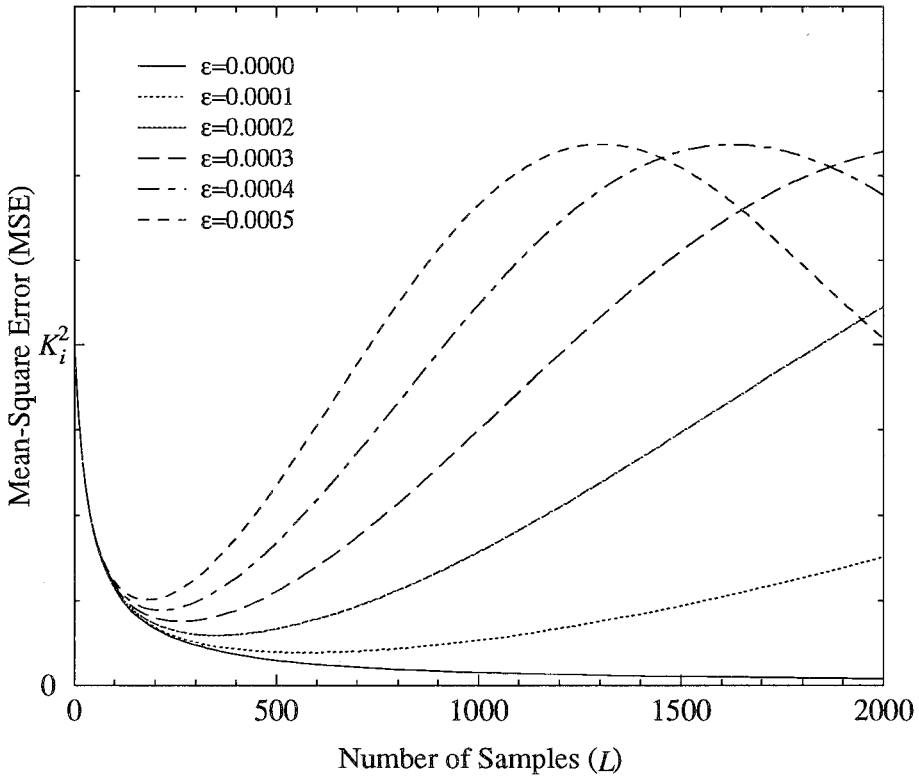

Figure 19. MSE vs. L. SNR = 15 dB, SIR = 10 dB, $\widehat{C} = C$, various ϵ.

when $\epsilon = 0.0001$ the MSE has a lower bound of about one-eighth of the interference power. In practice, the frequency estimator proposed in the next section produces more accurate estimates, so the MSE is generally lower.

The error in the estimate of C has only a slight affect on the MSE, even when $\widehat{C}$ is significantly incorrect. This is shown in Fig. 21 when $\epsilon = 0.0001$, SNR = 15 dB, SIR = 10 dB. Curves for $\widehat{C} = 0.5C$, $\widehat{C} = C$, and $\widehat{C} = 2C$ are shown. For most typical values of C and $\widehat{C}$, the effect of any error is slight, and although undesirable, it does not produce the same limit on L that error in the frequency estimate does. As a result, most of the emphasis in the next section will be on accurately estimating the frequency of the interfering tone.

For most applications the proposed scheme will eliminate the interference sufficiently to allow for reliable data communication. Nonetheless, it is possible to further reduce the mean-square error through the use of decision feedback.

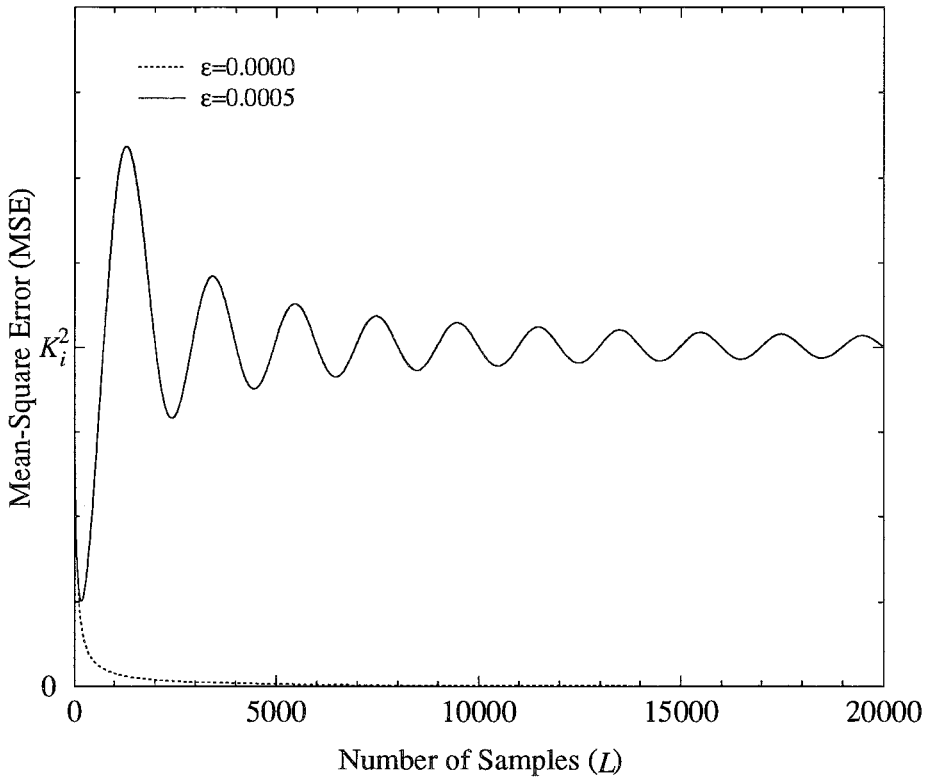

Figure 20. MSE vs. L. SNR = 15 dB, SIR = 10 dB, $\widehat{C} = C$, $\epsilon = 0.0005$.

3.2.3 A Decision Feedback Tone Canceller

The presence of the data and noise signals in the received samples are the primary reasons why the tone can not be measured precisely. Increasing the number of samples used by the estimator will decrease the significance of these signals, allowing better tone estimation, but unfortunately, imprecise frequency estimates limit the number of samples that can be used. Even if the frequency is known, the number of samples required may be prohibitively large. Consider a tone with SIR = 5 dB in noise with SNR = 15 dB. Fig. 22 contains a plot showing the number of samples required to achieve a given SRR, found by solving Eq. (3.12), in conjunction with Eq. (3.13), for L. For example, to increase the SRR to above 15 dB at least $L = 115$ samples are required. Since the number of samples is fairly small, any slight inaccuracy in the estimate of the frequency will have little effect. However, recalling Fig. 15, at a 15 dB SRR, the tone still noticeably affects the probability of transmission error.

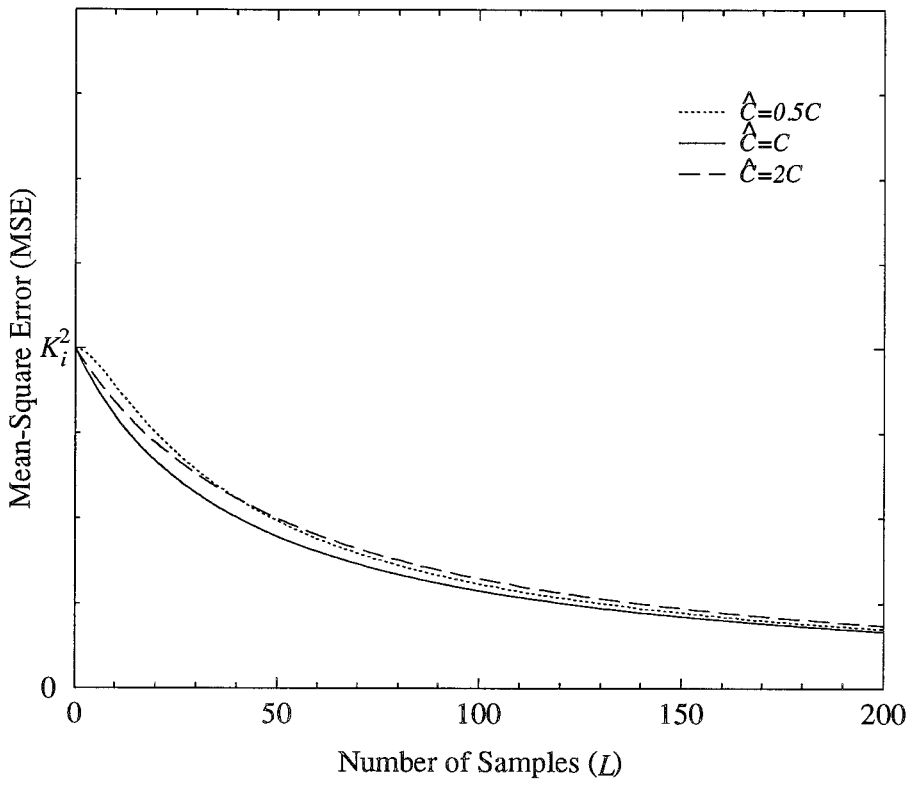

Figure 21. MSE vs. L. SNR = 15 dB, SIR = 10 dB, $\epsilon = 0.0001$, various $\widehat{C}$.

For negligible distortion due to the tone the SRR must be increased to above 25 dB. This is confirmed by recalling Fig. (15), which shows that the probability of error when the SIR is 25 dB is not substantially different from when no tone is present. Therefore, at least L = 1262 samples are required to effectively cancel the tone. Even if such a long tapped delay line were economically feasible, the immense susceptibility to inaccuracy in the frequency estimate would prevent the residue from reaching this goal.

As this example shows, the proposed system is capable of providing some improvement in system performance, but is generally incapable of achieving the ideal goal of a SRR above 25 dB. However, with a slight modification system performance can be drastically improved. To illustrate this modification, consider how the interference estimator would perform if the data signal was absent from the received signal. In this case, by following a procedure similar

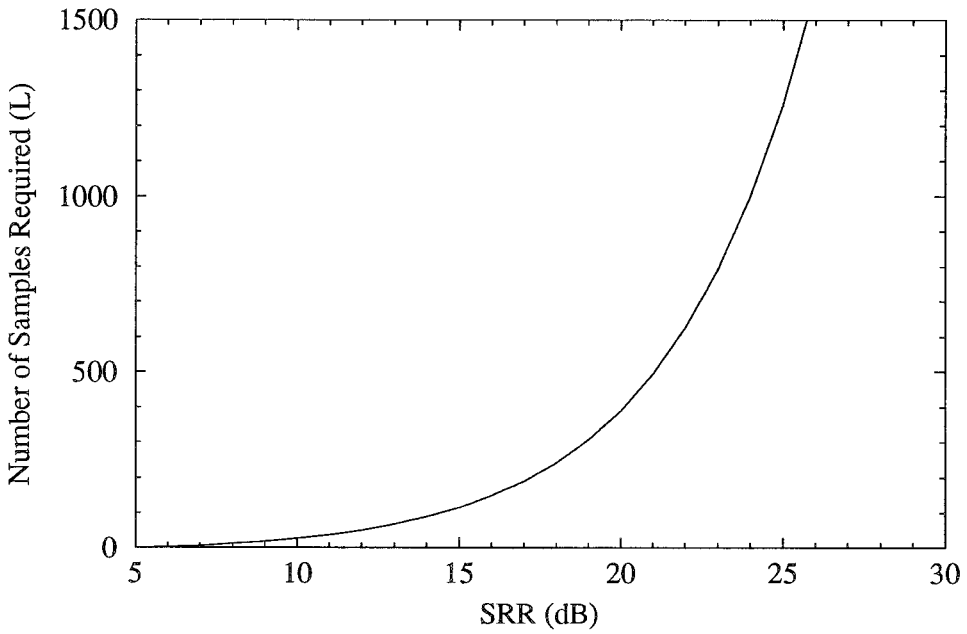

Figure 22. Number of samples vs. SRR, SNR = 15 dB, SIR = 5 dB.

to the one in Appendix A, the MMSE can be shown to be

$$\gamma'_{\min} = \frac{N_0}{L + N_0/K_i^2} \tag{3.21}$$

providing ω_i and C are known. By using this equation instead of Eq. (3.12), it is clear that for the tone in the previous example, the SRR would be 15.4 dB if the tone is estimated from only one sample. Only 10 samples would be need to increase the SRR to 25 dB. Clearly, if the data signal could be removed from the received samples before estimating the tone, the residue could easily be reduced to a negligible value, even if the frequency is not exactly known.

Even though the transmitted data signal is not known at the receiver, it is possible to reduce the effect of the data signal on the samples by employing decision feedback. Since the estimate of the interference in the current sample is based only on previously received samples (*i.e.* $n \geq 1$), it is possible to subtract the previously detected symbols, $\widehat{I}_{a-n}$, from the samples, R_{a-n}, before estimating the interference. By using this method the effect of the data signal is greatly reduced. Unfortunately, the minimum mean-square error and the optimum weights are very difficult to find in this case as they depend on the probability

of detection error, which in turn depends on the MMSE and the optimal weights. Even a numerical solution has proved elusive. However, using the estimator

$$\widehat{Z}_a = \frac{1}{L+\widehat{C}} \sum_{n=1}^{L} \left(R_{a-n} - \widehat{I}_{a-n} \right) e^{j\widehat{\omega}_i n} \tag{3.22}$$

produces excellent tone cancellation, as will be confirmed experimentally in the next chapter.

As noted, detailed mathematical analysis of the system performance when decision feedback is used is extremely difficult since the correctness of the detected symbols depend on many factors. Nonetheless, the usefulness of decision feedback can be shown by considering a few scenarios. If only a few transmission errors occur, $\widehat{I}_{a-n}$ usually equals I_{a-n}, so that $R_{a-n} - \widehat{I}_{a-n}$ usually does not depend on the data signal. As a result, the effect of the data signal is almost completely removed from $\widehat{Z}_a$. This leads to a lower residue, better tone cancellation, and fewer transmission errors. Since the tone canceller works without feedback, it is very tolerant of transmission errors. In fact, the feedback canceller generally performs no worse than the basic canceller when feedback is not used, even when nearly half the symbols are detected incorrectly. Clearly, under normal operating conditions, situations this severe are unlikely to arise. However, when the receiver tunes to a new signal, a large tone may be present, potentially causing almost all symbols to be in error. In this situation, the feedback canceller will initially performs worse than the basic canceller, usually achieving a SRR that is about 3 dB lower. Even at this lower performance level, however, the tone is reduced sufficiently to allow for a significant reduction in transmission errors. As the number of errors declines, more accurate interference estimates are produced, further decreasing the number of transmission errors, eventually leading to a much better SRR. On the other hand, if many transmission errors arise from noise with extremely strong power, or perhaps an error burst, the feedback canceller does not work well. However, since the source of the errors is not the tone, removing the tone will not alleviate the error problem. In the next chapter, a comparison of the performance of the feedback and basic cancellers will be presented.

Although the true MMSE of the feedback canceller is unknown, a crude bound can be found by assuming that no detection errors occur. In this case the data signal is completely removed from the received signal, and the MMSE is given by Eq. (3.21). An uppper bound on the performance gain is then

$$G'_{\max} = -10 \log \frac{N_0/K_i^2}{L + N_0/K_i^2} , \tag{3.23}$$

which is plotted in Fig. 23 for L = 32. Clearly these theoretical results are vastly superior to the ones in Fig. 17. Without the presence of the data signal, the noise power becomes the limiting factor controlling the performance. Cancellation can be applied to substantially weaker tones, and cancellation is much more effective, regardless of noise and tone power.

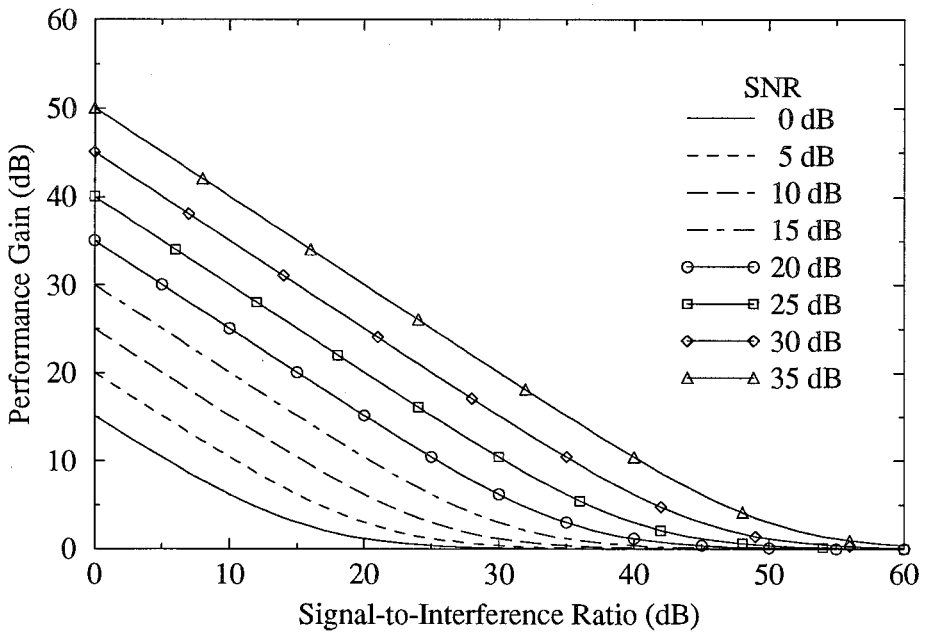

Figure 23. $G'_{\max}$ vs. SIR, L = 32, with decision feedback.

For the feedback canceller to work properly, another slight detail must be considered. Since the data signal power in the samples has been reduced, the power ratio, $\widehat{C}$ should

estimate the quantity

$$\frac{\mathbf{E}\left[\left|I_a - \widehat{I}_a\right|^2\right] + N_a}{K_i^2} \tag{3.24}$$

instead of $(\sigma_s^2 + N_0)/K_i^2$, as in Eq. (3.8). This change reflects the decreased power of the data signal relative to the power of the tone. Fortunately, producing this estimate is straightforward, as will be shown in the next section.

3.3 Estimation of Frequency and Power Ratio

The linear estimator of Z_a described in the previous section requires knowledge of the frequency of the tone and the ratio of signal and noise power to interference power. This information can be readily extracted from the power spectral density of the received signal. In this section a simple method for estimating the PSD will be presented, followed by a detailed description of how the frequency and power ratio can be estimated.

When attempting to determine the frequency of the interfering tone it is natural to analyse the received signal in the frequency domain. Fig. 24 contains a plot of the PSD of the received signal when quadrature amplitude modulation is used with root-raised cosine filters with a roll-off factor of $\alpha = 0.2$. The noise and tone have powers given by a SNR of 15 dB and a SIR of 15 dB. The frequency of the tone is $f_i = 0.1/T_s$. The PSD is characterized by (see Eq. 2.55)

$$\bar{\Phi}_R(f) = \sigma_s^2 \frac{1}{T_s} |H(f)|^2 + N_0 |H_R(f)|^2 + K_i^2 \delta(f - f_i) \; . \tag{3.25}$$

All the power in the tone is concentrated around the frequency of the tone, while the power in the data and noise signals is dispersed smoothly throughout the signal frequency band. The frequency of the tone can be found by finding the frequency where the impulse in the PSD

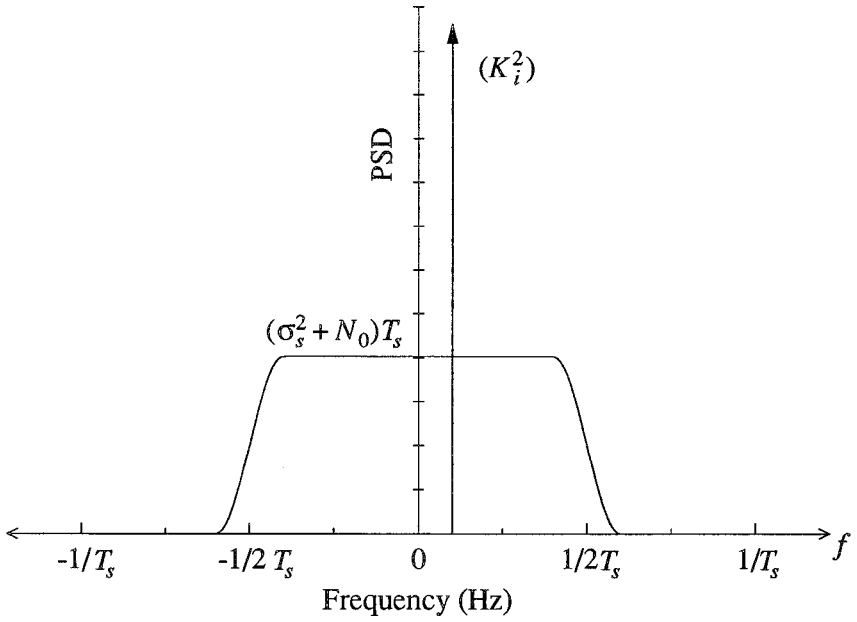

Figure 24. PSD of Received Signal. SNR = 15 dB, SIR = 15 dB, $\alpha = 0.2$.

occurs. This simple observation is the motivation for the proposed method for estimating the tone's frequency.

3.3.1 PSD Estimation

The PSD of a random process is based on all possible realizations of the process over all time. Since only one realization is observed at the receiver, only an estimate of the PSD can be generated. Furthermore, practical considerations limit the observation to a finite time interval. Methods for estimating the PSD fall in the realm of spectral analysis. Numerous techniques have been proposed in this mature field [29], offering solutions covering a wide range of accuracy and complexity. One technique, the periodogram, has been selected for use in this thesis because of its simplicity and computational efficiency [29]. As will be shown later, the estimate it produces of the PSD is sufficient to allow the frequency of the tone to be accurately determined. The periodogram is based on the finite-length discrete Fourier transform (FFT), a transform that can be performed efficiently and has hardware implementations readily available [30].

The periodogram is a set of values that describe the PSD of the signal at a set of discrete frequencies. It is calculated in a straightforward manner from a block of samples of the received signal. The signal is sampled at a rate of $1/T$ samples per second. To prevent aliasing, the sampling rate must meet the Nyquist sampling criterion, so T must be less than or equal to $T_s/2$, since the raised cosine filters limit the bandwidth of the signal to $|f| < 1/T_s$ [24]. To simplify analysis, the relationship between the symbol duration and the sampling period is required to be $T = T_s/N_x$, where N_x is an integer representing the number of samples per symbol. Clearly $N_x \geq 2$ is required to prevent aliasing.

As the received signal is sampled, the samples are collected in blocks containing N samples each. The sample stored in the n^{th} position of the d^{th} block shall be denoted by $r_d(n)$ and is defined as

$$r_d(n) \triangleq r(nT + dNT) \,, \tag{3.26}$$

for $n = 0, 1, \ldots, N-1$, and any integer d. The FFT of the d^{th} block is given by

$$R_d(k) \triangleq \sum_{n=0}^{N-1} r_d(n) e^{-j2\pi \frac{kn}{N}} \,, \tag{3.27}$$

for $k = -N/2, \ldots, -1, 0, 1, \ldots, N/2 - 1$. This transform has the property that the points in $\{R_d(k)\}$ are equal to the Fourier transform of a sampled and truncated version of the received signal, evaluated at k/NT Hz. Since efficient algorithms exist for computing the discrete Fourier transform when the block length is a power of two, it is necessary to choose N to be a power of two. To simplify analysis it is also desirable that N be made a multiple of N_x.

Once the FFT of a block has been calculated, its periodogram can be determined in a straightforward manner. The periodogram of the d^{th} block shall be denoted by $X_d(k)$ and is defined as

$$X_d(k) \triangleq \frac{1}{N} |R_d(k)|^2 \,. \tag{3.28}$$

The set of values $\{X_d(k)\}$ are estimates of the PSD of the received signal at the set of frequencies $\left\{\frac{k}{NT} \middle| \; k \in \mathbf{I},\; -\frac{N}{2} \leq k \leq \frac{N}{2} - 1\right\}$.

To show the relationship between the periodogram and the PSD of the received signal, it would be beneficial to find the probability distribution function (PDF) of the points in the periodogram. Ideally, a simple expression for the PDF of $\{X_d(k)\}$ could be found. Unfortunately, this is not the case. The difficulty arises primarily from the cyclostationary nature of the transmitted signal. Even finding an expression for the mean of $X_d(k)$ is a non-trivial matter. The discussion that follows is included only to illustrate some of the strengths and weaknesses of the periodogram approach to spectral estimation. It is not intended to be a thorough or exact analysis, as it was felt that this task is beyond the scope of this thesis.

To express the mean of each point in the periodogram in terms of the PSD of the received signal it is useful to use Eq. (3.27) and Eq. (3.28), so that

$$\begin{aligned}
\mathbf{E}[X_d(k)] &\triangleq \mathbf{E}\left[\tfrac{1}{N}|R_d(k)|^2\right] \\
&= \mathbf{E}\left[\frac{1}{N}\sum_{n=0}^{N-1} r_d^*(n)e^{j2\pi\frac{kn}{N}} \sum_{m=0}^{N-1} r_d(m)e^{-j2\pi\frac{km}{N}}\right] \\
&= \frac{1}{N}\sum_{n=0}^{N-1}\sum_{m=0}^{N-1} \mathbf{E}[r_d^*(n)r_d(m)]e^{-j2\pi\frac{k(m-n)}{N}} \; . \qquad (3.29)
\end{aligned}$$

Substituting Eq. (3.26) yields

$$\begin{aligned}
\mathbf{E}[X_d(k)] &= \frac{1}{N}\sum_{n=0}^{N-1}\sum_{m=0}^{N-1} \mathbf{E}[r^*(nT + dNT)r(mT + dNT)]e^{-j2\pi\frac{k(m-n)}{N}} \\
&= \frac{1}{N}\sum_{n=0}^{N-1}\sum_{m=0}^{N-1} \phi_R(nT + dNT; mT - nT)e^{-j2\pi\frac{k(m-n)}{N}} \; . \qquad (3.30)
\end{aligned}$$

This equation provides an expression for the mean of the periodogram in terms of the received signal's autocorrelation function. By substituting Eq. (2.53) for $\phi_R(nT + dNT; mT - nT)$ it is possible to express the mean as

$$\mathbf{E}[X_d(k)] = \frac{1}{N}\sum_{n=0}^{N-1}\sum_{m=0}^{N-1} \phi_V(nT + dNT; mT - nT)e^{-j2\pi\frac{k(m-n)}{N}}$$

$$+\frac{1}{N}\sum_{n=0}^{N-1}\sum_{m=0}^{N-1}\phi_N(mT-nT)e^{-j2\pi\frac{k(m-n)}{N}}$$
$$+\frac{1}{N}\sum_{n=0}^{N-1}\sum_{m=0}^{N-1}\phi_Z(mT-nT)e^{-j2\pi\frac{k(m-n)}{N}}$$
$$=E_V(d,k)+E_N(d,k)+E_Z(d,k)\ , \tag{3.31}$$

where

$$E_V(d,k)\triangleq\frac{1}{N}\sum_{n=0}^{N-1}\sum_{m=0}^{N-1}\phi_V(nT+dNT;mT-nT)e^{-j2\pi\frac{k(m-n)}{N}}\ , \tag{3.32}$$

$$E_N(d,k)\triangleq\frac{1}{N}\sum_{n=0}^{N-1}\sum_{m=0}^{N-1}\phi_N(mT-nT)e^{-j2\pi\frac{k(m-n)}{N}}\ , \tag{3.33}$$

and

$$E_Z(d,k)\triangleq\frac{1}{N}\sum_{n=0}^{N-1}\sum_{m=0}^{N-1}\phi_Z(mT-nT)e^{-j2\pi\frac{k(m-n)}{N}}\ . \tag{3.34}$$

Clearly, from the above equations, the mean is the sum of three components, with one component depending on the data signal, one depending on the noise, and the third depending on the tone. By analysing the three components separately it is possible to express the mean in terms of the PSD.

The first component is the most difficult to analyse due to the cyclostationary nature of the data signal. From Eq. (2.46),

$$\phi_V(nT+dNT;mT-nT)$$
$$=\sigma_s^2\frac{1}{T_s}\sum_{a=-\infty}^{\infty}\int_{-\infty}^{\infty}H^*(f)H\left(f+\tfrac{a}{T_s}\right)e^{j2\pi\frac{a(nT+dNT)}{T_s}}e^{j2\pi\left(f+\frac{a}{T_s}\right)(m-n)T}df\ . \tag{3.35}$$

However, since $\phi_V(t;\tau)$ is periodic with respect to t with a period of T_s,

$$\phi_V(nT+dNT;mT-nT)=\phi_V(nT;mT-nT) \tag{3.36}$$

since $dNT = dNT_s/N_x$ is a multiple of T_s.[4] In addition, when $|a|>1$, $H(f)$ and $H(f+a/T_s)$ do not overlap since $H(f)$ is band-limited to $|f|<1/T_s$. Therefore

[4] Since N is a multiple of N_x, N/N_x is an integer. The block number, d, is also an integer.

$H^*(f)H(f+a/T_s) \equiv 0$ when $|a| > 1$. As a result, only three terms in the summation with respect to a are non-zero. Therefore,

$$\phi_V(nT+dNT;mT-nT) = \sigma_s^2 \frac{1}{T_s} \sum_{a=-1}^{1} \int_{-\infty}^{\infty} H^*(f)H\left(f+\tfrac{a}{T_s}\right) e^{-j2\pi fnT} e^{j2\pi\left(f+\frac{a}{T_s}\right)mT} df \ . \tag{3.37}$$

Substituting Eq. (3.37) for $\phi_V(nT+dNT;mT-nT)$ in Eq. (3.32) yields

$$\begin{aligned} E_V(d,k) &= \tfrac{1}{N} \sum_{n=0}^{N-1} \sum_{m=0}^{N-1} \sigma_s^2 \tfrac{1}{T_s} \sum_{a=-1}^{1} \int_{-\infty}^{\infty} H^*(f)H\left(f+\tfrac{a}{T_s}\right) e^{-j2\pi fnT} e^{j2\pi\left(f+\frac{a}{T_s}\right)mT} df e^{-j2\pi\frac{k(m-n)}{N}} \\ &= \tfrac{1}{N}\sigma_s^2 \tfrac{1}{T_s} \sum_{a=-1}^{1} \int_{-\infty}^{\infty} H^*(f)H\left(f+\tfrac{a}{T_s}\right) \sum_{n=0}^{N-1} e^{-j2\pi\left(f-\frac{k}{NT}\right)nT} \sum_{m=0}^{N-1} e^{j2\pi\left(f+\frac{a}{T_s}-\frac{k}{NT}\right)mT} df \ . \end{aligned} \tag{3.38}$$

To clarify this expression define

$$\begin{aligned} G(f) &\triangleq \sum_{n=0}^{N-1} e^{j2\pi fnT} \\ &= \frac{1-\exp(j2\pi fNT)}{1-\exp(j2\pi fT)} \\ &= \frac{\sin \pi fNT}{\sin \pi fT} e^{j2\pi f(N-1)T} \ , \end{aligned} \tag{3.39}$$

so that

$$E_V(d,k) = \tfrac{1}{N}\sigma_s^2 \frac{1}{T_s} \sum_{a=-1}^{1} \int_{-\infty}^{\infty} H^*(f)H\left(f+\tfrac{a}{T_s}\right) G^*\left(f-\tfrac{k}{NT}\right) G\left(f+\tfrac{a}{T_s}-\tfrac{k}{NT}\right) df \ . \tag{3.40}$$

The magnitude of $G(f)$ is characterized by spikes occurring at multiples of $1/T = N_x/T_s$ Hz, and is small elsewhere. As a result, there can not be a spike at both $G(f)$ and $G(f+a/T_s)$ for the same value of f, so $G^*(f)G(f+a/T_s)$ is negligible when $a = \pm 1$ (if $N_x \geq 2$). Therefore, the integrals when $a = \pm 1$ can be ignored. Only when $a = 0$ does the integral contribute to $E_V(d,k)$, so

$$E_V(d,k) = \tfrac{1}{N}\sigma_s^2 \frac{1}{T_s} \int_{-\infty}^{\infty} |H(f)|^2 \left|G\left(f-\tfrac{k}{NT}\right)\right|^2 df \ . \tag{3.41}$$

To express this in terms of the PSD, recall from Eq. (2.48) that

$$\bar{\Phi}_V(f) = \sigma_s^2 \frac{1}{T_s} |H(f)|^2 \,, \tag{3.42}$$

so that

$$E_V(d,k) = \frac{1}{N} \int_{-\infty}^{\infty} \bar{\Phi}_V(f) \left| G\left(f - \tfrac{k}{NT}\right) \right|^2 df \,. \tag{3.43}$$

The noise component, given by Eq. (3.33), can be expressed in a similar format by

$$\begin{aligned} E_N(d,k) &\triangleq \frac{1}{N} \sum_{n=0}^{N-1} \sum_{m=0}^{N-1} \phi_N(mT - nT) e^{-j2\pi \frac{k(m-n)}{N}} \\ &= \frac{1}{N} \sum_{n=0}^{N-1} \sum_{m=0}^{N-1} \int_{-\infty}^{\infty} \Phi_N(f) e^{j2\pi f(m-n)T} df e^{-j2\pi \frac{k(m-n)}{N}} \\ &= \frac{1}{N} \int_{-\infty}^{\infty} \Phi_N(f) \sum_{n=0}^{N-1} e^{-j2\pi \left(f - \frac{k}{NT}\right) nT} \sum_{m=0}^{N-1} e^{j2\pi \left(f - \frac{k}{NT}\right) mT} df \\ &= \frac{1}{N} \int_{-\infty}^{\infty} \Phi_N(f) \left| G\left(f - \tfrac{k}{NT}\right) \right|^2 df \,. \end{aligned} \tag{3.44}$$

The tone component, given by Eq. (3.34) can be expressed in terms of the PSD of the tone by

$$\begin{aligned} E_Z(d,k) &\triangleq \frac{1}{N} \sum_{n=0}^{N-1} \sum_{m=0}^{N-1} \phi_Z(mT - nT) e^{-j2\pi \frac{k(m-n)}{N}} \\ &= \frac{1}{N} \sum_{n=0}^{N-1} \sum_{m=0}^{N-1} \int_{-\infty}^{\infty} \Phi_Z(f) e^{j2\pi f(m-n)T} df e^{-j2\pi \frac{k(m-n)}{N}} \\ &= \frac{1}{N} \int_{-\infty}^{\infty} \Phi_Z(f) \sum_{n=0}^{N-1} e^{-j2\pi \left(f - \frac{k}{NT}\right) nT} \sum_{m=0}^{N-1} e^{j2\pi \left(f - \frac{k}{NT}\right) mT} df \\ &= \frac{1}{N} \int_{-\infty}^{\infty} \Phi_Z(f) \left| G\left(f - \tfrac{k}{NT}\right) \right|^2 df \,. \end{aligned} \tag{3.45}$$

Combining the three components yields

$$\begin{aligned} \mathbf{E}[X_d(k)] &= E_V(d,k) + E_N(d,k) + E_Z(d,k) \\ &= \frac{1}{N} \int_{-\infty}^{\infty} \bar{\Phi}_V(f) \left| G\left(f - \tfrac{k}{NT}\right) \right|^2 df + \frac{1}{N} \int_{-\infty}^{\infty} \Phi_N(f) \left| G\left(f - \tfrac{k}{NT}\right) \right|^2 df \end{aligned}$$

$$+\frac{1}{N}\int_{-\infty}^{\infty}\Phi_Z(f)\left|G(f-\tfrac{k}{NT})\right|^2 df$$
$$=\frac{1}{N}\int_{-\infty}^{\infty}\left[\bar{\Phi}_V(f)+\Phi_N(f)+\Phi_Z(f)\right]\left|G(f-\tfrac{k}{NT})\right|^2 df\ . \tag{3.46}$$

By using Eq. (2.55) for the PSD of the received signal, this can be expressed as

$$\mathbf{E}[X_d(k)]=\frac{1}{N}\int_{-\infty}^{\infty}\bar{\Phi}_R(f)\left|G(f-\tfrac{k}{NT})\right|^2 df$$
$$=\int_{-\infty}^{\infty}\bar{\Phi}_R(f)W_N(f-\tfrac{k}{NT})df\ , \tag{3.47}$$

where

$$W_N(f)=\frac{1}{N}|G(f)|^2=\frac{\sin^2\pi fNT}{N\sin^2\pi fT} \tag{3.48}$$

is referred to as a window function. Examination of Eq. (3.47) reveals that the mean of the $X_d(k)$ is equal to the result of the convolution of the PSD of the received signal with the window function evaluated at $f=\frac{k}{NT}$. Since the mean of periodogram is not equal to the PSD of the signal, the periodogram is known as a biased estimator [31]. The convolution operation causes the PSD to appear slightly widened, with more power shifted into the sidelobes. For large N, the effect of the bias is less noticeable. In fact, as $N\to\infty$, $W_N(f)\to\delta(fT)$, so that

$$\lim_{N\to\infty}\mathbf{E}[X_d(k)]=\lim_{N\to\infty}\int_{-\infty}^{\infty}\bar{\Phi}_R(f)W_N(f-\tfrac{k}{NT})df$$
$$=\int_{-\infty}^{\infty}\bar{\Phi}_R(f)\delta([f-\tfrac{k}{NT}]T)df$$
$$=\int_{-\infty}^{\infty}\bar{\Phi}_R(f)\frac{1}{T}\delta(f-\tfrac{k}{NT})df$$
$$=\frac{1}{T}\bar{\Phi}_R(\tfrac{k}{NT})\ . \tag{3.49}$$

The primary implication of the bias is that for finite N, the impulse that results from the tone that occurs in the PSD is estimated as a finite-magnitude pulse in the periodogram. The shape of this pulse is proportionate to $W_N(f)$.

Fig. 25 shows a typical periodogram of a received signal with SNR = 15 dB and SIR = 15 dB, calculated from N = 16384 samples collected at N_x = 2 samples per symbol. The

predominant spike is due to the tone with frequency $f_i = 0.1/T_s$, and occurs at

$$k \cong f_i NT = 0.1NT/T_s = 0.1N/N_x \cong 819 \, . \tag{3.50}$$

By finding the position of the spike in the periodogram, it should be possible to estimate the frequency of the tone.

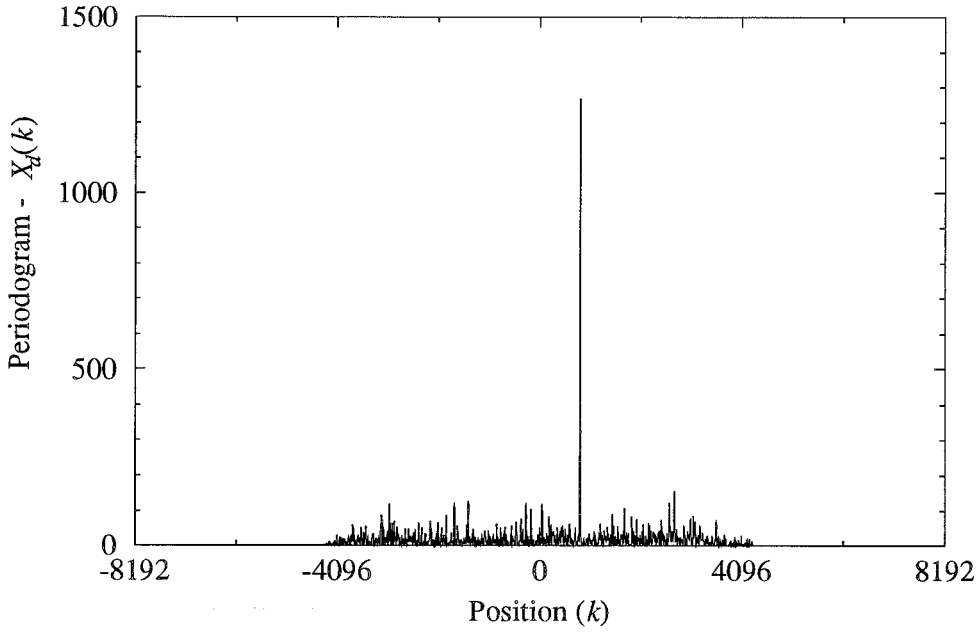

Figure 25. Periodogram of Received Signal. N = 16384, N_x = 2, SNR = 15 dB, SIR = 15 dB.

Fig. 25 also illustrates a problem inherent with the use of the periodogram. Since the PSD is dependent on the autocorrelation function of the received signal, it is essentially an average all possible realizations of the signal. The periodogram, on the other hand, is calculated from only a single realization. Compare Fig. 25 with the actual PSD of the signal as shown in Fig. 24. Note that the smooth portions of the spectrum appear very jagged in the periodogram. This is because the periodogram only estimates the PSD. Any given estimate can differ wildly from its desired value, even though it equals its desired value on average. This difference is a measure of the variance of the estimator. The smaller the variance, the more like likely the estimator will be close to its desired value. The variance of the periodogram is a very important consideration.

In the example given above, N was chosen to be excessively large to show how the periodogram can be useful. A value of N = 2048 is much more reasonable in terms of implementation complexity, and Fig. 26 shows why the periodogram by itself is generally impractical. The tone, marked by an arrow in the graph, is indistinguishable. Because of the larger bias associated with using a smaller value of N, the spike due to the tone is concealed by the random nature of the periodogram. If the tone had a weaker power, this problem would be even more pronounced.

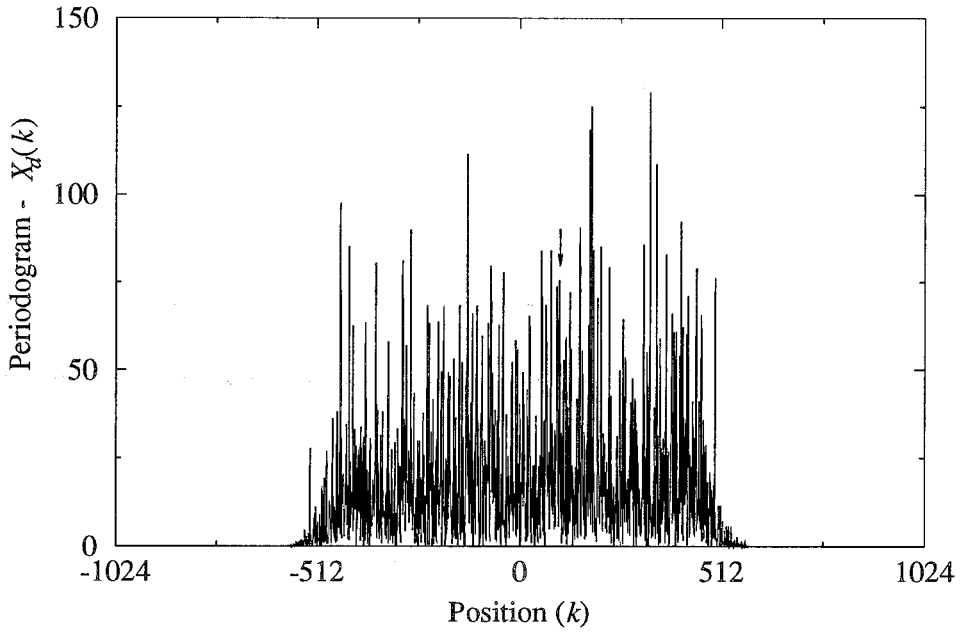

Figure 26. Periodogram of Received Signal. N = 2048, N_x = 2, SNR = 15 dB, SIR = 15 dB.

The number of samples used to produce the periodogram is an important parameter. When N samples are used, the periodogram estimates the PSD at N discrete frequencies in the range $\left[-\frac{N_x}{T_s}, \frac{N_x}{T_s}\right]$. By increasing N, more estimates are produced, which are more closely spaced in the frequency range. This reduces the need to use interpolation to estimate the PSD at frequencies not provided by the periodogram. In addition, increasing N causes the bias to be reduced which increases the magnitude of the spike due to the tone, making it easier to find. Clearly there is much to be gained by selecting a large value of N. Unfortunately, there are

some limitations. FFT algorithms have an order of $N \log N$, and therefore the amount of time required to perform the operation grows non-linearly with increasing N. Similarly, hardware implementations become increasingly more complex. Another drawback is that more time is required to collect the block of data if N is increased.

3.3.2 Average Periodogram

Because of the large variance, the periodogram of a single block can not be used by itself to estimate the PSD. Instead, it is desirable to compute the periodograms from several different blocks of samples and average the results together. The resulting estimate will be referred to as the average periodogram (AP). When D periodograms are averaged together, the resulting AP will be denoted by $X_D(k)$ and defined as

$$X_D(k) \triangleq \frac{1}{D} \sum_{d=0}^{D-1} X_d(k) \,, \tag{3.51}$$

where $X_d(k)$ is the periodogram calculated from the d^{th} block of samples using Eq. (3.28). Note that the same number of samples must be used for each periodogram, and no sample should be used for more than one periodogram. The sample blocks must not overlap.

The mean of the average periodogram can be determined easily by applying Eq. (3.47), so that

$$\begin{aligned} \mathbf{E}[X_D(k)] &= \frac{1}{D} \sum_{d=0}^{D-1} \mathbf{E}[X_d(k)] \\ &= \frac{1}{D} \sum_{d=0}^{D-1} \int_{-\infty}^{\infty} \bar{\Phi}_R(f) W_N\big(f - \tfrac{k}{NT}\big) df \\ &= \int_{-\infty}^{\infty} \bar{\Phi}_R(f) W_N\big(f - \tfrac{k}{NT}\big) df \,. \end{aligned} \tag{3.52}$$

Similarly, the variance is

$$\mathbf{Var}[X_D(k)] = \mathbf{E}\big[X_D^2(k)\big] - \mathbf{E}[X_D(k)]^2$$

$$= \frac{1}{D^2} \sum_{d=0}^{D-1} \sum_{e=0}^{D-1} \mathbf{E}[X_d(k)X_e(k)] - \frac{1}{D^2} \sum_{d=0}^{D-1} \sum_{e=0}^{D-1} \mathbf{E}[X_d(k)]\mathbf{E}[X_e(k)]$$
$$= \frac{1}{D^2} \sum_{d=0}^{D-1} \sum_{e=0}^{D-1} \mathbf{Cov}[X_d(k), X_e(k)] \,, \tag{3.53}$$

where $\mathbf{Cov}[\cdot,\cdot]$ denotes the covariance [28]. A detailed analysis of the covariance has not been included in this thesis for the sake of brevity. However, different periodograms are essentially uncorrelated, and the variances of all the periodograms are identical, independent of block number. Using these properties the variance of the AP can be expressed as

$$\begin{aligned} \mathbf{Var}[X_D(k)] &\cong \frac{1}{D^2} \sum_{d=0}^{D-1} \sum_{e=0}^{D-1} \mathbf{Var}[X_d(k)]\delta(e-d) \\ &= \frac{1}{D^2} \sum_{d=0}^{D-1} \mathbf{Var}[X_d(k)] \\ &= \frac{1}{D}\mathbf{Var}[X_d(k)] \,. \end{aligned} \tag{3.54}$$

As can be seen by Eq. (3.54), the variance of the AP is a fraction of the variance of a single periodogram. By increasing D it is possible to reduce the variance to any arbitrary level. Fig. 27 shows an AP calculated for the signal in the preceding example, calculated with $D = 8$ and $N = 2048$. Note that the random perturbations have been significantly reduced, allowing the tone to be detected easily. As more blocks of samples are processed and included in the AP, the variance decreases further. Unlike N, D is not a fixed parameter and can increase without bound. Given enough time, even the weakest tone can be detected in the AP.

Aside from N and L, the other important system design parameter is N_x, the number of samples per symbol. To prevent aliasing, N_x must be greater than or equal to two. However, the practice of taking $N_x > 2$ is questionable. Although the periodogram is proportionate to N_x, the tone spike is no more or less prominent with different values of N_x. Increasing N_x widens the frequency range over which the PSD is estimated, but all this additional range falls outside the signal frequency band. Since N remains unchanged, the points in the

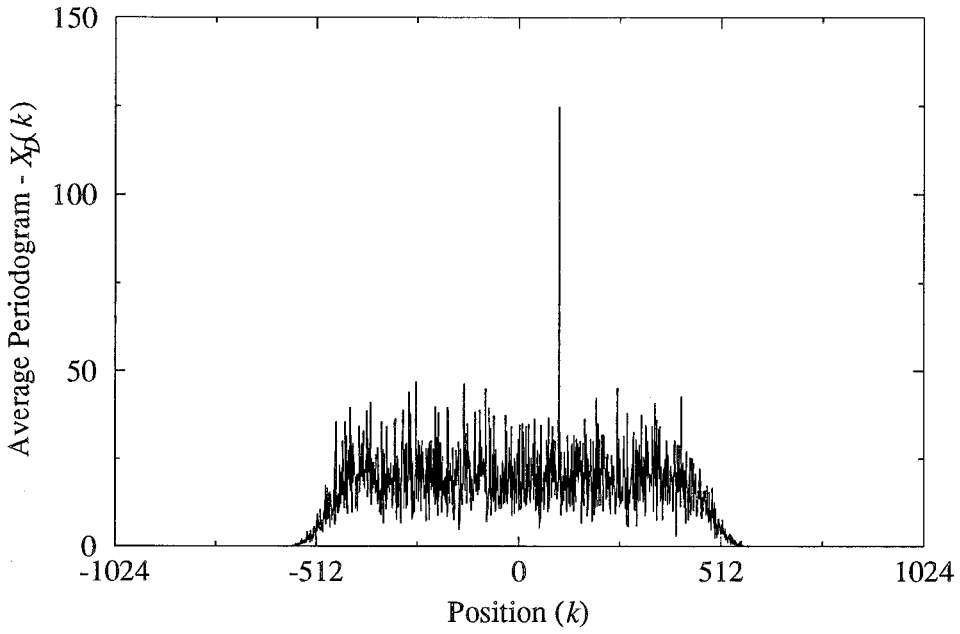

Figure 27. Average Periodogram (AP) of Received Signal.
D = 8, N = 2048, N_x = 2, SNR = 15 dB, SIR = 15 dB.

periodogram become more spread out so the frequency resolution is decreased, with fewer relevant estimates. On the other hand, collecting samples at a faster rate requires less time to collect a full block of N. However, in that shortened time span, a less valuable estimate of the PSD is produced. Therefore, it is concluded that two is the best value for N_x to estimate the PSD.

3.3.3 Symbol Rate Sampling

If the primary goal was estimating the PSD of the signal, the optimal value of N_x would be two. However, for the proposed tone canceller, estimating the frequency of the interfering tone is the main concern, accurate estimates of the true PSD are not really important. By taking $N_x = 1$ (*i.e.*, sampling below the Nyquist sampling rate), aliasing is introduced. The resulting average periodogram does not reflect the PSD of the received signal, but does contain sufficient information to accurately estimate the frequency of the interference. There are three reasons for doing this: *i*) the implementation is considerably easier, *ii*) the tone frequency can be estimated with greater accuracy, and *iii*) decision feedback (which will be discussed

in Subsection 3.3.6) can be used to further improve the results. Only one sample is collected per symbol, and it is collected at the symbol sampling instant. Throughout the remained of this chapter, only the case when $N_x = 1$ will be discussed.

In Appendix B, expressions for the mean and variance of the resulting AP are derived, when only one sample per symbol is collected. They are

$$\mathbf{E}[X_D(k)] = \sigma_s^2 + N_0 + K_i^2 Z_0(k) \tag{3.55}$$

and

$$\mathbf{Var}[X_D(k)] = \frac{1}{D}\left[\left(\sigma_s^2 + N_0\right)^2 + 2\left(\sigma_s^2 + N_0\right)K_i^2 Z_0(k)\right], \tag{3.56}$$

where

$$\begin{aligned} Z_0(k) &= W_N\left(f_i - \tfrac{k}{NT_s}\right) \\ &= \frac{\sin^2\left[\pi\left(f_i - \frac{k}{NT_s}\right)NT_s\right]}{N\sin^2\left[\pi\left(f_i - \frac{k}{NT_s}\right)T_s\right]} \\ &= \frac{\sin^2 \pi f_i NT_s}{N\sin^2 \frac{\pi}{N}[f_i NT_s - k]} \end{aligned} \tag{3.57}$$

is the mathematical formula that characterizes the effect of the tone on the points in the average periodogram. This spike is largest for the value of k closest to $f_i NT_s$, and is small for all other values of k. Also, note from Eq. (3.56) that the variance is inversely proportional to D.

3.3.4 Frequency Estimation

By using the average periodogram it is possible to estimate the frequency of the interfering tone. The presence of a tone in the received signal is indicated by a large spike in the AP, with the position of the spike depending on the frequency of the tone. By finding the position of the largest spike in the AP, the frequency of the tone can be determined. To illustrate this procedure, assume that enough blocks have processed so that the random nature of $X_D(k)$ is minimal, so $X_D(k) \cong \mathbf{E}[X_D(k)]$.

As noted in Appendix B, the mean of the average periodogram is

$$\mathbf{E}[X_D(k)] = \sigma_s^2 + N_0 + K_i^2 \frac{\sin^2 \pi f_i N T_s}{N \sin^2 \frac{\pi}{N}[f_i N T_s - k]} , \tag{3.58}$$

which attains its largest value when $k = k_i$, where k_i is the integer closest to $f_i N T_s$. To use this property, let $\widehat{k_i}$ be the position of the largest value in the average periodogram, so that $X_D\left(\widehat{k_i}\right) \geq X_D(k)$ for all $k \in \left[-\frac{N}{2}, \frac{N}{2} - 1\right]$. Then, one possible estimate for f_i is

$$\widehat{f_i} = \frac{\widehat{k_i}}{N T_s} . \tag{3.59}$$

Under normal operating conditions, the largest value of the AP always occurs at k_i, so this estimate can be quite reliable. The only problem arises when the tone is relatively weak and only a few blocks have been processed. In this case the tone is hidden in the random nature of the AP. However, as more blocks are processed, the variance decreases and the tone spike becomes prominent. As this problem only occurs for an extremely short time while the receiver tunes to a new channel, it can be disregarded. In general, it is safe to assume that $\widehat{k_i} = k_i$, and that assumption will be made for the remainder of this section. Although the estimate of Eq. (3.59) is very reliable, it is limited by the frequency resolution of the AP to an accuracy of

$$\left| f_i - \widehat{f_i} \right| \leq \frac{1}{2 N T_s} . \tag{3.60}$$

There is no error only if $f_i N T_s$ happens to be an integer.

By considering the shape of the tone pulse, it is possible to fine-tune the estimate of the frequency to achieve significantly better performance. The shape of the spike is governed by

$$Z_0(k) = \frac{\sin^2 (\pi f_i N T_s)}{N \sin^2 \left(\frac{\pi}{N}[f_i N T_s - k]\right)} , \tag{3.61}$$

which is plotted in Fig. 28 for $N = 2048$ and $f_i T_s = 0.05$, so $f_i N T_s = 102.4$. As expected, it appears as a large spike, which falls at $k_i = 102$. Fig. 29 shows the same function for points

around k_i only. The points marked with a circle are for integral k, and indicate the points for which the average periodogram has been calculated. The dashed line shows the values of $Z_0(k)$ when k is not an integer. In this case, $Z_0(k)$ reaches its peak at some point not included in the AP. That is, $Z_0(k)$ is at a maximum at $f_i NT_s = 102.4$, while the largest value in the mean of the AP is at $k_i = 102$. It is useful to define the difference between the two points as

$$\delta_i = f_i NT_s - k_i \ . \tag{3.62}$$

Note that $|\delta_i| \leq 1/2$. By finding $\widehat{\delta}_i$ as an estimate for δ_i, the frequency of the tone can be estimated as

$$\widehat{f}_i = \frac{k_i}{NT_s} + \frac{\widehat{\delta}_i}{NT_s} \ . \tag{3.63}$$

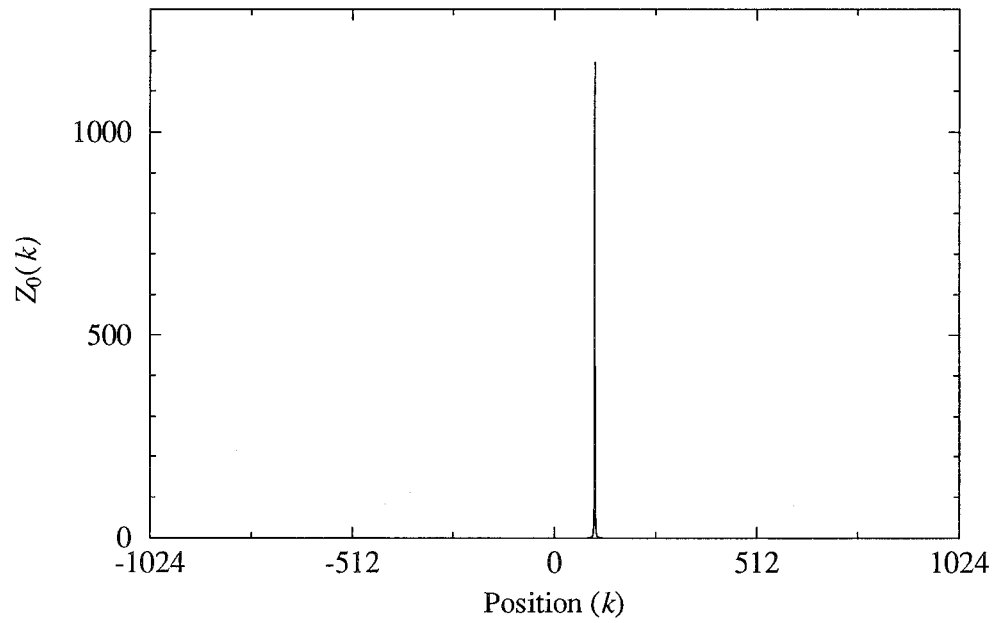

Figure 28. Plot of $Z_0(k)$ vs. k, for $N = 2048$ and $f_i T_s = 0.05$.

To estimate δ_i, a simple interpolation procedure is used. The second largest point in $\mathbf{E}[X_D(k)]$ occurs at $k_i + 1$ if $\delta_i > 0$ or at $k_i - 1$ if $\delta_i < 0$. Consider the ratio of the largest point in $\mathbf{E}[X_D(k)]$ to the second largest point. Let

$$B = \frac{\mathbf{E}[X_D(k_i)] - (\sigma_s^2 + N_0)}{\mathbf{E}[X_D(k_i \pm 1)] - (\sigma_s^2 + N_0)}$$

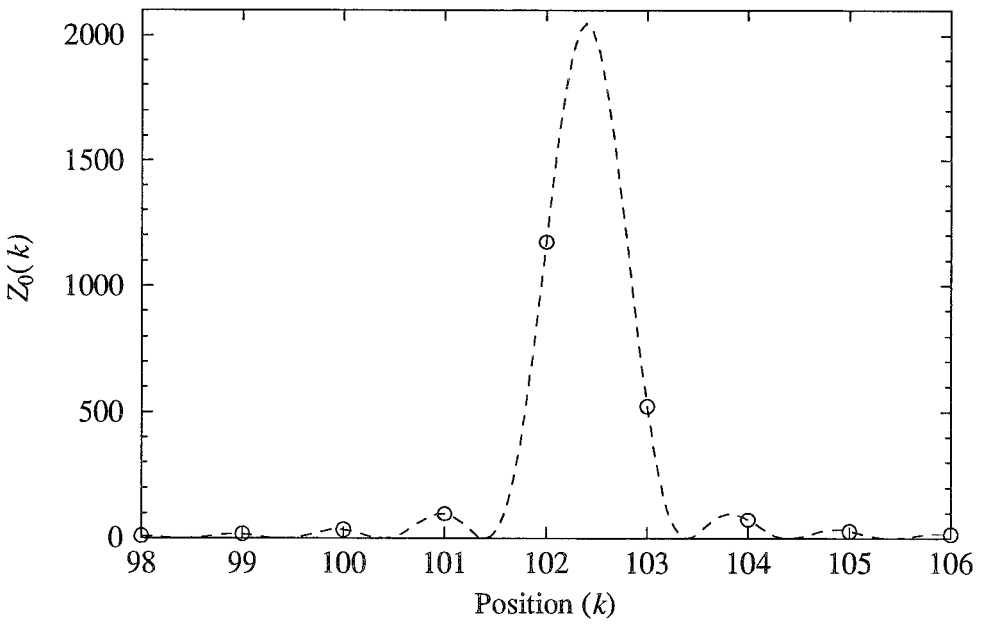

Figure 29. Plot of $Z_0(k)$ vs. k, for $N = 2048$ and $f_i T_s = 0.05$. For points around $f_i N T_s$ only.

$$
\begin{aligned}
&= \frac{Z_0(k_i)}{Z_0(k_i \pm 1)} \\
&= \frac{\frac{\sin^2(\pi f_i N T_s)}{N \sin^2\left(\frac{\pi}{N}[f_i N T_s - k_i]\right)}}{\frac{\sin^2(\pi f_i N T_s)}{N \sin^2\left(\frac{\pi}{N}[f_i N T_s - (k_i \pm 1)]\right)}} \\
&= \frac{\sin^2\left(\frac{\pi}{N}[f_i N T_s - (k_i \pm 1)]\right)}{\sin^2\left(\frac{\pi}{N}[f_i N T_s - k_i]\right)} \, .
\end{aligned} \tag{3.64}
$$

Substituting, $\delta_i = f_i N T_s - k_i$ into the above equation yields

$$
B = \frac{\sin^2\left(\frac{\pi}{N}[\delta_i \mp 1]\right)}{\sin^2\left(\frac{\pi}{N}\delta_i\right)} = \frac{\sin^2\left(\frac{\pi}{N}[\pm 1 - \delta_i]\right)}{\sin^2\left(\frac{\pi}{N}\delta_i\right)} \, . \tag{3.65}
$$

Since $|\delta_i| \leq \frac{1}{2}$, both $\frac{\pi}{N}\delta_i$ and $\frac{\pi}{N}[\pm 1 - \delta_i]$ are small, so the approximation $\sin x \cong x$ can be used. Therefore

$$
B \cong \frac{\left[\frac{\pi}{N}\right]^2 [\pm 1 - \delta_i]^2}{\left[\frac{\pi}{N}\right]^2 [\delta_i]^2} = \left[\frac{\pm 1}{\delta_i} - 1\right]^2 \, . \tag{3.66}
$$

Taking the positive square root of both sides yields

$$
\sqrt{B} \cong \frac{\pm 1}{\delta_i} - 1 \, , \tag{3.67}
$$

which implies

$$\delta_i \cong \frac{\pm 1}{1+\sqrt{B}} \,. \tag{3.68}$$

To take advantage of this relationship, note that $X_D(k) \cong \mathbf{E}[X_D(k)]$ for large D, so using

$$B = \frac{X_D(k_i) - (\sigma_s^2 + N_0)}{X_D(k_i \pm 1) - (\sigma_s^2 + N_0)} \tag{3.69}$$

in Eq. 3.68 produces a satisfactory estimate of δ_i. Since N_0 is unknown, this method cannot be used directly. However, since typically $\sigma_s^2 \gg N_0$, the effect of the noise can be disregarded, and σ_s^2 used in place of $\sigma_s^2 + N_0$. Alternatively, a method for estimating $\sigma_s^2 + N_0$, such as the one discussed along with estimating the power ratio in Section 3.3.5, can be used instead.

In summary, the frequency of the interfering tone can be estimated as follows. First, find the largest value in the average periodogram, and let k_i denote its position. If the largest neighbour of $X_D(k_i)$ is $X_D(k_i + 1)$, find the ratio

$$B = \frac{X_D(k_i) - \sigma_s^2}{X_D(k_i + 1) - \sigma_s^2} \,, \tag{3.70}$$

and estimate the frequency of the tone by

$$\widehat{f}_i = \frac{k_i}{NT_s} + \frac{\frac{1}{1+\sqrt{B}}}{NT_s} \,. \tag{3.71}$$

On the other hand, if the largest neighbour is $X_D(k_i - 1)$, find the ratio

$$B = \frac{X_D(k_i) - \sigma_s^2}{X_D(k_i - 1) - \sigma_s^2} \,, \tag{3.72}$$

and estimate the frequency of the tone by

$$\widehat{f}_i = \frac{k_i}{NT_s} - \frac{\frac{1}{1+\sqrt{B}}}{NT_s} \,. \tag{3.73}$$

3.3.5 Power Ratio Estimation

For proper cancellation of the interfering tone, the ratio $C = (\sigma_s^2 + N_0)/K_i^2$ must be estimated as well as the frequency of the tone. This estimate can also be extracted from the average periodogram.

To produce this estimate, a couple of intermediate quantities must be generated. The first one is the average of all points in the AP. Let

$$S_1 = \frac{1}{N} \sum_{k=-\frac{N}{2}}^{\frac{N}{2}-1} X_D(k) \, . \tag{3.74}$$

The second quantity is the sum of only a few points in the AP, centered around the position of the tone spike, k_i. Let M denote the number of points to sum, where M is odd, and let $c = (M-1)/2$. This quantity is then given by

$$S_2 = \sum_{k=k_i-c}^{k_i+c} X_D(k) \, . \tag{3.75}$$

Once S_1 and S_2 have been calculated, estimators for $\sigma_s^2 + N_0$ and K_i^2 can be generated with

$$\theta_1 = \frac{NG_M(\delta_i)S_1 - S_2}{NG_M(\delta_i) - M} \tag{3.76}$$

and

$$\theta_2 = \frac{S_2 - MS_1}{NG_M(\delta_i) - M} \, , \tag{3.77}$$

respectively, where the function

$$G_M(\delta_i) \triangleq \frac{1}{N} \sum_{k=k_i-c}^{k_i+c} Z_0(k) \tag{3.78}$$

represents the fraction of the power of the tone that is contained in the M points centered around k_i. This is a function of δ_i, which was defined in Eq. (3.62) and measures how close the frequency of the tone is to the spike in the AP. Fig. 30 contains plots of $G_M(\delta_i)$ for various values of M when $N = 2048$. In practice, $G_M(\delta_i)$ can be approximated by using linear

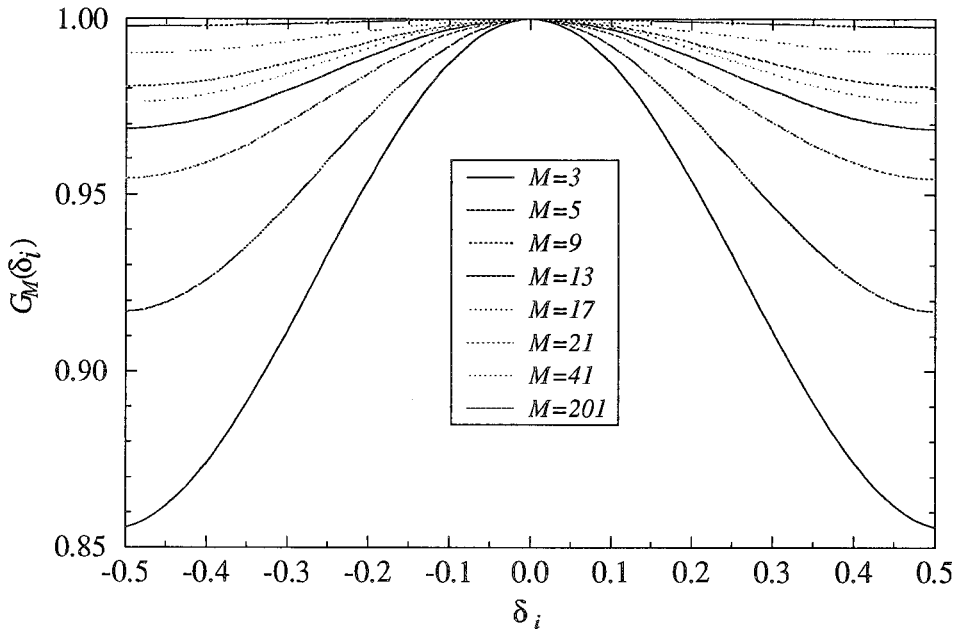

Figure 30. Plot of $G_M(\delta_i)$ vs. δ_i, for N = 2048 and for various values of M.

interpolation, and since δ_i is unknown at the receiver, the quantity $\widehat{\delta_i} = \widehat{f_i} NT_s - \widehat{k_i}$ is used in its place. As confirmed by the experimental results in the next chapter, this approximation has little impact the performance of the interference canceller.

In Appendix C, it is shown that θ_1 and θ_2 are unbiased estimators for $\sigma_s^2 + N_0$ and K_i^2, respectively. It is also shown that their variances are approximately

$$\mathbf{Var}[\theta_1] \cong \frac{1}{(N-M)D}\left[\left(\sigma_s^2 + N_0\right)^2 + \left(\sigma_4^2 - 2\left(\sigma_s^2\right)^2\right)\frac{N-M}{N}\right] \tag{3.79}$$

and

$$\mathbf{Var}[\theta_2] \cong \frac{1}{ND}\left[\left(\sigma_s^2 + N_0\right)^2 \frac{M}{N-M} + 2\left(\sigma_s^2 + N_0\right)K_i^2\right]. \tag{3.80}$$

Note that $\mathbf{Var}[\theta_1]$ and $\mathbf{Var}[\theta_2]$ are roughly proportional to $1/ND$. This implies that these estimates are very accurate for large N, and, in addition, the accuracy increases as more blocks are added to the AP. Because of these properties, the quantity

$$\widehat{C} = \frac{\theta_1}{\theta_2} \tag{3.81}$$

can be used as an estimate for the power ratio $C = \left(\sigma_s^2 + N_0\right)/K_i^2$. Note, however, that $\widehat{C}$ is not an unbiased estimator for C since division is not a linear operation. Nonetheless, it

is generally sufficient for the purposes of the tone canceller, usually providing very reliable estimates of the power ratio. There is, unfortunately, a situation where this is not the case. When the tone is very weak, C can be a very large number. In fact, $C \rightarrow \infty$ as $K_i^2 \rightarrow 0$. The same can not be said for $\widehat{C}$, however. By inspecting Eq. (3.80), it is apparent that the variance of θ_2 does not tend to zero as $K_i^2 \rightarrow 0$. Because of this non-zero variance, θ_2 can be much larger than K_i^2 when the tone is weak. As a result, $\widehat{C}$ does not tend to infinity as $K_i^2 \rightarrow 0$, but instead levels off at some maximum value. In implications of this problem are explored more thoroughly in the next chapter.

In summary, the estimate for the power ratio can be found by first calculating S_1 and S_2 with Eqs. (3.74) and (3.75), and then using the results to calculate θ_1 and θ_2 with Eqs. (3.76) and (3.77). Then calculate

$$\widehat{C} = \frac{\theta_1}{\theta_2} \tag{3.82}$$

as an estimate for $C = \left(\sigma_s^2 + N_0\right)/K_i^2$. The estimate θ_1 could also be used by the frequency estimator instead of $\sigma_s^2 + N_0$ in Eq. (3.69).

3.3.6 Decision Feedback for Frequency and Power Ratio Estimation

As in the case of the interference estimator (see Subsection 3.2.3), the strong presence of the data signal in the received samples is the primary factor limiting the accuracy of the parameter estimators. Here, too, the use of decision feedback significantly improves results and is very easy to implement. As each sample, $r_d(n)$, is received by the parameter estimator, the corresponding detected symbol, $\widehat{I}_{n+dN}$, is subtracted from it. The periodogram for the d^{th} block is then calculated as

$$X_d(k) = \frac{1}{N}\left|\sum_{n=0}^{N-1}\left(r_d(n) - \widehat{I}_{n+dN}\right)e^{-j2\pi\frac{kn}{N}}\right|^2 . \tag{3.83}$$

The average periodogram resulting when decision feedback is used has essentially the same properties as the one described earlier in this section. Theoretical analysis is difficult, but

by replacing σ_s^2 with $\sigma_\epsilon^2 \triangleq \mathbf{E}\left[\left|I_a - \widehat{I}_a\right|^2\right]$, the mean and variance are approximately (see Eqs. (3.55) and (3.56))

$$\mathbf{E}[X_D(k)] \cong \sigma_\epsilon^2 + N_o + K_i^2 Z_0(k) \,, \tag{3.84}$$

and

$$\mathbf{Var}[X_D(k)] \cong \frac{1}{D}\left[\left(\sigma_\epsilon^2 + N_0\right)^2 + 2\left(\sigma_\epsilon^2 + N_0\right)K_i^2 Z_0(k)\right] \,. \tag{3.85}$$

By using the same procedure described earlier, an accurate estimate of f_i can be produced. Also, the quantity $\widehat{C}$ estimates $\left(\sigma_\epsilon^2 + N_0\right)/K_i^2$ when feedback is used, instead of $\left(\sigma_s^2 + N_0\right)/K_i^2$. However, if feedback is also used by the interference estimator, $\widehat{C}$ estimates the desired value.

3.4 Summary and Conclusion

Fig. 31 contains a block diagram of the proposed tone interference canceller. The received signal, $r(t)$, after demodulation and filtering, is sampled at the symbol sampling instants, $t = aT_s$. From each sample, R_a, an estimate of the interference present in the sample, $\widehat{Z}_a$, is subtracted. The resulting decision variable, R'_a, is used by the symbol detector to produce the detected symbol, $\widehat{I}_a$, which is expected to be the same as the transmitted symbol. Since the tone interference has been removed from the decision variable, this is likely to be the case.

To estimate the interference present in each sample, a simple tapped delay line is used, as is shown in Fig. 32. The tone is estimated as

$$\widehat{Z}_a = \sum_{n=1}^{L} \widehat{\mathrm{w}}_n \left(R_{a-n} - \widehat{I}_{a-n}\right) \,, \tag{3.86}$$

where $\{R_{a-n}\}$ are previously received samples, and $\{I_{a-n}\}$ are previously detected symbols. The weights, $\{\widehat{\mathrm{w}}_n\}$, are calculated by

$$\widehat{\mathrm{w}}_n = \frac{1}{L + \widehat{C}} \exp\left(j2\pi \widehat{f}_i n T_s\right) \,, \tag{3.87}$$

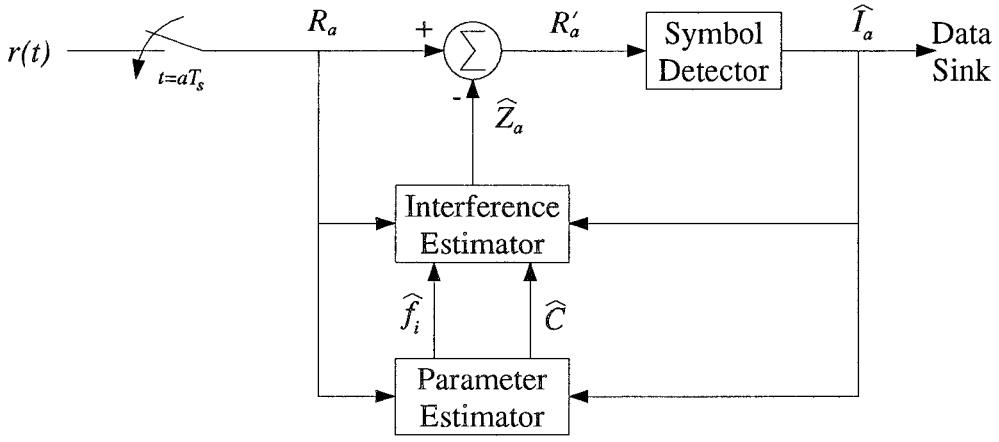

Figure 31. Tone Interference Canceller.

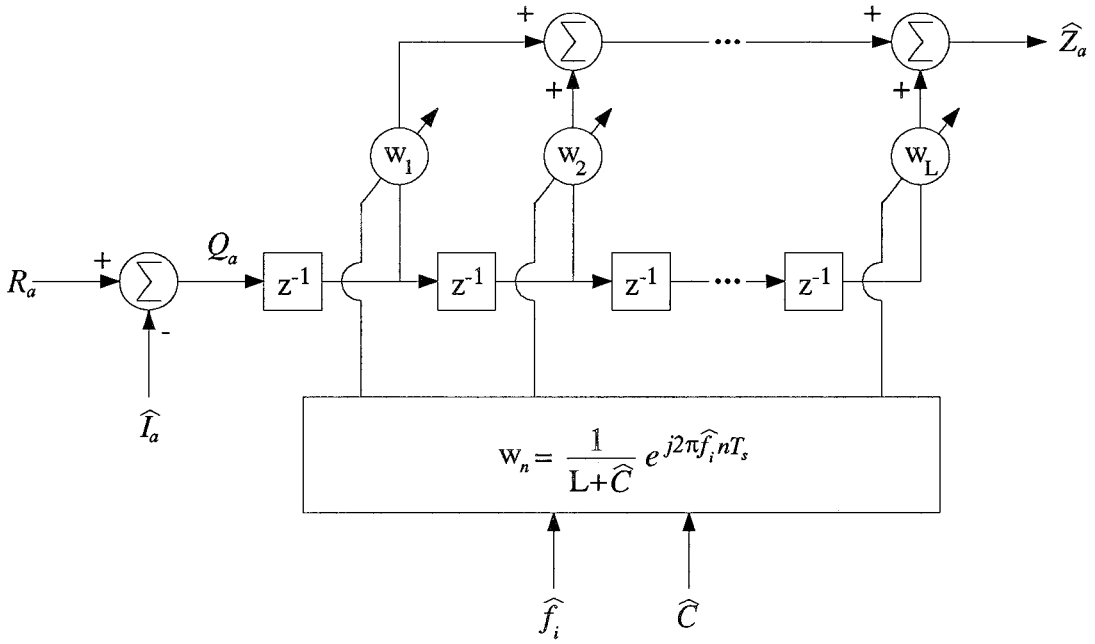

Figure 32. Interference Estimator

where $\widehat{f}_i$ is an estimate of the frequency of the interfering tone, and $\widehat{C}$ is an estimate of $(\sigma_\epsilon^2 + N_0)/K_i^2$. The quantity σ_ϵ^2 equals $\mathbf{E}\left[\left|I_a - \widehat{I}_a\right|^2\right]$, an unknown value that depends on the power of the transmitted symbols and the probability of detection error. Both $\widehat{f}_i$ and $\widehat{C}$ are generated by the parameter estimator. The number of samples used, L, is a fixed design parameter. It should be selected to be as large as possible, but inaccuracies in $\widehat{f}_i$ place a theoretical limit on how large it can be.

In practice, the cost of a long tapped delay line will be the primary limitation on L. However, an alternate realization can be used that is considerably cheaper. To motivate this realization, let

$$Q_a = R_a - \widehat{I}_a \ , \tag{3.88}$$

so that

$$\begin{aligned}
\widehat{Z}_a &= \sum_{n=1}^{L} \mathrm{w}_n Q_{a-n} \\
&= \frac{1}{L+\widehat{C}} \sum_{n=1}^{L} Q_{a-n} e^{j2\pi \widehat{f}_i n T_s} \\
&= \frac{1}{L+\widehat{C}} \sum_{n=0}^{L-1} Q_{a-(n+1)} e^{j2\pi \widehat{f}_i (n+1) T_s} \\
&= \frac{1}{L+\widehat{C}} \left[\sum_{n=1}^{L} Q_{a-(n+1)} e^{j2\pi \widehat{f}_i (n+1) T_s} + Q_{a-1} e^{j2\pi \widehat{f}_i T_s} - Q_{a-(L+1)} e^{j2\pi \widehat{f}_i (L+1) T_s} \right] \\
&= \left[\frac{1}{L+\widehat{C}} \sum_{n=1}^{L} Q_{a-1-n} e^{j2\pi \widehat{f}_i n T_s} \right] e^{j2\pi \widehat{f}_i T_s} + \mathrm{w}_1 Q_{a-1} - \mathrm{w}_{(L+1)} Q_{a-(L+1)} \\
&= \widehat{Z}_{a-1} e^{j2\pi \widehat{f}_i T_s} + \mathrm{w}_1 Q_{a-1} - \mathrm{w}_{(L+1)} Q_{a-(L+1)} \ .
\end{aligned} \tag{3.89}$$

This equation provides a means for generating the interference estimate at $t = aT_s$ by updating the estimate from the previous sampling instant. Using this property, the interference can be estimated with the device shown in Fig. 33. Since this implementation requires fewer adders and multipliers, a much larger value of L can be used without significantly increasing cost.

The frequency and power ratio are estimated from the AP computed from the received signal. The detected symbol is subtracted from the received sample, and the result is stored in a buffer of length N. Let $r_d(n)$ denote the n^{th} value stored in the buffer while processing the d^{th} block. Then

$$r_d(n) = R_{n+dN} - \widehat{I}_{n+dN} \ . \tag{3.90}$$

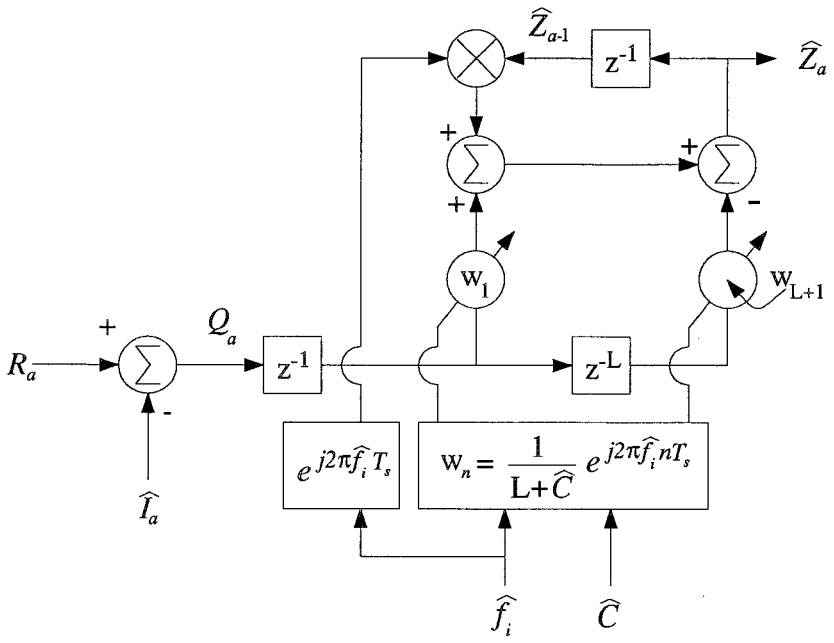

Figure 33. Reduced Complexity Realization of Interference Estimator

When the buffer is full, a FFT is performed on the data. The transformed block, $\{R_d(k)\}$ also contains N values. The d^{th} periodogram is computed from the transformed block as

$$X_d(k) = \tfrac{1}{N}|R_d(k)|^2 \,. \tag{3.91}$$

This periodogram is included in a running average of all the previously computed periodograms. This average periodogram is

$$X_D(k) = \tfrac{1}{D}\sum_{d=0}^{D-1} X_d(k) \,, \tag{3.92}$$

where D is the total number of blocks currently processed. The block length, N, is another fixed design parameter. It too should be selected to be as large as possible, however economic considerations limit its size.

From the data in the average periodogram, $\widehat{f}_i$ and $\widehat{C}$ are calculated. To estimate the frequency, the largest value in the AP is found, and its position is denoted by k_i. If $X_D(k_i+1)$ is found to be greater than $X_D(k_i-1)$, the quantity

$$B = \frac{X_D(k_i) - \theta_1}{X_D(k_i+1) - \theta_1} \tag{3.93}$$

is computed, where θ_1 is an estimate for $\sigma_\epsilon^2 + N_0$. If no estimate is available, a value of zero can be used instead. With B, the quantity $\widehat{\delta}_i$ is computed by $\widehat{\delta}_i = 1/\left(1+\sqrt{B}\right)$, and the frequency is estimated as $\widehat{f}_i = \left(k_i + \widehat{\delta}_i\right)/(NT_s)$. If, however, $X_D(k_i+1)$ is found to be less than $X_D(k_i-1)$, the quantity

$$B = \frac{X_D(k_i) - \theta_1}{X_D(k_i - 1) - \theta_1} \tag{3.94}$$

is computed instead, and, with $\widehat{\delta}_i = -1/\left(1+\sqrt{B}\right)$, the frequency is estimated as $\widehat{f}_i = \left(k_i + \widehat{\delta}_i\right)/(NT_s)$.

To estimate the power ratio, the quantities

$$S_1 = \tfrac{1}{N} \sum_{k=-\frac{N}{2}}^{\frac{N}{2}-1} X_D(k)\,, \tag{3.95}$$

and

$$S_2 = \sum_{k=k_i-c}^{k_i+c} X_D(k) \tag{3.96}$$

are calculated from the average periodogram, where $c = (M-1)/2$, with M being the number of points to sum around the spike caused by the tone. With S_1 and S_2, the quantities

$$\theta_1 = \frac{NG_M\left(\widehat{\delta}_i\right)S_1 - S_2}{NG_M\left(\widehat{\delta}_i\right) - M}\,, \tag{3.97}$$

and

$$\theta_2 = \frac{S_2 - MS_1}{NG_M\left(\widehat{\delta}_i\right) - M} \tag{3.98}$$

are computed, where $G_M\left(\widehat{\delta}_i\right)$ is the fraction of the tone spike that is contained within the M points centered around k_i. Note that θ_1 is an unbiased estimator of $\sigma_s^2 + N_0$, and θ_2 is an unbiased estimator of K_i^2. The estimate $\widehat{C}$ is finally generated by $\widehat{C} = \theta_1/\theta_2$.

Using the procedure outlined above, extremely effective interference cancellation will be achieved. Theoretically, near-optimal performance in terms of the MSE is possible. In the next chapter, experimental results are presented to support this claim.

Chapter Four

Computer Simulation Results

4.1 Introduction

The theoretical analysis of the proposed interference canceller included in the previous chapter indicated that it should have near-optimal performance in the MMSE sense. Furthermore, using decision feedback and increasing L are both expected to yield better tone cancellation since these actions directly affect the theoretical bound on performance. On the other hand, the block length, N, and the number of blocks processed, D, do not affect the bound, but they do affect how close to the bound the canceller performs.

To support these theoretical claims, computer simulations were employed. This chapter contains a summary of the simulation results, confirming that effective cancellation of tone interference is possible. After a description of the simulation system in Section 4.2, the simulation results when decision feedback is not employed are discussed in Section 4.3. In Section 4.4 the results when decision feedback is employed are studied.

4.2 Computer Simulation System

All the experimental results presented in this chapter were produced by computer simulation of the communication system and interference canceller. Appendix D contains a complete listing of the source code, written entirely in *C*. All results in this chapter pertain to a 16–QAM system with root raised-cosine filters with a roll-off factor of $\alpha = 0.2$, and the average transmitted signal power is $P_s = 10/T_s$. The frequency of the interfering tone and its initial phase were arbitrarily selected as $f_i = 0.05/T_s$, and $\phi_i = 0.0$. Of course, these values were not available for use by the tone canceller. The tests were performed over a wide range of tone and noise powers.

The interference canceller was implemented using the reduced-complexity model of Fig. 33, and the frequency and power ratio estimates were generated from APs using symbol-rate sampling. Unless otherwise stated, a filter length of $L = 32$ was used, and a total of $D = 32$ blocks length of $N = 2048$ were used to compute the AP. In addition, a value of $M = 21$ was used in Eq. (3.75) and Eqs. (3.76)-(3.77) to generate the intermediate estimates θ_1 and θ_2.

To accurately measure the average residual power, a very large number of trials must be executed to ensure statistical convergence of the results. Since a total of $ND = 65536$ samples were processed for each trial, convergence was hastened by using the average over the last $ND/4 = 16384$ samples as the estimate of the residue for that trial. Since the samples in a single trial are not strictly independent, each trial was repeated 2000 times with different random data, and the results were averaged together.

4.3 Cancellation Without Decision Feedback

In Section 3.2, the theoretical performance of the linear MMSE estimator was studied, and the maximum performance gain was plotted in Fig. 17. For the sake of convenience

in comparison, this figure is repeated in Fig. 34. As noted, this data represents a bound that limits the performance gain of all tone interference cancellers that use linear estimates without employing decision feedback to reduce the effect of the data signal. In Fig. 35 the simulated results for the proposed canceller are presented. By inspecting this graph it is clear that if the SIR is less than about 20 dB, some cancellation of the tone is possible. This performance is almost identical to the theoretical bound in Fig. 17. If the SIR is in the 20–40 dB range, very little cancellation occurs. Again, this performance is in agreement with the bound. However, if the SIR is greater than about 40 dB a minor problem is apparent. In this region the canceller exhibits a negative gain, indicating that additional distortion is being introduced. While this situation is undesirable, it should be pointed out that this additional distortion is very insignificant, since it is proportionate to the strength of the tone, which itself is very weak in this region.

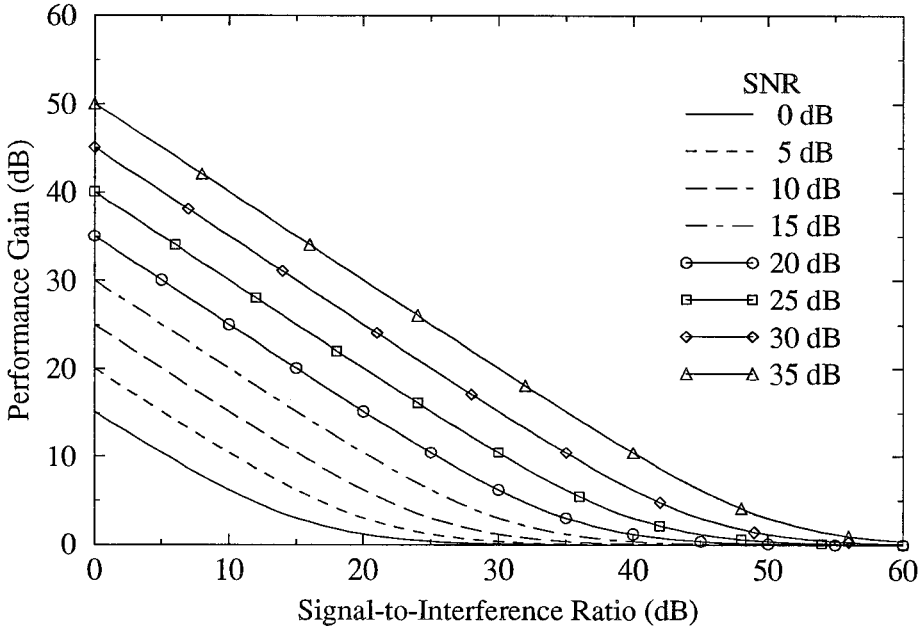

Figure 34. Theoretical Performance Gain vs. SIR, L = 32, N = 2048, D = 32, without decision feedback

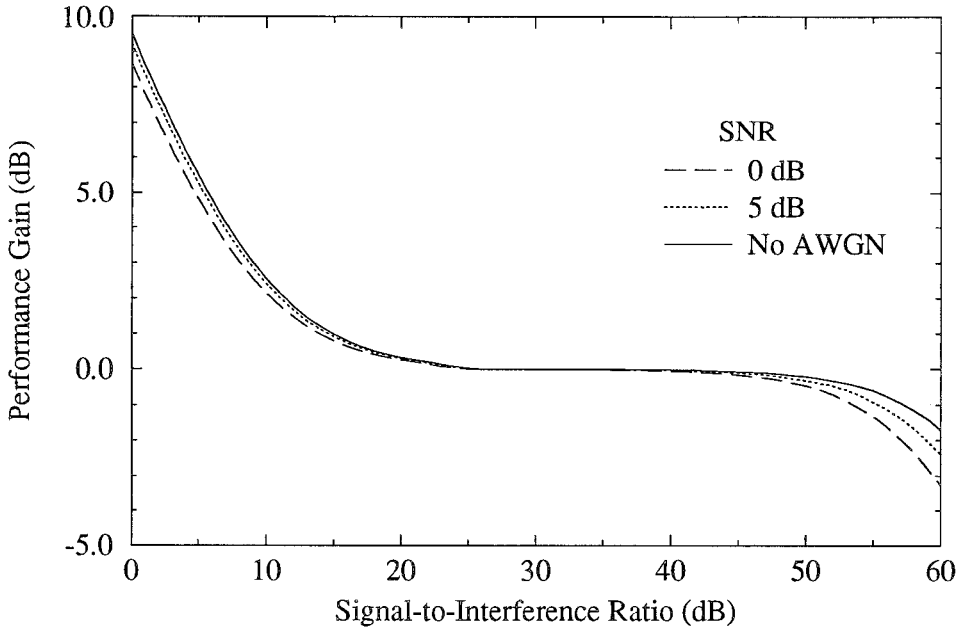

Figure 35. Simulated Performance Gain vs. SIR, L = 32, N = 2048, D = 32, without decision feedback

Another way to express the effectiveness of the interference cancellation is consider to the SRR, which is plotted in Fig. 36 for the simulated results. Clearly all tones with a SIR greater than 0 dB are reduced to residues with SRRs of greater that 8 dB. As such, the probability of transmission error will be lower that if no attempt was made to cancel a strong interfering tone. As noted, when the SIR is greater that about 40 dB, the SRR is less that the SIR, but the SRR is nonetheless greater than 40 dB when the tone is this weak. Clearly this will have no practical effect on the probability of transmission error. As the SIR increases without bound, the SRR, instead of also increasing, actually levels off to a residue floor. Results of simulation when no tone is present have indicated that this floor is at about 60 dB. The proposed canceller can not reduce the residue below the floor, and interference that is weaker than the floor will be increased to that level. This phenomenon is a result of inaccuracies in the estimate of the power ratio, and in particular, the problem with θ_2 not tending to zero

as $K_i^2 \rightarrow 0$ that was discussed in Subsection 3.3.5. Fortunately, since the variance of θ_2 is inversely proportional to D, the residue floor decreases as D is increased. As the amount of time that the receiver has been tuned to a single TV station increases, more blocks are included in the AP, thereby reducing the variance of θ_2, leading to a lower residue floor. This is confirmed through simulation in the next section.

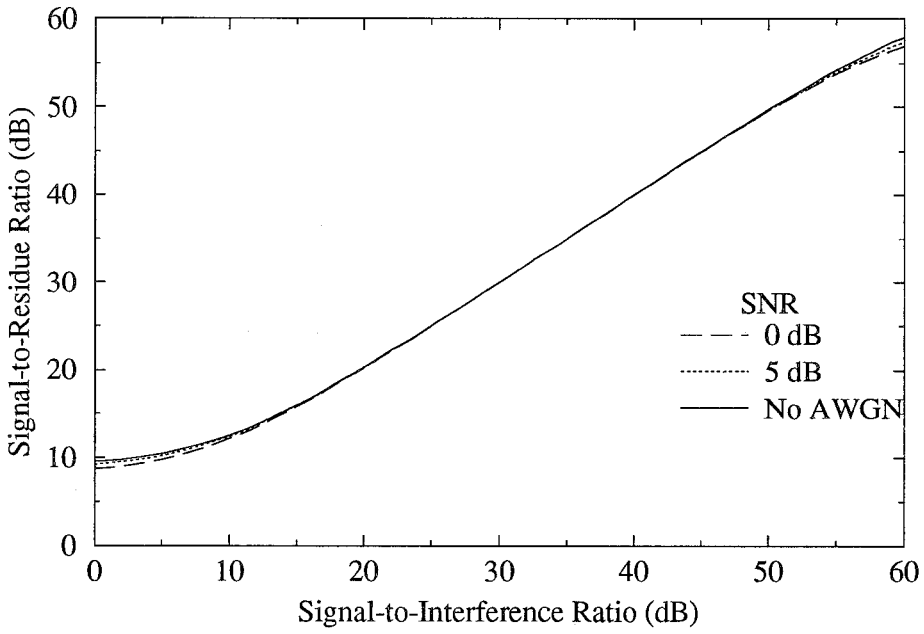

Figure 36. Simulated SRR vs. SIR, L = 32, N = 2048, D = 32, without decision feedback

With the exception of the introduction of distortion when the tone is weak, the proposed canceller performs as well as can be expected. For practical purposes, the bound has been achieved. However, without the use of decision feedback, the gain is limited to less than 8 dB. Significantly better results can be achieved when the detected symbols are used to reduce the power of the transmitted data in the received signal by means of a feedback mechanism.

4.4 Cancellation with Decision Feedback

As noted in Section 3.2, using the detected symbols to reduce the power of the data signal before attempting to estimate the tone is expected to provide substantially better interference cancellation. The theoretical bound in this case, presented originally in Fig. 23, is repeated in Fig. 37. Comparison with the simulated results, which are shown in Fig. 38, confirms that the performance gain is better than when feedback is not employed, and that the results are very close to the bound over a wide range of distortion conditions. Of course, when the tone is weak (*i.e.*, SIR > 50 dB) additional distortion is still introduced due to the residue floor, but it is at a noticeably lower level. Also, when the noise is strong (*i.e.*, SNR < 10 dB), the performance gain is somewhat lower than predicted by the bound. This occurs because of the high number of transmission errors that occur at these noise levels. Since the data is not completely removed less accurate estimates of the tone are produced. Unfortunately, without knowing the true MMSE it is impossible to determine whether this is a problem with the proposed estimator using sub-optimal weights or actually a property of the optimal estimator. Nonetheless, performance is better at these noise levels than when decision feedback is not used. In addition, since reliable communication is not possible when the noise is this strong, the performance of the canceller is not particularly relevant.

Aside from using decision feedback, the theoretical bound can only be improved by increasing the number of samples on which the estimate of the tone is based. In the previous performance results a value of $L = 32$ samples was used. In Fig. 39 the theoretical bound on performance when $L = 1000$ is shown. Note that by using the reduced complexity model of Fig. 33, it is possible to implement the proposed canceller economically with such a large value of L, since the number of multipliers and adders does not increase with L, as in the case of the transervsal filter. This is a distinct advantage over traditional linear estimators. Simulated performance evaluation results are presented in Fig. 40. Other than the residue

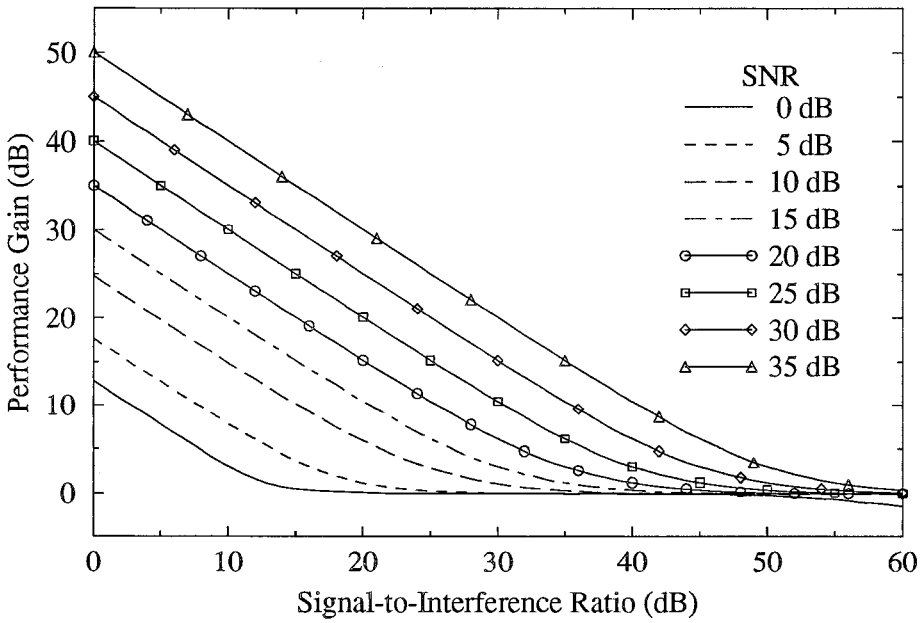

Figure 37. Theoretical Performance Gain vs. SIR, L = 32, N = 2048, D = 32, with decision feedback.

floor, which is substantially higher, the performance is slightly sub-optimal in the regions where the performance gain is small (*i.e.* $G' < 10$ dB). Inaccuracy in the frequency estimates are the likely cause. Nonetheless, performance is considerably better that when L = 32, with about 15 dB better cancellation.

As more blocks are included in the AP, it is expected that more reliable estimates of f_i and C will be produced. In particular, the reduced variance of θ_2 should lead to a reduction of the residue floor. This is confirmed by the simulated performance results depiction in Fig. 41, which shows that performance gain after D = 128 blocks have been processed, as opposed to the results presented in Fig. 38 when D = 32. Note that the residue floor does not affect the performance for any of the interference conditions depicted in this graph.

Although performance improves over time as D increases, the parameter N is much more important. The results of repeating the simulation with N = 32 and D = 2048 are presented

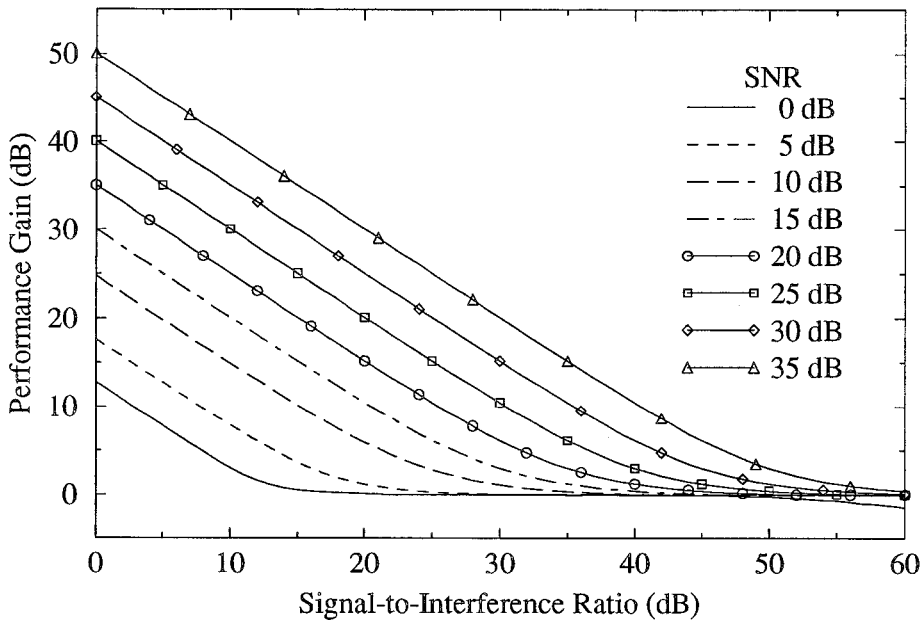

Figure 38. Simulated Performance Gain vs. SIR, L = 32, N = 2048, D = 32, with decision feedback.

in Fig. 42. Note that even though the same total number of samples have been processed as in the simulation of Fig. 38, the residue floor is much higher. Otherwise, the results are still very acceptable.

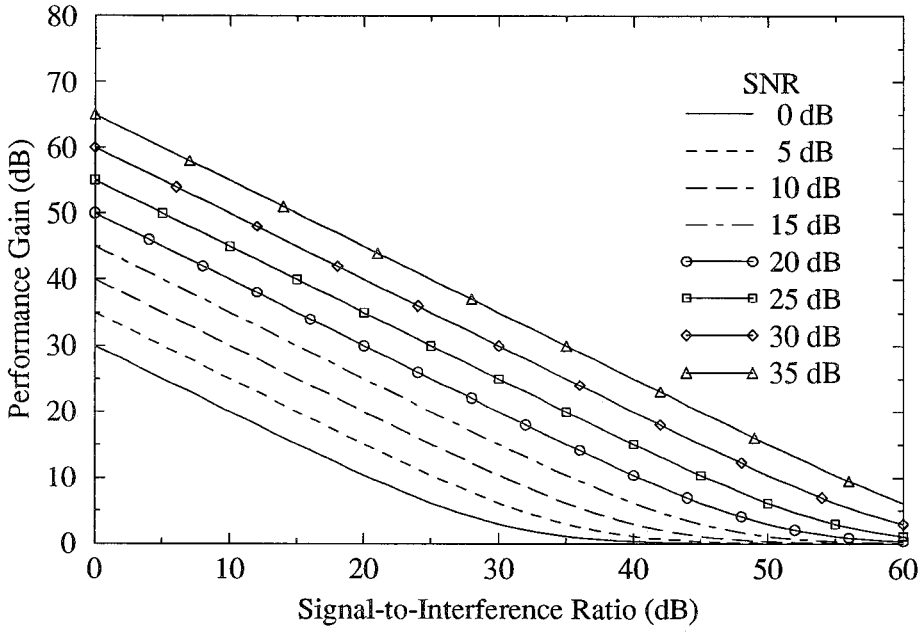

Figure 39. Theoretical Performance Gain vs. SIR, $L = 1000$, $N = 2048$, $D = 32$.

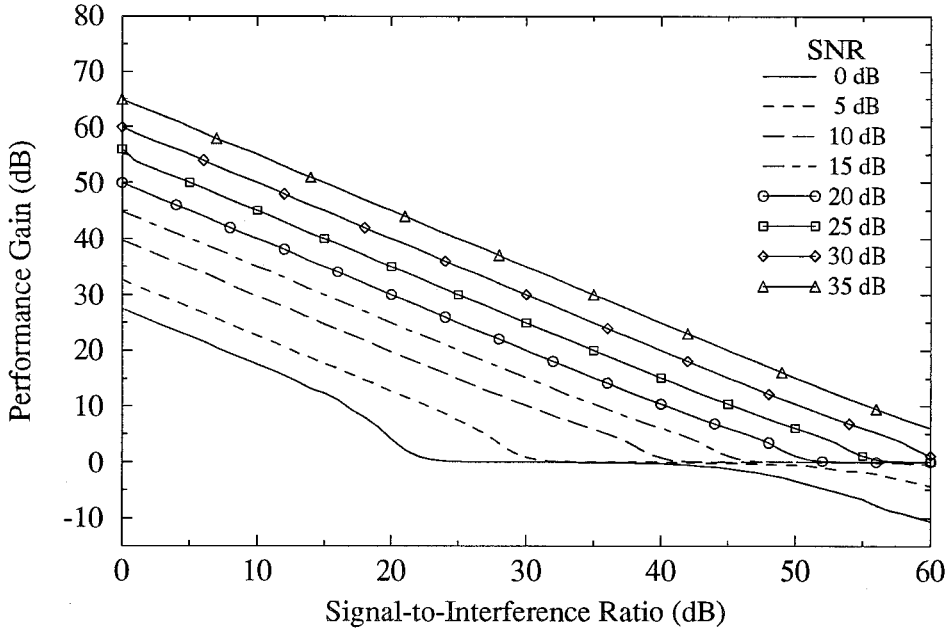

Figure 40. Simulated Performance Gain vs. SIR, $L = 1000$, $N = 2048$, $D = 32$.

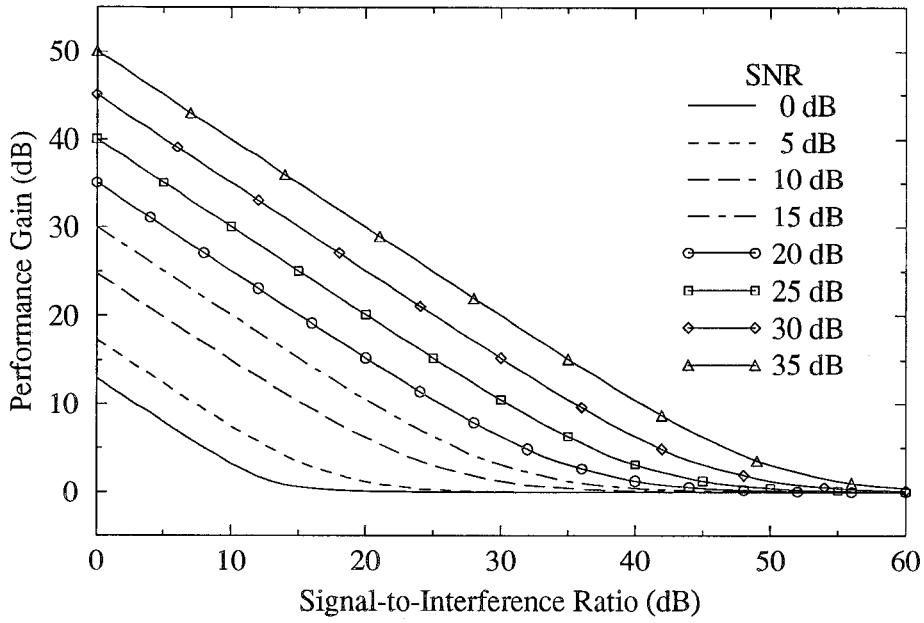

Figure 41. Simulated Performance Gain vs. SIR, $L = 32$, $N = 2048$, $D = 128$.

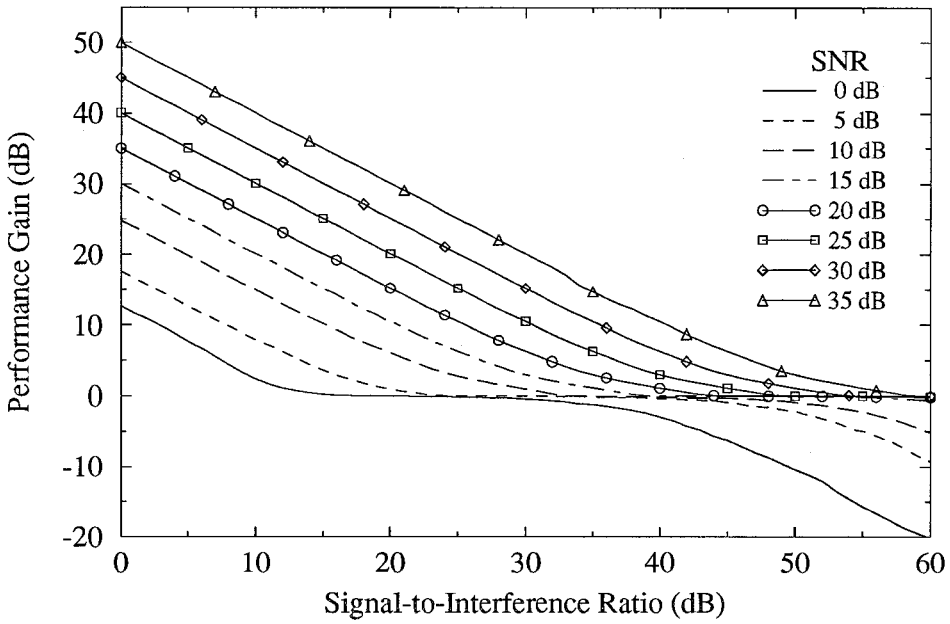

Figure 42. Simulated Performance Gain vs. SIR, $L = 32$, $N = 32$, $D = 2048$.

Chapter Five

Conclusions and Future Research Topics

The various all-digital HDTV systems currently being considered by the FCC are capable of delivering high resolution, wide aspect ratio video signals to home viewers over existing cable TV networks. The impressive compression rates of the source encoders allow for transmission without the use of additional bandwidth. Furthermore, the powerful error protection ensures high quality image reception under normal operating conditions. The presence of a strong interfering tone, however, may defeat the ability of the error correcting codes, leading to severe image degradation. In this case the use of some form of tone cancellation may be required at the receiver.

In this thesis an effective tone canceller has been proposed. This device is based on a linear estimator, and is a suboptimal direct implementation of the minimum mean-square error estimator, with performance that is very close to the theoretical optimum under most

circumstances. Simulated performance analysis confirmed that cancellation can be applied to reduce the tone to negligible levels, thereby allowing impairment-free image reception.

Finally, the following is a list of topics which can be considered for further research.

- **MULTIPLE TONES**

  If multiple tones, closely spaced in frequency as in the case of CTB, interfere with the HDTV signal, some cancellation is expected from using the proposed device directly, but performance may be far from optimal. Further theoretical and experimental analysis is required. One the other hand, for cancelling tones that are well separated some modifications will definitely have to be made. However, these modifications should be relatively minor as this problem was a secondary design consideration of the proposed system. Nonetheless, extensive analysis and testing is required to support this claim.

- **NON-STATIONARY TONES**

  The performance of the proposed canceller should be investigation if the interfering tone is non-stationary. Methods for tracking slow variations in the tone's frequency and power should be developed.

- **THRESHOLD CANCELLATION**

  To prevent distortion from being introduced because of the residue floor, methods for determining if the tone is below a certain threshold, and hence too weak to cancel should be developed. Under this condition the canceller would be disabled.

- **ALTERNATIVE FREQUENCY ESTIMATION METHODS**

  Although the use of the periodogram provides an extremely reliable estimate of the tone's frequency, it may be unduly complex. Since the accuracy provided is excessive, a less complicated method may be capable of providing adequate results. In addition, the periodogram is ill-suited for tracking frequency variations and distinguishing between

closely spaced tones. In hindsight, the periodogram may not be the most versatile tool for frequency estimation. Alternate methods should be investigated.

References

[1] R. E. Wiley, "A U.S. HDTV Update," in *HDTV '90 Colloquiem Proceedings*, vol. 1, (Ottawa), pp. 1.4.1–1.4.5, 1990.

[2] D. Wood and J. Tejerina, "The Current EBU Analysis of the CIF and CDR HDTV Production Formats," in *HDTV '90 Colloquiem Proceedings*, vol. 1, (Ottawa), pp. 4A.2.1–4A.2.15, 1990.

[3] FCC Advisory Committee on Advanced Television Service, "ATV System Recommendations," *IEEE Transactions on Broadcasting*, vol. BC-39, pp. 2–245, Mar. 1993.

[4] R. Hopkins, "Digital HDTV Broadcasting," *IEEE Transactions on Broadcasting*, vol. BC-37, pp. 123–127, Dec. 1991.

[5] J. A. Krauss, "Source Coding, Channel Coding, and Modulation Techniques Used in the DigiCipher System," *IEEE Transactions on Broadcasting*, vol. BC-37, pp. 158–161, Dec. 1991.

[6] G. W. Beakley, "Channel Coding for Digital HDTV Terrestrial Broadcasting," *IEEE Transactions on Broadcasting*, vol. BC-37, pp. 137–140, Dec. 1991.

[7] P. Nasiopoulos and R. K. Ward, *HDTV: Advanced Television for the 1990's*. Univ. of British Columbia, Aug. 1992.

[8] J. N. Slater, *Modern Television Systems to HDTV and beyond.* London: Pitman, 1991.

[9] E. R. Bartlett, *Cable Television Technology and Operations: HDTV and NTSC Systems.* New York: McGraw-Hill, 1990.

[10] J. A. Chiddix, "Fiber Backbone Trunking in Cable Television Networks: An Evolutionary Adoption of New Technology," *IEEE LCS Magazine*, vol. 1, pp. 32–37, Feb. 1990.

[11] J. N. Slater, *Cable Television Technology.* Chichester, U.K.: Ellis Horwood, 1988.

[12] W. S. Ciciora, "An Introduction to Cable Television in the United States," *IEEE LCS Magazine*, vol. 1, pp. 19–25, Feb. 1990.

[13] R. Joshi, J. C. Anbak, and R. Prasad, "A Method for Intermodulation Noise Calculations in a Cable Television Network with HD-MAC, PAL, and RM Radio Signals," *IEEE Transactions on Broadcasting*, vol. BC-38, pp. 177–185, Sept. 1992.

[14] K. A. Simons, "The Decibel Relationships Between Amplifier Distortion Products," *Proceedings of the IEEE*, vol. 88, pp. 1071–1086, July 1970.

[15] T. Williams, "Composite Triple Beat: A New Look and a New Problem," *Specs Technology*, pp. 2–6, 1992.

[16] F. G. Stremler, *Introduction to Communication Systems.* Reading, Mass.: Addison-Wesley, 2nd ed., 1982.

[17] T. Kasparis, "Suppression of Nonstationary Sinusoidal Interference using Transform Domain Median Filtering," *IEE Electronics Letters*, vol. 29, no. 2, pp. 176–178, 1993.

[18] R. C. DiPietro, "An FFT Based Technique for Suppressing Narrow-Band Interference in PN Spread Spectrum Communication Systems," in *Proc. of Int'l Conf. on Acoustics, Speech, and Signal Processing*, (Glasgow, Scotland), pp. 1360–1363, May 1990.

[19] B. Widrow *et al.*, "Adaptive Noise Cancelling: Principles and Applications," *Proceedings of the IEEE*, vol. 63, pp. 1692–1716, Dec. 1975.

[20] D. V. Bhaskar Rao and S. Y. Jung, "Adaptive Notch Filtering for the Retrieval of Sinusoids in Noise," *IEEE Transactions on Acoustics, Speech, and Signal Processing*, vol. ASSP-32, pp. 791–802, Aug. 1984.

[21] G. C. Goodwin *et al.*, "Sinusoidal Disturbance Rejection with Application to Helicopter Flight Data Estimation," *IEEE Transactions on Acoustics, Speech, and Signal Processing*, vol. ASSP-34, pp. 479–484, June 1986.

[22] W. K. Pratt, *Digital Image Processing*. New York: John Wiley & Sons, 2nd ed., 1991.

[23] S. Lin and D. J. Costello, Jr., *Error Control Coding: Fundamentals and Applications*. Englewood Cliffs, N.J.: Prentice-Hall, 1983.

[24] J. G. Proakis, *Digital Communications*. New York: McGraw-Hill, 2nd ed., 1989.

[25] H. Meyr and G. Ascheid, *Synchronization in Digital Communication*, vol. 1. New York: John Wiley & Sons, 1990.

[26] A. Papoulis, *Probability, Random Variables, and Stochastic Processes*. New York: McGraw-Hill, 1984.

[27] M. L. Honig and D. G. Messerschmitt, *Adpative Filters: Structures, Algorithms and Applications*. Boston: Kluwer, 1984.

[28] S. M. Ross, *A First Course in Probability*. New York: Macmillan, 2nd ed., 1984.

[29] S. Kay, *Modern Spectral Estimation: Theory and Application*. Englewood Cliggs, N.J.: Prentice Hall, 1988.

[30] J. G. Proakis and D. Manolakis, *Digital Signal Processing*. New York: MacMillan, 2nd ed., 1992.

[31] N. Mohanty, *Signal Processing: Signals, Filtering, and Detection*. New York: Van Nostrand Reinhold, 1987.

Appendix A
MMSE Tone Estimator

In this appendix the assertion that $\widehat{Z}_a$, given by

$$\widehat{Z}_a = \sum_{n=1}^{L} \mathrm{w}_n R_{a-n} \ , \tag{A.1}$$

is the linear minimum mean-squared estimator of Z_a when

$$\mathrm{w}_n = \frac{1}{L+C} e^{j\omega_i n} \ , \tag{A.2}$$

where $C = \left(\sigma_s^2 + N_0\right)/K_i^2$ and $\omega_i = 2\pi f_i T_s$ is proved. This is accomplished by showing that the partial derivatives of the MSE with respect to the real and imaginary parts of each w_n are equal to zero. To begin, note that the MSE is

$$\begin{aligned}
\gamma &= \mathbf{E}\left[\left|Z_a - \widehat{Z}_a\right|^2\right] \\
&= Z_a^* Z_a - Z_a^* \mathbf{E}\left[\widehat{Z}_a\right] - Z_a \mathbf{E}\left[\widehat{Z}_a^*\right] + \mathbf{E}\left[\widehat{Z}_a^* \widehat{Z}_a\right] \\
&= Z_a^* Z_a - Z_a^* \sum_{n=1}^{L} \mathrm{w}_n \mathbf{E}[R_{a-n}] - Z_a \sum_{n=1}^{L} \mathrm{w}_n^* \mathbf{E}\left[R_{a-n}^*\right] \\
&\qquad + \sum_{n=1}^{L} \sum_{m=1}^{L} \mathrm{w}_n^* \mathrm{w}_m \mathbf{E}\left[R_{a-n}^* R_{a-m}\right] \ .
\end{aligned} \tag{A.3}$$

To use this expression, recall from Section 2.6 that since I_a and N_a are zero mean random variables,

$$\begin{aligned}
\mathbf{E}[R_a] &= \mathbf{E}[I_a + N_a + Z_a] \\
&= Z_n \ ,
\end{aligned} \tag{A.4}$$

and

$$\begin{aligned}
\mathbf{E}[R_n^* R_m] &= \mathbf{E}[I_n^* I_m] + \mathbf{E}[N_n^* N_m] + Z_n^* Z_m \\
&= \sigma_s^2 \delta(m-n) + N_0 \delta(m-n) + Z_n^* Z_m \ .
\end{aligned} \tag{A.5}$$

Substituting these expressions into Eq. (A.3) yields

$$\gamma = Z_a^* Z_a - Z_a^* \sum_{n=1}^{L} \mathrm{w}_n Z_{a-n} - Z_a \sum_{n=1}^{L} \mathrm{w}_n^* Z_{a-n}^* + \sum_{n=1}^{L}\sum_{m=1}^{L} \mathrm{w}_n^* \mathrm{w}_m \left[(\sigma_s^2 + N_0)\delta(m-n) + Z_{a-n}^* Z_{a-m} \right] . \tag{A.6}$$

From the definition of Z_a given by Eq. (2.62) it is clear that

$$\begin{aligned} Z_{a-n} &= z(aT_s - nT_s) \\ &= K_i e^{j2\pi f_i (a-n)T_s} e^{j\phi_i} \\ &= K_i e^{j2\pi f_i a T_s} e^{j\phi_i} e^{-j2\pi f_i n T_s} \\ &= Z_a e^{-j2\pi f_i n T_s} \\ &= Z_a e^{-j\omega_i n} , \end{aligned} \tag{A.7}$$

so Eq. (A.6) becomes

$$\gamma = Z_a^* Z_a - Z_a^* Z_a \sum_{n=1}^{L} \mathrm{w}_n e^{-j\omega_i n} - Z_a Z_a^* \sum_{n=1}^{L} \mathrm{w}_n^* e^{j\omega_i n} + Z_a^* Z_a \sum_{n=1}^{L}\sum_{m=1}^{L} \mathrm{w}_n^* \mathrm{w}_m e^{-j\omega_i (m-n)} + \left(\sigma_s^2 + N_0\right) \sum_{n=1}^{L} \mathrm{w}_n^* \mathrm{w}_n . \tag{A.8}$$

By noting that $Z_a^* Z_a = K_i^2$, the above equation can be expressed as

$$\gamma = K_i^2 \left[1 - \sum_{n=1}^{L} \mathrm{w}_n e^{-j\omega_i n} - \sum_{n=1}^{L} \mathrm{w}_n^* e^{j\omega_i n} + \sum_{n=1}^{L}\sum_{m=1}^{L} \mathrm{w}_n^* \mathrm{w}_m e^{-j\omega_i (m-n)} \right] + \left(\sigma_s^2 + N_0\right) \sum_{n=1}^{L} \mathrm{w}_n^* \mathrm{w}_n . \tag{A.9}$$

To find the partial derivatives it is convenient to express each w_n in terms of its real and imaginary components. Let $x_n = \mathbf{Re}[\mathrm{w}_n]$ and $y_n = \mathbf{Im}[\mathrm{w}_n]$ so that $\mathrm{w}_n = x_n + jy_n$. Then Eq. (A.9) becomes

$$\gamma = K_i^2 \left[1 - \sum_{n=1}^{L} (x_n + jy_n) e^{-j\omega_i n} - \sum_{n=1}^{L} (x_n - jy_n) e^{j\omega_i n} \right]$$

$$
\begin{aligned}
&+ K_i^2 \sum_{n=1}^{L} \sum_{m=1}^{L} (x_n - jy_n)(x_n + jy_n) e^{-j\omega_i(m-n)} \\
&+ (\sigma_s^2 + N_0) \sum_{n=1}^{L} (x_n^2 + y_n^2) \\
&= K_i^2 \left[1 - \sum_{n=1}^{L} x_n \left(e^{-j\omega_i n} + e^{j\omega_i n} \right) - j \sum_{n=1}^{L} y_n \left(e^{-j\omega_i n} - e^{j\omega_i n} \right) \right] \\
&+ K_i^2 \sum_{n=1}^{L} \sum_{m=1}^{L} (x_n - jy_n)(x_n + jy_n) e^{-j\omega_i(m-n)} \\
&+ (\sigma_s^2 + N_0) \sum_{n=1}^{L} (x_n^2 + y_n^2) \\
&= (\sigma_s^2 + N_0) \sum_{n=1}^{L} (x_n^2 + y_n^2) + K_i^2 \left[1 - 2 \sum_{n=1}^{L} x_n \cos(\omega_i n) - 2 \sum_{n=1}^{L} y_n \sin(\omega_i n) \right] \\
&+ K_i^2 \sum_{n=1}^{L} \sum_{m=1}^{L} [x_n x_m + j x_n y_m - j y_n x_m + y_n y_m] e^{-j\omega_i(m-n)} \, . \qquad \text{(A.10)}
\end{aligned}
$$

The derivative of γ with respect to x_c for $c = 1, \ldots, L$ is

$$
\begin{aligned}
\frac{\partial \gamma}{\partial x_c} &= (\sigma_s^2 + N_0) 2x_c + K_i^2 [-2 \cos(\omega_i c)] \\
&\quad + K_i^2 \sum_{n=1}^{L} \sum_{m=1}^{L} [x_n \delta(m-c) + \delta(n-c) x_m] e^{-j\omega_i(m-n)} \\
&\quad + jK_i^2 \sum_{n=1}^{L} \sum_{m=1}^{L} [\delta(n-c) y_m - y_n \delta(m-c)] e^{-j\omega_i(m-n)} \\
&= 2(\sigma_s^2 + N_0) x_c - 2K_i^2 \cos(\omega_i c) \\
&\quad + K_i^2 \sum_{n=1}^{L} \left[x_n e^{-j\omega_i(c-n)} + x_n e^{-j\omega_i(n-c)} \right] \\
&\quad + jK_i^2 \sum_{n=1}^{L} \left[y_n e^{-j\omega_i(n-c)} - y_n e^{-j\omega_i(c-n)} \right] \\
&= 2(\sigma_s^2 + N_0) x_c - 2K_i^2 \cos(\omega_i c) \\
&\quad + 2K_i^2 \sum_{n=1}^{L} [x_n \cos[\omega_i(n-c)] + y_n \sin[\omega_i(n-c)]] \, . \qquad \text{(A.11)}
\end{aligned}
$$

To show that this is equal to zero when the coefficients are given by Eq. (3.8), it is necessary

to substitute

$$x_n = \mathbf{Re}[\mathrm{w}_n] = \frac{1}{L+C}\cos(\omega_i n)\ , \tag{A.12}$$

and

$$y_n = \mathbf{Im}[\mathrm{w}_n] = \frac{1}{L+C}\sin(\omega_i n) \tag{A.13}$$

into Eq. (A.11). This leads to

$$\begin{aligned}
\frac{\partial\gamma}{\partial x_c} &= 2\big(\sigma_s^2 + N_0\big)\frac{1}{L+C}\cos(\omega_i c) - 2K_i^2\cos(\omega_i c) \\
&\quad + 2K_i^2\sum_{n=1}^{L}\left[\frac{1}{L+C}\cos(\omega_i n)\cos[\omega_i(n-c)] + \frac{1}{L+C}\sin(\omega_i n)\sin[\omega_i(n-c)]\right] \\
&= 2\big(\sigma_s^2 + N_0\big)\frac{1}{L+C}\cos(\omega_i c) - 2K_i^2\left(\frac{L+C}{L+C}\right)\cos(\omega_i c) \\
&\quad + 2K_i^2\frac{1}{L+C}\sum_{n=1}^{L}\cos[\omega_i(n-n+c)] \\
&= 2\cos(\omega_i c)\frac{1}{L+C}\big[\big(\sigma_s^2 + N_0\big) - K_i^2(L+C) + K_i^2 L\big] \\
&= 2\cos(\omega_i c)\frac{1}{L+C}\left[\big(\sigma_s^2 + N_0\big) - K_i^2\left(L + \frac{\sigma_s^2 + N_0}{K_i^2}\right) + K_i^2 L\right] \\
&= 2\cos(\omega_i c)\frac{1}{L+C}[0] \\
&= 0
\end{aligned} \tag{A.14}$$

for all $c = 1, \ldots, L$.

Following a similar procedure for the derivatives with respect to y_c yields

$$\begin{aligned}
\frac{\partial\gamma}{\partial y_c} &= 2\big(\sigma_s^2 + N_0\big)y_c - 2K_i^2\sin(\omega_i c) \\
&\quad + 2K_i^2\sum_{n=1}^{L}[-x_n\sin[\omega_i(n-c)] + y_n\cos[\omega_i(n-c)]]\ ,
\end{aligned} \tag{A.15}$$

and substituting for x_n and y_n yields

$$\frac{\partial\gamma}{\partial y_c} = 2\big(\sigma_s^2 + N_0\big)\frac{1}{L+C}\sin(\omega_i c) - 2K_i^2\sin(\omega_i c)$$

$$
\begin{aligned}
&+ 2K_i^2 \sum_{n=1}^{L} \left[\frac{-1}{L+C} \cos(\omega_i n) \sin[\omega_i(n-c)] + \frac{1}{L+C} \sin(\omega_i n) \cos[\omega_i(n-c)] \right] \\
&= 2(\sigma_s^2 + N_0) \frac{1}{L+C} \sin(\omega_i c) - 2K_i^2 \left(\frac{L+C}{L+C} \right) \sin(\omega_i c) \\
&\quad + 2K_i^2 \frac{1}{L+C} \sum_{n=1}^{L} \sin[\omega_i(n-n+c)] \\
&= 2\sin(\omega_i c) \frac{1}{L+C} \left[(\sigma_s^2 + N_0) - K_i^2(L+C) + K_i^2 L \right] \\
&= 2\sin(\omega_i c) \frac{1}{L+C} \left[(\sigma_s^2 + N_0) - K_i^2 \left(L + \frac{\sigma_s^2 + N_0}{K_i^2} \right) + K_i^2 L \right] \\
&= 2\sin(\omega_i c) \frac{1}{L+C} [0] \\
&= 0
\end{aligned}
\tag{A.16}
$$

for all $c = 1, \ldots, L$. The results in Eq. (A.14) and (A.16) show that the partial derivatives of γ are all equal to zero when

$$
\mathrm{w}_n = \frac{1}{L+C} e^{j\omega_i n} \,. \tag{A.17}
$$

To complete the proof it should be shown that the point given by $\{\mathrm{w}_n\}$ relates to the global minimum of γ, and not a local minimum, or a maximum or saddle. However, it was felt that such completeness is beyond the scope of this thesis. Nonetheless, it can safely be assumed that the coefficients given by Eq. (3.8) do minimize γ and therefore

$$
\widehat{Z}_a = \frac{1}{L+C} \sum_{n=1}^{L} R_{a-n} e^{j\omega_i n} \tag{A.18}
$$

is the linear MMSE estimator of Z_a.

Appendix B
Derivation of Mean and Variance of Average Periodogram with One Sample per Symbol

In this appendix, expressions for the mean and variance of the points in the average periodogram are developed. This analysis is only valid if one sample per symbol is collected, at the symbol sampling instant. It is tailored specifically for QAM signals. The proof begins by finding various moments of the components in the received samples (Section B.1). These are used to find similar moments of the finite Fourier transformed blocks (Section B.2). These results are in turn used to find the mean and covariance of the periodograms (Section B.3). Finally, the mean and variance of the average periodogram is determined (Section B.4).

B.1 Signal Samples

Using Eq. (2.28), the samples of the received signal, $r_d(n)$, can be expressed in terms of samples of the three component signals as

$$\begin{aligned} r_d(n) &\triangleq r(nT_s + dNT_s) \\ &= v(nT_s + dNT_s) + n(nT_s + dNT_s) + z(nT_s + dNT_s) \\ &= v_d(n) + n_d(n) + z_d(n) \ . \end{aligned} \tag{B.1}$$

The three components will be treated separately.

The first component is due to the transmitted data signal, and each sample can be expressed by using Eq. (2.34) as

$$\begin{aligned} v_d(n) &\triangleq v(nT_s + dNT_s) \\ &= \sum_{a=-\infty}^{\infty} I_a h(nT_s + dNT_s - aT_s) \end{aligned}$$

$$= \sum_{c=-\infty}^{\infty} I_{(n+dN-c)} h(cT_s)$$
$$= I_{(n+dN)} \,, \tag{B.2}$$

since $h(cT_s) = \delta(c)$ because of there is no intersymbol interference due to the Nyquist filtering assumed (see Eq. (2.6)).

For all typical QAM signal constellations with each symbol equally likely, the following properties hold: $\mathbf{E}[I_a] = 0$, $\mathbf{E}[I_a I_a] = 0$, and $\mathbf{E}[I_a^* I_a I_a] = 0$. Let $\sigma_s^2 = \mathbf{E}[I_a^* I_a]$ and $\sigma_4^2 = \mathbf{E}[I_a^* I_a I_a^* I_a]$. As it is assumed that no correlation exists between the symbols transmitted at different times, the following properties hold:

$$\mathbf{E}[I_a^* I_b] = \sigma_s^2 \delta(b-a) \,, \tag{B.3}$$

and

$$\begin{aligned}
\mathbf{E}[I_a^* I_b I_c^* I_d] &= \sigma_4^2 \delta(b-a)\delta(d-c)\delta(c-a) \\
&\quad + \left(\sigma_s^2\right)^2 \delta(b-a)\delta(d-c)[1-\delta(c-a)] \\
&\quad + \left(\sigma_s^2\right)^2 \delta(d-a)\delta(c-b)[1-\delta(c-a)] \\
&= \left[\sigma_4^2 - 2\left(\sigma_s^2\right)^2\right] \delta(b-a)\delta(d-c)\delta(c-a) \\
&\quad + \left(\sigma_s^2\right)^2 \delta(b-a)\delta(d-c) \\
&\quad + \left(\sigma_s^2\right)^2 \delta(d-a)\delta(c-b) \,.
\end{aligned} \tag{B.4}$$

From these properties the following moments can be found:

$$\mathbf{E}[v_d(n)] = \mathbf{E}\left[I_{(n+dN)}\right] = 0 \,, \tag{B.5}$$

$$\begin{aligned}
\mathbf{E}[v_d^*(n) v_e(m)] &= \mathbf{E}\left[I_{(n+dN)}^* I_{(m+eN)}\right] \\
&= \sigma_s^2 \delta(m-n+(e-d)N) \\
&= \sigma_s^2 \delta(m-n)\delta(e-d) \,,
\end{aligned} \tag{B.6}$$

$$\mathbf{E}[v_d(n)v_e(m)] = \mathbf{E}\left[I_{(n+dN)}I_{(m+eN)}\right]$$
$$= 0\,, \tag{B.7}$$

$$\mathbf{E}[v_d^*(n_1)v_d(m_1)v_e(n_2)] = \mathbf{E}\left[I^*_{(n_1+dN)}I_{(m_1+dN)}I_{(n_2+eN)}\right]$$
$$= 0\,, \tag{B.8}$$

and

$$\begin{aligned}\mathbf{E}[v_d^*(n_1)v_d(m_1)v_e^*(n_2)v_d(m_2)] &= \mathbf{E}\left[I^*_{(n_1+dN)}I_{(m_1+dN)}I^*_{(n_2+eN)}I_{(m_2+eN)}\right] \\ &= \left[\sigma_4^2 - 2\left(\sigma_s^2\right)^2\right]\delta(m_1-n_1)\delta(m_2-n_2)\delta(n_2-n_1+(e-d)N) \\ &\quad + \left(\sigma_s^2\right)^2\delta(m_1-n_1)\delta(m_2-n_2) \\ &\quad + \left(\sigma_s^2\right)^2\delta(m_2-n_1+(e-d)N)\delta(n_2-m_1+(e-d)N) \\ &= \left[\sigma_4^2 - 2\left(\sigma_s^2\right)^2\right]\delta(m_1-n_1)\delta(m_2-n_2)\delta(n_2-n_1)\delta(e-d) \\ &\quad + \left(\sigma_s^2\right)^2\delta(m_1-n_1)\delta(m_2-n_2) \\ &\quad + \left(\sigma_s^2\right)^2\delta(m_2-n_1)\delta(n_2-m_1)\delta(e-d)\,. \end{aligned} \tag{B.9}$$

The second component of Eq. (B.1), $n_d(n)$, is due to the AWGN signal. The samples $n_d(n)$ are statistically independent complex Gaussian random variables with zero mean and a variance of N_0. Any zero mean complex Gaussian random variable, Y, with variance σ_Y^2, can be treated as two real Gaussian random variables, F and G, such that $Y = F + jG$. F and G are statistically independent with identical distributions, zero mean, and variances of $\sigma_Y^2/2$. Therefore they have the properties

$$\mathbf{E}[F] = \mathbf{E}[G] = 0\,, \tag{B.10}$$

$$\mathbf{E}\left[F^2\right] = \mathbf{E}\left[G^2\right] = \frac{\sigma_Y^2}{2}\,, \tag{B.11}$$

$$\mathbf{E}\left[F^3\right] = \mathbf{E}\left[G^3\right] = 0\,, \tag{B.12}$$

$$\mathbf{E}\left[F^4\right] = \mathbf{E}\left[G^4\right] = 3\left(\frac{\sigma_Y^2}{2}\right)^2 = \frac{3}{4}\left(\sigma_Y^2\right)^2 , \tag{B.13}$$

and

$$\mathbf{E}[FG] = \mathbf{E}[F]\mathbf{E}[G] = 0 . \tag{B.14}$$

Using these properties, the following moments of Y can be found:

$$\mathbf{E}[Y] = \mathbf{E}[F + jG] = \mathbf{E}[F] + j\mathbf{E}[G] = 0 , \tag{B.15}$$

$$\mathbf{E}[Y^*Y] = \mathbf{E}\left[F^2 + G^2\right] = \frac{\sigma_Y^2}{2} + \frac{\sigma_Y^2}{2} = \sigma_Y^2 , \tag{B.16}$$

$$\mathbf{E}[YY] = \mathbf{E}\left[F^2 + j2FG - G^2\right] = \frac{\sigma_Y^2}{2} - j2(0) - \frac{\sigma_Y^2}{2} = 0 , \tag{B.17}$$

$$\begin{aligned}\mathbf{E}[Y^*YY] &= \mathbf{E}\left[F^3 + jF^2G + FG^2 + jG^3\right] \\ &= 0 + j\frac{\sigma_Y^2}{2}(0) + (0)\frac{\sigma_Y^2}{2} + j(0) \\ &= 0 ,\end{aligned} \tag{B.18}$$

and

$$\begin{aligned}\mathbf{E}[Y^*YY^*Y] &= \mathbf{E}\left[F^4 + 2F^2G^2 + G^4\right] \\ &= \frac{3}{4}\left(\sigma_Y^2\right)^2 + 2\left(\frac{\sigma_Y^2}{2}\right)\left(\frac{\sigma_Y^2}{2}\right) + \frac{3}{4}\left(\sigma_Y^2\right)^2 \\ &= 2\left(\sigma_Y^2\right)^2 .\end{aligned} \tag{B.19}$$

For statistically independent samples of a Gaussian random process, the following properties exist:

$$\mathbf{E}[Y_a^*Y_b] = \sigma_Y^2\delta(b-a) , \tag{B.20}$$

and

$$\mathbf{E}[Y_a^*Y_bY_c^*Y_d] = 2\left(\sigma_Y^2\right)^2\delta(b-a)\delta(d-c)\delta(c-a)$$

$$+ \left(\sigma_Y^2\right)^2 \delta(b-a)\delta(d-c)[1-\delta(c-a)]$$

$$+ \left(\sigma_Y^2\right)^2 \delta(d-c)\delta(c-b)[1-\delta(c-a)]$$

$$= \left(\sigma_Y^2\right)^2 \delta(b-a)\delta(d-c) + \left(\sigma_Y^2\right)^2 \delta(d-a)\delta(c-b) \; . \tag{B.21}$$

Extending these properties to samples of the noise signal yields

$$\mathbf{E}[n_d(n)] = 0 \; , \tag{B.22}$$

$$\mathbf{E}[n_d^*(n)n_e(m)] = N_0\delta(m-n)\delta(e-d) \; , \tag{B.23}$$

$$\mathbf{E}[n_d(n)n_e(m)] = 0 \; , \tag{B.24}$$

$$\mathbf{E}[n_d^*(n_1)n_d(m_1)n_e(n_2)] = 0 \; , \tag{B.25}$$

and

$$\mathbf{E}[n_d^*(n_1)n_d(m_1)n_e^*(n_2)n_e(m_2)] = N_0^2\delta(m_1-n_1)\delta(m_2-n_2)$$

$$+ N_0^2\delta(m_2-n_1)\delta(n_2-m_1)\delta(e-d) \; . \tag{B.26}$$

Finally, the third component of Eq. (B.1), $z_d(n)$, is deterministic and is a result of the interfering tone. From Eq. (2.42), it can be expressed as

$$z_d(n) \triangleq z(nT_s + dNT_s)$$

$$= K_i e^{j2\pi f_i n T_s} e^{j2\pi f_i dNT_s} e^{j\phi_i} \; . \tag{B.27}$$

B.2 Finite Fourier Transform

The FFT of the d^{th} block of samples, as defined in Eq. (3.27), is

$$R_d(k) \triangleq \sum_{n=0}^{N-1} r_d(n) e^{-j2\pi\frac{kn}{N}} \; . \tag{B.28}$$

This can be expressed in terms of the three component signals by defining

$$V_d(k) \triangleq \sum_{n=0}^{N-1} v_d(n) e^{-j2\pi \frac{kn}{N}} , \tag{B.29}$$

$$N_d(k) \triangleq \sum_{n=0}^{N-1} n_d(n) e^{-j2\pi \frac{kn}{N}} , \tag{B.30}$$

and

$$Z_d(k) \triangleq \sum_{n=0}^{N-1} z_d(n) e^{-j2\pi \frac{kn}{N}} , \tag{B.31}$$

so that

$$R_d(k) = V_d(k) + N_d(k) + Z_d(k) . \tag{B.32}$$

Once again, each of the components will be treated separately.

Moments of the first component can be found by applying the moments given in Eqs. (B.5)-(B.9). Therefore,

$$\begin{aligned} \mathbf{E}[V_d(k)] &= \sum_{n=0}^{N-1} \mathbf{E}[v_d(n)] e^{-j2\pi \frac{kn}{N}} \\ &= 0 , \end{aligned} \tag{B.33}$$

$$\begin{aligned} \mathbf{E}[V_d^*(k) V_e(l)] &= \sum_{n=0}^{N-1} \sum_{m=0}^{N-1} \mathbf{E}[v_d^*(n) v_e(m)] e^{-j2\pi \frac{lm}{N}} e^{j2\pi \frac{kn}{N}} \\ &= \sum_{n=0}^{N-1} \sum_{m=0}^{N-1} \sigma_s^2 \delta(m-n) \delta(e-d) e^{-j2\pi \frac{lm-kn}{N}} \\ &= \sigma_s^2 \sum_{n=0}^{N-1} e^{-j2\pi \frac{(l-k)n}{N}} \delta(e-d) \\ &= \sigma_s^2 N \delta(l-k) \delta(e-d) , \end{aligned} \tag{B.34}$$

$$\begin{aligned} \mathbf{E}[V_d(k) V_e(l)] &= \sum_{n=0}^{N-1} \sum_{m=0}^{N-1} \mathbf{E}[v_d(n) v_e(m)] e^{-j2\pi \frac{lm}{N}} e^{-j2\pi \frac{kn}{N}} \\ &= 0 , \end{aligned} \tag{B.35}$$

$$\mathbf{E}[V_d^*(k)V_d(k)V_e(l)] = \sum_{n_1=0}^{N-1}\sum_{m_1=0}^{N-1}\sum_{n_2=0}^{N-1}\mathbf{E}[v_d^*(n_1)v_d(m_1)v_e(n_2)]e^{-j2\pi\frac{ln_2}{N}}e^{-j2\pi\frac{k(m_1-n_1)}{N}}$$
$$= 0\,, \tag{B.36}$$

and

$$\begin{aligned}
&\mathbf{E}[V_d^*(k)V_d(k)V_e^*(l)V_e(l)] \\
&= \sum_{n_1=0}^{N-1}\sum_{m_1=0}^{N-1}\sum_{n_2=0}^{N-1}\sum_{m_2=0}^{N-1}\mathbf{E}[v_d^*(n_1)v_d(m_1)v_e^*(n_2)v_e(m_2)]e^{-j2\pi\frac{k(m_1-n_1)}{N}}e^{-j2\pi\frac{l(m_2-n_2)}{N}} \\
&= \sum_{n_1=0}^{N-1}\sum_{m_1=0}^{N-1}\sum_{n_2=0}^{N-1}\sum_{m_2=0}^{N-1}\left[\begin{array}{l}\left[\sigma_4^2-\left(\sigma_s^2\right)^2\right]\delta(m_1-n_1)\delta(m_2-n_2)\delta(n_2-n_1)\delta(e-d) \\ \qquad\qquad\qquad\qquad\qquad\qquad\times e^{-j2\pi\frac{k(m_1-n_1)}{N}}e^{-j2\pi\frac{l(m_2-n_2)}{N}} \\ \quad+\left(\sigma_s^2\right)^2\delta(m_1-n_1)\delta(m_2-n_2)e^{-j2\pi\frac{k(m_1-n_1)}{N}}e^{-j2\pi\frac{l(m_2-n_2)}{N}} \\ \quad+\left(\sigma_s^2\right)^2\delta(m_2-n_1)\delta(n_2-m_1)\delta(e-d)e^{-j2\pi\frac{k(m_1-n_1)}{N}}e^{-j2\pi\frac{l(m_2-n_2)}{N}}\end{array}\right] \\
&= \left[\sigma_4^2-2\left(\sigma_s^2\right)^2\right]\sum_{n_1=0}^{N-1}\sum_{n_2=0}^{N-1}\delta(n_2-n_1)\delta(e-d)e^{-j2\pi\frac{k(n_1-n_1)}{N}}e^{-j2\pi\frac{l(n_2-n_2)}{N}} \\
&\quad+\left(\sigma_s^2\right)^2\sum_{n_1=0}^{N-1}\sum_{n_2=0}^{N-1}e^{-j2\pi\frac{k(n_1-n_1)}{N}}e^{-j2\pi\frac{l(n_2-n_2)}{N}} \\
&\quad+\left(\sigma_s^2\right)^2\sum_{n_1=0}^{N-1}\sum_{n_2=0}^{N-1}\delta(e-d)e^{-j2\pi\frac{k(n_2-n_1)}{N}}e^{-j2\pi\frac{l(n_1-n_2)}{N}} \\
&= \left[\sigma_4^2-2\left(\sigma_s^2\right)^2\right]N\delta(e-d)+\left(\sigma_s^2\right)^2N^2+\left(\sigma_s^2\right)^2N^2\delta(l-k)\delta(e-d)\,.
\end{aligned} \tag{B.37}$$

Using Eqs. (B.22)-(B.26), the moments of the second component of Eq. (B.32), $N_d(k)$ can be found. They are:

$$\mathbf{E}[N_d(k)] = \sum_{n=0}^{N-1}\mathbf{E}[n_d(n)]e^{-j2\pi\frac{kn}{N}}$$
$$= 0\,, \tag{B.38}$$

$$\mathbf{E}[N_d^*(k)N_e(l)] = \sum_{n=0}^{N-1}\sum_{m=0}^{N-1}\mathbf{E}[n_d^*(n)n_e(m)]e^{-j2\pi\frac{lm}{N}}e^{j2\pi\frac{kn}{N}}$$
$$= \sum_{n=0}^{N-1}\sum_{m=0}^{N-1}N_0\delta(m-n)\delta(e-d)e^{-j2\pi\frac{lm-kn}{N}}$$

$$= N_0 \sum_{n=0}^{N-1} e^{-j2\pi\frac{(l-k)n}{N}} \delta(e-d)$$
$$= N_0 N \delta(l-k)\delta(e-d)\ , \tag{B.39}$$

$$\mathbf{E}[N_d(k)N_e(l)] = \sum_{n=0}^{N-1}\sum_{m=0}^{N-1} \mathbf{E}[n_d(n)n_e(m)] e^{-j2\pi\frac{lm}{N}} e^{-j2\pi\frac{kn}{N}}$$
$$= 0\ , \tag{B.40}$$

$$\mathbf{E}[N_d^*(k)N_d(k)N_e(l)] = \sum_{n_1=0}^{N-1}\sum_{m_1=0}^{N-1}\sum_{n_2=0}^{N-1} \mathbf{E}[n_d^*(n_1)n_d(m_1)n_e(n_2)] e^{-j2\pi\frac{ln_2}{N}} e^{-j2\pi\frac{k(m_1-n_1)}{N}}$$
$$= 0\ , \tag{B.41}$$

and

$$\begin{aligned}
&\mathbf{E}[N_d^*(k)N_d(k)N_e^*(l)N_e(l)] \\
&\quad= \sum_{n_1=0}^{N-1}\sum_{m_1=0}^{N-1}\sum_{n_2=0}^{N-1}\sum_{m_2=0}^{N-1} \mathbf{E}[n_d^*(n_1)n_d(m_1)n_e^*(n_2)n_e(m_2)] e^{-j2\pi\frac{k(m_1-n_1)}{N}} e^{-j2\pi\frac{l(m_2-n_2)}{N}} \\
&\quad= \sum_{n_1=0}^{N-1}\sum_{m_1=0}^{N-1}\sum_{n_2=0}^{N-1}\sum_{m_2=0}^{N-1} N_0^2 \delta(m_1-n_1)\delta(m_2-n_2) e^{-j2\pi\frac{k(m_1-n_1)}{N}} e^{-j2\pi\frac{l(m_2-n_2)}{N}} \\
&\qquad+ \sum_{n_1=0}^{N-1}\sum_{m_1=0}^{N-1}\sum_{n_2=0}^{N-1}\sum_{m_2=0}^{N-1} N_0^2 \delta(m_2-n_1)\delta(n_2-m_1)\delta(e-d) e^{-j2\pi\frac{k(m_1-n_1)}{N}} e^{-j2\pi\frac{l(m_2-n_2)}{N}} \\
&\quad= N_0^2 \sum_{n_1=0}^{N-1}\sum_{n_2=0}^{N-1} e^{-j2\pi\frac{k(n_1-n_1)}{N}} e^{-j2\pi\frac{l(n_2-n_2)}{N}} \\
&\qquad+ N_0^2 \sum_{n_1=0}^{N-1}\sum_{n_2=0}^{N-1} \delta(e-d) e^{-j2\pi\frac{k(n_2-n_1)}{N}} e^{-j2\pi\frac{l(n_1-n_2)}{N}} \\
&= N_0^2 N^2 + N_0^2 N^2 \delta(l-k)\delta(e-d)\ .
\end{aligned} \tag{B.42}$$

For the third component of Eq. (B.32), the FFT can be computed directly. Using Eq. (B.27), $Z_d(k)$ can be expressed as

$$Z_d(k) \triangleq \sum_{n=0}^{N-1} z_d(n) e^{-j2\pi\frac{kn}{N}}$$

$$
\begin{aligned}
&= \sum_{n=0}^{N-1} K_i e^{j2\pi f_i n T_s} e^{j2\pi f_i d N T_s} e^{j\phi_i} e^{-j2\pi \frac{kn}{N}} \\
&= K_i e^{j2\pi f_i d N T_s} e^{j\phi_i} \sum_{n=0}^{N-1} e^{j2\pi \left(f_i - \frac{k}{NT_s}\right) n T_s} \\
&= K_i e^{j2\pi f_i d N T_s} e^{j\phi_i} \frac{\sin\left[\pi\left(f_i - \frac{k}{NT_s}\right) N T_s\right]}{\sin\left[\pi\left(f_i - \frac{k}{NT_s}\right) T_s\right]} \frac{e^{j\pi\left(f_i - \frac{k}{NT_s}\right) N T_s}}{e^{j\pi\left(f_i - \frac{k}{NT_s}\right) T_s}} \\
&= K_i e^{j2\pi f_i d N T_s} e^{j\phi_i} \frac{\sin\left[\pi(f_i N T_s - k)\right]}{\sin\left[\frac{\pi}{N}(f_i N T_s - k)\right]} \frac{e^{j\pi(f_i N T_s - k)}}{e^{j\frac{\pi}{N}(f_i N T_s - k)}} \; . \qquad \text{(B.43)}
\end{aligned}
$$

Note that

$$
\begin{aligned}
|Z_d(k)|^2 &= K_i^2 \frac{\sin^2\left[\pi(f_i N T_s - k)\right]}{\sin^2\left[\frac{\pi}{N}(f_i N T_s - k)\right]} \\
&= K_i^2 \frac{\sin^2\left[\pi f_i N T_s\right]}{\sin^2\left[\frac{\pi}{N}(f_i N T_s - k)\right]} \; . \qquad \text{(B.44)}
\end{aligned}
$$

It is useful to define the function

$$
Z_0(k) = \frac{\sin^2 \pi f_i N T_s}{N \sin^2 \frac{\pi}{N}(f_i N T_s - k)} \; , \qquad \text{(B.45)}
$$

so that

$$
|Z_d(k)|^2 = K_i^2 N Z_0(k) \; . \qquad \text{(B.46)}
$$

B.3 The Periodogram

From the definition of the periodogram in Eq. (3.28),

$$
X_d(k) \triangleq \tfrac{1}{N} |R_d(k)|^2 \; , \qquad \text{(B.47)}
$$

it has a mean of

$$
\mathbf{E}[X_d(k)] = \tfrac{1}{N} \mathbf{E}\left[|R_d(k)|^2\right] \; , \qquad \text{(B.48)}
$$

and a covariance of

$$\mathbf{Cov}[X_d(k), X_e(l)] = \tfrac{1}{N^2}\mathbf{Cov}\left[|R_d(k)|^2, |R_e(l)|^2\right] . \tag{B.49}$$

To evaluate these expressions, substitute Eq. (B.32) for $R_d(k)$ so that

$$\begin{aligned} |R_d(k)|^2 = {} & |V_d(k)|^2 + V_d^*(k)N_d(k) + V_d^*(k)Z_d(k) \\ & + N_d^*(k)V_d(k) + |N_d(k)|^2 + N_d^*(k)Z_d(k) \\ & + Z_d^*(k)V_d(k) + Z_d^*(k)N_d(k) + |Z_d(k)|^2 . \end{aligned} \tag{B.50}$$

Taking the expectation yields

$$\begin{aligned} \mathbf{E}\left[|R_d(k)|^2\right] = {} & \mathbf{E}\left[|V_d(k)|^2\right] + \mathbf{E}[V_d^*(k)]\mathbf{E}[N_d(k)] + \mathbf{E}[V_d^*(k)]Z_d(k) \\ & + \mathbf{E}[N_d^*(k)]V_d(k) + \mathbf{E}\left[|N_d(k)|^2\right] + \mathbf{E}[N_d^*(k)]Z_d(k) \\ & + Z_d^*(k)V_d\mathbf{E}[V_d(k)] + Z_d^*(k)\mathbf{E}[N_d(k)] + |Z_d(k)|^2 , \\ = {} & \mathbf{E}\left[|V_d(k)|^2\right] + \mathbf{E}\left[|N_d(k)|^2\right] + |Z_d(k)|^2 . \end{aligned} \tag{B.51}$$

The expression for $\mathbf{E}\left[|R_d(k)|^2|R_e(l)|^2\right]$, needed for the covariance, has eighty-one terms, but most are equal to zero. All terms with exactly one or three data or noise components have zero mean, and therefore are omitted. Also, terms with $\mathbf{E}[V_d(k)V_e(l)]$ and $\mathbf{E}[N_d(k)N_e(l)]$ are also equal to zero, and are omitted too. The remaining terms are

$$\begin{aligned} & \mathbf{E}\left[|R_d(k)|^2|R_e(l)|^2\right] \\ & \quad = \mathbf{E}\left[|V_d(k)|^2|V_e(l)|^2\right] + \mathbf{E}\left[|V_d(k)|^2|N_e(l)|^2\right] + \mathbf{E}\left[|V_d(k)|^2\right]|Z_e(l)|^2 \\ & \quad + \mathbf{E}\left[|N_d(k)|^2|V_e(l)|^2\right] + \mathbf{E}\left[|N_d(k)|^2|N_e(l)|^2\right] + \mathbf{E}\left[|N_d(k)|^2\right]|Z_e(l)|^2 \\ & \quad + |Z_d(k)|^2\mathbf{E}\left[|V_e(l)|^2\right] + |Z_d(k)|^2\mathbf{E}\left[|N_e(l)|^2\right] + |Z_d(k)|^2|Z_e(l)|^2 \\ & \quad + \mathbf{E}[V_d^*(k)V_e(l)]\mathbf{E}[N_d(k)N_e^*(l)] + \mathbf{E}[V_d(k)V_e^*(l)]\mathbf{E}[N_d^*(k)N_e^*(l)] \\ & \quad + \mathbf{E}[V_d^*(k)V_e(l)]Z_d(k)Z_e^*(l) + \mathbf{E}[V_d(k)V_e^*(l)]Z_d^*(k)Z_e(l) \end{aligned}$$

$$+ \mathbf{E}[N_d^*(k)N_e^*(l)]Z_d(k)Z_e^*(l) + \mathbf{E}[N_d(k)N_e^*(l)]Z_d^*(k)Z_e(l)\,. \tag{B.52}$$

From Eqs. (B.51) and (B.52), it is clear that

$$\begin{aligned}
&\mathbf{Cov}\Big[|R_d(k)|^2, |R_e(l)|^2\Big] \\
&\quad = \mathbf{E}\Big[|V_d(k)|^2|V_e(l)|^2\Big] - \mathbf{E}\Big[|V_d(k)|^2\Big]\mathbf{E}\Big[|V_e(l)|^2\Big] \\
&\qquad + \mathbf{E}\Big[|N_d(k)|^2|N_e(l)|^2\Big] - \mathbf{E}\Big[|N_d(k)|^2\Big]\mathbf{E}\Big[|N_e(l)|^2\Big] \\
&\qquad + \mathbf{E}[V_d^*(k)V_e(l)]\mathbf{E}[N_d(k)N_e^*(l)] + \mathbf{E}[V_d(k)V_e^*(l)]\mathbf{E}[N_d^*(k)N_e^*(l)] \\
&\qquad + \mathbf{E}[V_d^*(k)V_e(l)]Z_d(k)Z_e^*(l) + \mathbf{E}[V_d(k)V_e^*(l)]Z_d^*(k)Z_e(l) \\
&\qquad + \mathbf{E}[N_d^*(k)N_e^*(l)]Z_d(k)Z_e^*(l) + \mathbf{E}[N_d(k)N_e^*(l)]Z_d^*(k)Z_e(l)\,.
\end{aligned} \tag{B.53}$$

Substituting Eqs. (B.34), (B.37), (B.39), and (B.42) into Eqs. (B.51) and (B.53) yields

$$\mathbf{E}\Big[|R_d(k)|^2\Big] = \sigma_s^2 N + N_0 N + K_i^2 N Z_0(k)\,, \tag{B.54}$$

and

$$\begin{aligned}
&\mathbf{Cov}\Big[|R_d(k)|^2, |R_e(l)|^2\Big] \\
&\quad = \Big[\sigma_4^2 - 2\big(\sigma_s^2\big)^2\Big]N\delta(e-d) + \big(\sigma_s^2\big)^2 N^2 \\
&\qquad + \big(\sigma_s^2\big)^2 N^2\delta(l-k)\delta(e-d) - \big(\sigma_s^2\big)^2 N^2 \\
&\qquad + N_0^2 N^2 + N_0^2 N^2\delta(l-k)\delta(e-d) - N_0^2 N^2 \\
&\qquad + \sigma_s^2 N_0 N^2\delta(l-k)\delta(e-d) + \sigma_s^2 N_0 N^2\delta(l-k)\delta(e-d) \\
&\qquad + \sigma_s^2 N\delta(l-k)\delta(e-d)Z_d(k)Z_e^*(l) + \sigma_s^2 N\delta(l-k)\delta(e-d)Z_d^*(k)Z_e(l) \\
&\qquad + N_0 N\delta(l-k)\delta(e-d)Z_d(k)Z_e^*(l) + N_0 N\delta(l-k)\delta(e-d)Z_d^*(k)Z_e(l)\,, \\
&\quad = \Big[\sigma_4^2 - 2\big(\sigma_s^2\big)^2\Big]N\delta(e-d) + \Big[\big(\sigma_s^2\big)^2 + 2\sigma_s^2 N_0 + N_0^2\Big]N^2\delta(l-k)\delta(e-d) \\
&\qquad + 2\big[\sigma_s^2 + N_0\big]N|Z_d(k)|^2\delta(l-k)\delta(e-d) \\
&\quad = \big(\sigma_s^2 + N_0\big)^2 N^2\delta(l-k)\delta(e-d) + 2\big(\sigma_s^2 + N_0\big)K_i^2 N^2 Z_0(k)\delta(l-k)\delta(e-d)
\end{aligned}$$

$$+ \left[\sigma_4^2 - 2\left(\sigma_s^2\right)^2\right] N\delta(e-d) \; . \tag{B.55}$$

As a result,

$$\mathbf{E}[X_d(k)] = \sigma_s^2 + N_0 + K_i^2 Z_0(k) \; , \tag{B.56}$$

and

$$\begin{aligned}\mathbf{Cov}[X_d(k), X_e(l)] = \left(\sigma_s^2 + N_0\right)^2 \delta(l-k)\delta(e-d) + 2\left(\sigma_s^2 + N_0\right) K_i^2 Z_0(k)\delta(l-k)\delta(e-d) \\ + \tfrac{1}{N}\left[\sigma_4^2 - 2\left(\sigma_s^2\right)^2\right]\delta(e-d) \; .\end{aligned} \tag{B.57}$$

B.4 The Average Periodogram

From Eq. (3.51), the average periodogram is computed as

$$X_D(k) = \tfrac{1}{D} \sum_{d=0}^{D-1} X_d(k) \; . \tag{B.58}$$

Using Eq. (B.56), the mean of the average periodogram is

$$\begin{aligned}\mathbf{E}[X_D(k)] &= \tfrac{1}{D} \sum_{d=0}^{D-1} \mathbf{E}[X_d(k)] \\ &= \tfrac{1}{D} \sum_{d=0}^{D-1} \left[\sigma_s^2 + N_0 + K_i^2 Z_0(k)\right] \\ &= \sigma_s^2 + N_0 + K_i^2 Z_0(k) \; .\end{aligned} \tag{B.59}$$

The covariance between different points in the average periodogram is

$$\begin{aligned}\mathbf{Cov}[X_D(k), X_D(l)] &= \tfrac{1}{D^2} \sum_{d=0}^{D-1} \sum_{e=0}^{D-1} \mathbf{Cov}[X_d(k), X_e(l)] \\ &= \tfrac{1}{D^2} \sum_{d=0}^{D-1} \sum_{e=0}^{D-1} \left[\left(\sigma_s^2 + N_0\right)^2 + 2\left(\sigma_s^2 + N_0\right) K_i^2 Z_0(k)\right] \delta(l-k)\delta(e-d) \\ &+ \tfrac{1}{D^2} \sum_{d=0}^{D-1} \sum_{e=0}^{D-1} \tfrac{1}{N}\left[\sigma_4^2 - 2\left(\sigma_s^2\right)^2\right]\delta(e-d)\end{aligned}$$

$$= \frac{1}{D}\left[\left(\sigma_s^2 + N_0\right)^2 + 2\left(\sigma_s^2 + N_0\right)K_i^2 Z_0(k)\right]\delta(l-k) + \frac{1}{ND}\left[\sigma_4^2 - 2(\sigma_s^2)^2\right] . \tag{B.60}$$

Note that for two different points in the periodogram, there is a slight correlation, as indicated by the second term in Eq. (B.60). Note that the second term is much smaller that the first, since it is divided by N. Therefore for the variance the second term is negligible, so

$$\mathbf{Var}[X_D(k)] = \frac{1}{D}\left[\left(\sigma_s^2 + N_0\right)^2 + 2\left(\sigma_s^2 + N_0\right)K_i^2 Z_0(k)\right] . \tag{B.61}$$

In summary, Eqs. (B.59) and (B.61) provide expressions for the mean and variance of the points in the average periodogram, when D blocks of N samples collected at the symbol sampling instants are used to calculate the average periodogram. These expressions are in terms of the transmitted energy per symbol, σ_s^2, the one-sided noise spectral density, N_0, the power of the interfering tone, K_i^2, and the function

$$Z_0(k) = \frac{\sin^2(\pi f_i N T_s)}{N \sin^2\left(\frac{\pi}{N}[f_i N T_s - k]\right)} . \tag{B.62}$$

These results are used extensively throughout Section 3.3.

Appendix C
Power Ratio Estimator

In Section 3.3.5, two estimators, denoted by θ_1 and θ_2 were presented in conjunction with a method for estimating the power ratio, $C = (\sigma_s^2 + N_0)/K_i^2$. In this appendix it is proved that θ_1 and θ_2 are unbiased estimators of $\sigma_s^2 + N_0$ and K_i^2, respectively, and expressions for their variances are derived.

Recall that the two estimators are calculated from the two intermediate quantities, S_1 and S_2, that are define by Eq. (3.74) and Eq. (3.75), respectively. To analyse θ_1 and θ_2 it is first necessary to find the means, variances, and covariance of S_1 and S_2.

In Eq. (3.74) the first quantity, S_1, is defined as

$$S_1 \triangleq \frac{1}{N} \sum_{k=-\frac{N}{2}}^{\frac{N}{2}-1} X_D(k) \,. \tag{C.1}$$

Its mean can be found by using Eq. (B.59) as an expression for $\mathbf{E}[X_D(k)]$, so that

$$\begin{aligned} \mathbf{E}[S_1] &= \frac{1}{N} \sum_{k=-\frac{N}{2}}^{\frac{N}{2}-1} \mathbf{E}[X_D(k)] \\ &= \frac{1}{N} \sum_{k=-\frac{N}{2}}^{\frac{N}{2}-1} \left[\sigma_s^2 + N_0 + K_i^2 Z_0(k)\right] \\ &= \sigma_s^2 + N_0 + \frac{1}{N} K_i^2 \sum_{k=-\frac{N}{2}}^{\frac{N}{2}-1} Z_0(k) \,. \end{aligned} \tag{C.2}$$

To simplify this equation it is important to note that

$$\begin{aligned} Z_0(k) &= \frac{1}{N} \left| \sum_{n=0}^{N-1} e^{-j2\pi \left(f_i - \frac{k}{NT_s}\right) nT_s} \right|^2 \\ &= \frac{1}{N} \sum_{n=0}^{N-1} \sum_{m=0}^{N-1} e^{-j2\pi \left(f_i - \frac{k}{NT_s}\right)(m-n)T_s} \,, \end{aligned} \tag{C.3}$$

which follows from the definition of $Z_0(k)$ given in Appendix B, in particular Eq. (B.43). Using this identity it is easy to see that

$$\begin{aligned}
\sum_{k=-\frac{N}{2}}^{\frac{N}{2}-1} Z_0(k) &= \sum_{k=-\frac{N}{2}}^{\frac{N}{2}-1} \frac{1}{N} \sum_{n=0}^{N-1}\sum_{m=0}^{N-1} e^{-j2\pi\left(f_i-\frac{k}{NT_s}\right)(m-n)T_s} \\
&= \sum_{n=0}^{N-1}\sum_{m=0}^{N-1} e^{-j2\pi f_i(m-n)T_s} \frac{1}{N} \sum_{k=-\frac{N}{2}}^{\frac{N}{2}-1} e^{j2\pi\frac{k(m-n)}{N}} \\
&= \sum_{n=0}^{N-1}\sum_{m=0}^{N-1} e^{-j2\pi f_i(m-n)T_s}\delta(m-n) \\
&= \sum_{n=0}^{N-1} e^{-j2\pi f_i(n-n)T_s} \\
&= N\ . \qquad \text{(C.4)}
\end{aligned}$$

Substituting this into Eq. (C.2) yields

$$\mathbf{E}[S_1] = \sigma_s^2 + N_0 + K_i^2\ , \qquad \text{(C.5)}$$

which is, of course, the total power in the received symbols.

To find the variance of S_1, Eq. (B.60) is used for the covariance of $X_D(k)$ and $X_D(l)$. This leads to

$$\begin{aligned}
\mathbf{Var}[S_1] &= \frac{1}{N^2} \sum_{k=-\frac{N}{2}}^{\frac{N}{2}-1}\sum_{l=-\frac{N}{2}}^{\frac{N}{2}-1} \mathbf{Cov}[X_D(k), X_D(l)] \\
&= \frac{1}{N^2} \sum_{k=-\frac{N}{2}}^{\frac{N}{2}-1}\sum_{l=-\frac{N}{2}}^{\frac{N}{2}-1} \left(\begin{array}{c} \frac{1}{D}\left[\left(\sigma_s^2+N_0\right)^2 + 2\left(\sigma_s^2+N_0\right)K_i^2 Z_0(k)\right]\delta(l-k) \\ + \frac{1}{ND}\left[\sigma_4^2 - 2\left(\sigma_s^2\right)^2\right] \end{array} \right) \\
&= \frac{1}{N^2 D} \sum_{k=-\frac{N}{2}}^{\frac{N}{2}-1} \left[\left(\sigma_s^2+N_0\right)^2 + 2\left(\sigma_s^2+N_0\right)K_i^2 Z_0(k)\right] + \frac{1}{N^3 D} N^2 \left[\sigma_4^2 - 2\left(\sigma_s^2\right)^2\right] \\
&= \frac{1}{ND}\left[\left(\sigma_s^2+N_0\right)^2 + 2\left(\sigma_s^2+N_0\right)K_i^2 + \left(\sigma_4^2 - 2\left(\sigma_s^2\right)^2\right)\right]\ . \qquad \text{(C.6)}
\end{aligned}$$

Recall that the second quantity, S_2, defined in Eq. (3.75), is the sum of only a few points in the AP, centered around the position of the tone spike, k_i. Let M denote the number of

points to sum, where M is odd, and let $c = (M-1)/2$. This quantity is therefore defined as

$$S_2 \triangleq \sum_{k=k_i-c}^{k_i+c} X_D(k) \; . \tag{C.7}$$

Its mean can be found by using Eq. (B.59) for $\mathbf{E}[X_D(k)]$, and is

$$\begin{aligned} \mathbf{E}[S_2] &= \sum_{k=k_i-c}^{k_i+c} \mathbf{E}[X_D(k)] \\ &= \sum_{k=k_i-c}^{k_i+c} \left[\sigma_s^2 + N_0 + K_i^2 Z_0(k)\right] \\ &= \left(\sigma_s^2 + N_0\right) M + K_i^2 \sum_{k=k_i-c}^{k_i+c} Z_0(k) \; . \end{aligned} \tag{C.8}$$

The summation of $Z_0(k)$ over $k \in [k_i - c, k_i + c]$ requires some attention. From Eq. (B.62), it is useful to note that

$$\begin{aligned} \sum_{k=k_i-c}^{k_i+c} Z_0(k) &= \sum_{k=k_i-c}^{k_i+c} \frac{\sin^2\left(\pi f_i N T_s\right)}{N \sin^2\left(\frac{\pi}{N}[f_i N T_s - k]\right)} \\ &= \sum_{k=-c}^{c} \frac{\sin^2\left(\pi f_i N T_s\right)}{N \sin^2\left(\frac{\pi}{N}[f_i N T_s - (k + k_i)]\right)} \\ &= \sum_{k=-c}^{c} \frac{\sin^2\left(\pi[\delta_i + k_i]\right)}{N \sin^2\left(\frac{\pi}{N}[\delta_i - k]\right)} \\ &= \sum_{k=-c}^{c} \frac{\sin^2\left(\pi \delta_i\right)}{N \sin^2\left(\frac{\pi}{N}[\delta_i - k]\right)} \; , \end{aligned} \tag{C.9}$$

which depends on δ_i and on the number of points used in the sum. The function

$$G_M(\delta_i) \triangleq \tfrac{1}{N} \sum_{k=k_i-c}^{k_i+c} Z_0(k) \tag{C.10}$$

represents the fraction of the total power of the tone that is contained within the M points centered around k_i. Since most of the power is contained in the spike, $G_M(\delta_i)$ is usually very close to unity. For the remainder of this Appendix, $G_M(\delta_i)$ will be abbreviated to G to simplify notation. Substituting Eq. (C.10) into Eq. (C.8) yields

$$\mathbf{E}[S_2] = \left(\sigma_s^2 + N_0\right) M + K_i^2 N G \; . \tag{C.11}$$

As in the case of S_1, the variance of S_2 can be found by using Eq. (B.60) as an expression for the covariance of $X_D(k)$ and $X_D(l)$. This leads to

$$\begin{aligned}
\mathbf{Var}[S_2] &= \sum_{k=k_i-c}^{k_i+c} \sum_{l=k_i-c}^{k_i+c} \mathbf{Cov}[X_D(k), X_D(l)] \\
&= \sum_{k=k_i-c}^{k_i+c} \sum_{l=k_i-c}^{k_i+c} \left(\begin{array}{c} \frac{1}{D}\left[\left(\sigma_s^2+N_0\right)^2 + 2\left(\sigma_s^2+N_0\right)K_i^2 Z_0(k)\right]\delta(l-k) \\ + \frac{1}{ND}\left[\sigma_4^2 - 2\left(\sigma_s^2\right)^2\right] \end{array} \right) \\
&= \frac{1}{D} \sum_{k=k_i-c}^{k_i+c} \left[\left(\sigma_s^2+N_0\right)^2 + 2\left(\sigma_s^2+N_0\right)K_i^2 Z_0(k)\right] + \frac{1}{ND} M^2 \left[\sigma_4^2 - 2\left(\sigma_s^2\right)^2\right] \\
&= \frac{1}{D}\left[\left(\sigma_s^2+N_0\right)^2 M + 2\left(\sigma_s^2+N_0\right)K_i^2 NG\right] + \frac{M^2}{ND}\left[\sigma_4^2 - 2\left(\sigma_s^2\right)^2\right] . \qquad \text{(C.12)}
\end{aligned}$$

To find expressions for the variances of θ_1 and θ_2, the covariance of S_1 and S_2 must be known. This is easily shown to be

$$\begin{aligned}
\mathbf{Cov}[S_1, S_2] &= \frac{1}{N} \sum_{k=-\frac{N}{2}}^{\frac{N}{2}-1} \sum_{l=k_i-c}^{k_i+c} \mathbf{Cov}[X_D(k), X_D(l)] \\
&= \frac{1}{N} \sum_{k=-\frac{N}{2}}^{\frac{N}{2}-1} \sum_{l=k_i-c}^{k_i+c} \left(\begin{array}{c} \frac{1}{D}\left[\left(\sigma_s^2+N_0\right)^2 + 2\left(\sigma_s^2+N_0\right)K_i^2 Z_0(k)\right]\delta(l-k) \\ + \frac{1}{ND}\left[\sigma_4^2 - 2\left(\sigma_s^2\right)^2\right] \end{array} \right) \\
&= \frac{1}{ND} \sum_{l=k_i-c}^{k_i+c} \left[\left(\sigma_s^2+N_0\right)^2 + 2\left(\sigma_s^2+N_0\right)K_i^2 Z_0(k)\right] + \frac{1}{N^2 D} NM \left[\sigma_4^2 - 2\left(\sigma_s^2\right)^2\right] \\
&= \frac{1}{ND}\left[\left(\sigma_s^2+N_0\right)^2 M + 2\left(\sigma_s^2+N_0\right)K_i^2 NG + \left(\sigma_4^2 - 2\left(\sigma_s^2\right)^2\right)M\right] . \qquad \text{(C.13)}
\end{aligned}$$

Armed with the joint moments of S_1 and S_2, analysis can proceed to θ_1 and θ_2. Recall from Eq. (3.76) that the estimator θ_1 is generated by

$$\theta_1 = \frac{NGS_1 - S_2}{NG - M} . \qquad \text{(C.14)}$$

Using Eqs. (C.5) and (C.11) for $\mathbf{E}[S_1]$ and $\mathbf{E}[S_2]$ respectively, it is clear that

$$\mathbf{E}[\theta_1] = \frac{NG\mathbf{E}[S_1] - \mathbf{E}[S_2]}{NG - M}$$

$$= \frac{NG[\sigma_s^2 + N_0 + K_i^2] - [(\sigma_s^2 + N_0)M + K_i^2 NG]}{NG - M}$$
$$= \frac{(\sigma_s^2 + N_0)[NG - M]}{NG - M}$$
$$= \sigma_s^2 + N_0 \, . \tag{C.15}$$

Therefore θ_1 is an unbiased estimator of $\sigma_s^2 + N_0$. Its variance can readily be found to be

$$\begin{aligned}\mathbf{Var}[\theta_1] &= \tfrac{1}{(NG-M)^2}\mathbf{Var}[NGS_1 - S_2] \\ &= \tfrac{1}{(NG-M)^2}\left[N^2G^2\mathbf{Var}[S_1] - 2NG\mathbf{Cov}[S_1, S_2] + \mathbf{Var}[S_2]\right] \, . \end{aligned} \tag{C.16}$$

By using Eqs. (C.6), (C.12), and (C.13), this variance can be expressed as

$$\begin{aligned}\mathbf{Var}[\theta_1] &= \tfrac{1}{(NG-M)^2}\left(\begin{array}{l} N^2G^2\tfrac{1}{ND}\left[(\sigma_s^2 + N_0)^2 + 2(\sigma_s^2 + N_0)K_i^2 + \left(\sigma_4^2 - 2(\sigma_s^2)^2\right)\right] \\ \quad - 2NG\tfrac{1}{ND}\left[\begin{array}{l}(\sigma_s^2 + N_0)^2 M + 2(\sigma_s^2 + N_0)K_i^2 NG \\ \quad + \left(\sigma_4^2 - 2(\sigma_s^2)^2\right)M\end{array}\right] \\ \quad + \tfrac{1}{D}\left[(\sigma_s^2 + N_0)^2 M + 2(\sigma_s^2 + N_0)K_i^2 NG\right] + \tfrac{M^2}{ND}\left[\sigma_4^2 - 2(\sigma_s^2)^2\right]\end{array}\right) \\ &= \tfrac{1}{(NG-M)^2}\left(\begin{array}{l}(\sigma_s^2 + N_0)^2\left[\tfrac{N^2G^2}{ND} - 2\tfrac{NMG}{ND} + \tfrac{M}{D}\right] \\ \quad + 2(\sigma_s^2 + N_0)K_i^2 NG\left[\tfrac{NG}{ND} - 2\tfrac{NG}{ND} + \tfrac{1}{D}\right] \\ \quad + \left(\sigma_4^2 - 2(\sigma_s^2)^2\right)\left[\tfrac{N^2G^2}{ND} - 2\tfrac{NMG}{ND} + \tfrac{M^2}{ND}\right]\end{array}\right) \\ &= \tfrac{1}{(NG-M)^2}\left(\begin{array}{l}\tfrac{1}{D}(\sigma_s^2 + N_0)^2\left[NG^2 - 2MG + M\right] \\ \quad + \tfrac{1}{D}2(\sigma_s^2 + N_0)K_i^2 NG[G - 2G + 1] \\ \quad + \tfrac{1}{D}\left(\sigma_4^2 - 2(\sigma_s^2)^2\right)\left[NG^2 - 2MG + \tfrac{M^2}{N}\right]\end{array}\right) \\ &= \tfrac{1}{(NG-M)D}\left(\begin{array}{l}(\sigma_s^2 + N_0)^2\left[G + \tfrac{M(1-G)}{NG-M}\right] \\ \quad + 2(\sigma_s^2 + N_0)K_i^2 NG\dfrac{1-G}{NG-M} \\ \quad + \left(\sigma_4^2 - 2(\sigma_s^2)^2\right)\dfrac{NG-M}{N}\end{array}\right) \, . \end{aligned} \tag{C.17}$$

This expression, although exact, is a little too cumbersome for practical use. A reasonable approximation can be made by assuming that G is exactly equal to one. This assumption

greatly simplifies Eq. (C.17), yielding

$$\mathbf{Var}[\theta_1] \cong \tfrac{1}{(N-M)D}\left[\left(\sigma_s^2+N_0\right)^2+\left(\sigma_4^2-2\left(\sigma_s^2\right)^2\right)\frac{N-M}{N}\right] \tag{C.18}$$

as an approximate expression for the variance.

The second estimator, θ_2, can also be analysed in a straightforward manner. Recall from Eq. (3.77) that

$$\theta_2 = \frac{S_2 - MS_1}{NG-M} \,. \tag{C.19}$$

By using Eqs. (C.5) and (C.11) its mean can be found to be

$$\begin{aligned}
\mathbf{E}[\theta_2] &= \frac{\mathbf{E}[S_2]-M\mathbf{E}[S_1]}{NG-M} \\
&= \frac{\left[\left(\sigma_s^2+N_0\right)M+K_i^2NG\right]-M\left[\sigma_s^2+N_0+K_i^2\right]}{NG-M} \\
&= \frac{K_i^2[NG-M]}{NG-M} \\
&= K_i^2 \,.
\end{aligned} \tag{C.20}$$

Therefore θ_2 is an unbiased estimator of K_i^2. Its variance can readily be found to be

$$\begin{aligned}
\mathbf{Var}[\theta_2] &= \tfrac{1}{(NG-M)^2}\mathbf{Var}[S_2-MS_1] \\
&= \tfrac{1}{(NG-M)^2}\left[\mathbf{Var}[S_2]-2M\mathbf{Cov}[S_1,S_2]+M^2\mathbf{Var}[S_1]\right] \,.
\end{aligned} \tag{C.21}$$

By using Eqs. (C.6), (C.12), and (C.13), this variance can be expressed as

$$\begin{aligned}
\mathbf{Var}[\theta_2] &= \tfrac{1}{(NG-M)^2}\left(\begin{array}{l}
\frac{1}{D}\left[\left(\sigma_s^2+N_0\right)^2M+2\left(\sigma_s^2+N_0\right)K_i^2NG\right]+\frac{M^2}{ND}\left[\sigma_4^2-2\left(\sigma_s^2\right)^2\right] \\
\quad -2M\frac{1}{ND}\left[\begin{array}{l}\left(\sigma_s^2+N_0\right)^2M+2\left(\sigma_s^2+N_0\right)K_i^2NG \\ \quad +\left(\sigma_4^2-2\left(\sigma_s^2\right)^2\right)M\end{array}\right] \\
\quad +M^2\frac{1}{ND}\left[\left(\sigma_s^2+N_0\right)^2+2\left(\sigma_s^2+N_0\right)K_i^2+\left(\sigma_4^2-2\left(\sigma_s^2\right)^2\right)\right]
\end{array}\right) \\
&= \tfrac{1}{(NG-M)^2}\left(\begin{array}{l}
\left(\sigma_s^2+N_0\right)^2\left[\frac{M}{D}-2\frac{M^2}{ND}+\frac{M^2}{ND}\right] \\
\quad +2\left(\sigma_s^2+N_0\right)K_i^2\left[\frac{NG}{D}-2\frac{MNG}{ND}+\frac{M^2}{ND}\right] \\
\quad +\left(\sigma_4^2-2\left(\sigma_s^2\right)^2\right)\left[\frac{M^2}{ND}-2\frac{M^2}{ND}+\frac{M^2}{ND}\right]
\end{array}\right)
\end{aligned}$$

$$= \frac{1}{(NG-M)^2}\left(\begin{array}{l}\frac{1}{D}\left(\sigma_s^2+N_0\right)^2 M\frac{N-M}{N} \\ \\ \quad +\frac{1}{D}2\left(\sigma_s^2+N_0\right)K_i^2\left[G(N-M)-\frac{M}{N}(NG-M)\right]\end{array}\right)$$

$$= \frac{1}{(NG-M)D}\left(\begin{array}{l}\left(\sigma_s^2+N_0\right)^2\frac{M}{N}\frac{(N-M)}{(NG-M)} \\ \\ \quad +2\left(\sigma_s^2+N_0\right)K_i^2\left[G\frac{N-M}{NG-M}-\frac{M}{N}\right]\end{array}\right). \tag{C.22}$$

As in the case of the variance of θ_1, this expression, is a little too cumbersome for practical use. By assuming G equals one Eq. (C.22) simplifies to

$$\mathbf{Var}[\theta_2] \cong \frac{1}{ND}\left[\left(\sigma_s^2+N_0\right)^2\frac{M}{N-M}+2\left(\sigma_s^2+N_0\right)K_i^2\right] \tag{C.23}$$

as an approximate expression for the variance.

To summarize, the preceding proof showed that θ_1 and θ_2 are unbiased estimates of $\sigma_s^2+N_0$ and K_i^2, respectively. Furthermore, these estimators have variances that are approximately given by

$$\mathbf{Var}[\theta_1] \cong \frac{1}{(N-M)D}\left[\left(\sigma_s^2+N_0\right)^2+\left(\sigma_4^2-2\left(\sigma_s^2\right)^2\right)\frac{N-M}{N}\right] \tag{C.24}$$

and

$$\mathbf{Var}[\theta_2] \cong \frac{1}{ND}\left[\left(\sigma_s^2+N_0\right)^2\frac{M}{N-M}+2\left(\sigma_s^2+N_0\right)K_i^2\right]. \tag{C.25}$$

Appendix D
Source Code Listings

This appendix provides complete listings of the source code for all the programs used in generating results for this thesis. Section D.1 contains listings for the programs used to determine the positions of the CTB, Section D.2 contains listings for the program used to determine the probability of transmission error, and Section D.3 contains a complete listing the tone canceller simulator.

D.1 Positions of CTB

To determine the positions of the triple beats, three separate filters are used. The first, **list**, generates a list of all the distinct beats. The second, **merge**, determines the distinct positions of the beats and the number of beats at each position. The final filter, **channel**, sums the number of beats falling within each channel. They are executed in order with the command:

% **list | sort | merge | channel**

```
/* List the positions of all the beats (Unsorted output) */

#include <math.h>
#define N       35

double freqs[N] = {
    54, 60, 66, 76, 82,
    174, 180, 186, 192, 198, 204, 210,
    120, 126, 132, 138, 144, 150, 156, 162, 168,
    216, 222, 228, 234, 240, 246, 252, 258, 264, 270, 276, 282, 288, 294
};

main()
{
    int a, b, c;
    int i;

    for (a=0; a < N; a++)
        freqs[a] += 1.25;

    for (a=0; a < N; a++)
        printf("%6.2f A\n", 3*freqs[a]);        /* 3rd Harmonic */

    for (a=0; a < N; a++)
        printf("%6.2f B\n", freqs[a]);

    for (a=0; a < N; a++)
        printf("%6.2f C\n", freqs[a]);

    for (a=0; a < N; a++) {
        for (b=0; b < N; b++) {
            if (b == a)
                continue;
            printf("%6.2f D\n", fabs(2*freqs[a]+freqs[b]));
            printf("%6.2f D\n", fabs(2*freqs[a]-freqs[b]));
        }
    }

    for (a=0; a < N; a++) {
        for (b=a+1; b < N; b++) {
            for (c=b+1; c < N; c++) {
                printf("%6.2f E\n", fabs(freqs[a] + freqs[b] + freqs[c]));
                printf("%6.2f E\n", fabs(freqs[a] + freqs[b] - freqs[c]));
                printf("%6.2f E\n", fabs(freqs[a] - freqs[b] + freqs[c]));
                printf("%6.2f E\n", fabs(freqs[a] - freqs[b] - freqs[c]));
            }
        }
    }

    for (a=0; a < N; a++)
        printf("%6.2f F\n", 2*freqs[a]);

    for (a=0; a < N; a++) {
        for (b=a+1; b < N; b++) {
            printf("%6.2f G\n", fabs(freqs[a]+freqs[b]));
            printf("%6.2f G\n", fabs(freqs[a]-freqs[b]));
        }
    }
}
```



```
#define NV      7

main()
{
    double f, f0;
    char chr[2];
    int i, n[NV];

    for (i=0; i < NV; i++)
        n[i] = 0;

    scanf("%lf%1s", &f0, chr);
    n[chr[0] - 'A']++;

    while (scanf("%lf%1s", &f, chr) == 2) {
        if (f != f0) {
            printf("%6.2f", f0);
            for (i=0; i < NV; i++) {
                printf(" %3d", n[i]);
                n[i] = 0;
            }
            printf("\n");
            f0 = f;
        }
        n[chr[0] - 'A']++;
    }

    printf("%6.2f", f0);
    for (i=0; i < NV; i++)
        printf(" %3d", n[i]);
    printf("\n");
}
```

```
#define N       35
#define NV      7

double freqs[N] = {
    54, 60, 66, 76, 82,
    120, 126, 132, 138, 144, 150, 156, 162, 168,
    174, 180, 186, 192, 198, 204, 210,
    216, 222, 228, 234, 240, 246, 252, 258, 264, 270, 276, 282, 288, 294
};

int chan[N] = {
    2, 3, 4, 5, 6,
    14, 15, 16, 17, 18, 19, 20, 21, 22,
    7, 8, 9, 10, 11, 12, 13,
    23, 24, 25, 26, 27, 28, 29, 30, 31, 32, 33, 34, 35, 36
};

main()
{
    double f, fa;
    int a, i, n[NV], nc[NV+1];

    scanf("%lf", &f);
    for (i=0; i < NV; i++)
        scanf("%d", &n[i]);

    for (a=0; a < N; a++) {
        fa = freqs[a];
        while (f < fa) {
            scanf("%lf", &f);
            for (i=0; i < NV; i++)
                scanf("%d", &n[i]);
        }

        for (i=0; i < NV+1; i++)
            nc[i] = 0;

        while (f < fa + 6) {
            if (n[0] > 0 || n[3] > 0 || n[4] > 0)
                nc[NV]++;
            for (i=0; i < NV; i++)
                nc[i] += n[i];

            scanf("%lf", &f);
            for (i=0; i < NV; i++)
                scanf("%d", &n[i]);
        }
        printf("%2d", chan[a]);
        for (i=0; i < NV+1; i++)
            printf(" %3d", nc[i]);
        printf(" -- %d\n", nc[0] + nc[3] + nc[4]);
    }
}
```

D.2 Probability of Symbol Error

To determine the probability of a symbol detection error in the presence of AWGN an interfering tone, the program **error** was used. Numerical integration is implemented with five-point Gaussian quadrature interpolation.

```
/* Program to generate plot of Pe vs. SNR for a various SIRs */
#include <stdio.h>
#include <math.h>

/* Local function prototypes */
static double theory1(int SNR);
static double theory2(int SNR, int SIR);
static double eval(double Ki, double No, double phi);
static double F1(double No, double eps);

main()
{
    int SIR, SNR;

    for (SNR=0; SNR < 35; SNR++) {
        printf("%d", SNR);
        for (SIR = 0; SIR < 35; SIR += 5)
            printf(" %g", theory2(SNR, SIR));
        printf(" %g\n", theory1(SNR));
    }
}

static double theory1(int SNR)
{
    double No, P, a;

    No = 10.0 / 4.0 * exp10(-SNR/10.0);

    P = erf(1.0 / sqrt(No));
    a = 0.75*P + 0.25;
    P = 1 - a*a;

    return (P < 1e-15) ? 1e-15 : P;
}

static double X[5] = { -0.9061798459,
                       -0.5384693101,
                        0.0,
                        0.5384693101,
                        0.9061798459
                     };

static double A[5] = {  0.2369268851,
                        0.4786286705,
                        0.5688888888,
                        0.4786286705,
                        0.2369268851
                     };

static double theory2(int SNR, int SIR)
{
    double No, Ki;
    double P;
    int n, m;

    No = 10.0 / 4.0 * exp10(-SNR/10.0);
    Ki = sqrt(10.0 / 4.0 * exp10(-SIR/10.0));

    P = 0.0;
    for (n=0; n < 20; n++)
        for (m=0; m < 5; m++)
            P += A[m] * eval(Ki, No, (X[m]+2*n+1) * (M_PI/80.0));

    P *= M_PI/80.0;
    P = 4.0 * P / (2.0*M_PI);

    P = 1.0 - P;
```



```
    return (P < 1e-15) ? 1e-15 : P;
}

static double eval(double Ki, double No, double phi)
{
    return F1(No, Ki*cos(phi)) * F1(No, Ki*sin(phi));
}

static double F1(double No, double eps)
{
    double E1;

    E1 = erf((1+eps)/sqrt(No)) + erf((1-eps)/sqrt(No));

    return 0.25 + 0.375*E1;
}
```

D.3 Tone Canceller Simulator

In the following pages the source code for the simulator is listed. The program is separated into two files: **tx.c** contains the main routines for the transmitter, channel, and receiver; and **cancel.c** contains the routines required by the interference canceller.

```
#include <stdio.h>
#include <fcntl.h>
#include <sys/stat.h>
#include <math.h>
#include <memory.h>

#define TRUE    1
#define FALSE   0

typedef struct {
    double Ki, freq, phi;
} IMITYPE;

typedef struct {
    double *R, *I;
} CMPLX;

/* Global function prototypes */
double drand48(void);
CMPLX cancel(CMPLX rc);

/* Global parameters */
int N = 2048;                   /* Number of samples per block */
int D = 32;                     /* Number of blocks to process */
int L = 32;                     /* Number of symbols to use */
int M = 0;                      /* Width of S2 */

/* Local function prototypes */
static double doblock(int d);
static CMPLX transmit(int N);
static CMPLX noise(double No, int N);
static CMPLX imi(IMITYPE *V, int d, int N);
static double getPower(CMPLX rv, CMPLX rn, CMPLX rc, CMPLX ro);
static int read_params(int argc, char *argv[]);

double No;
IMITYPE *V;

main(int argc, char *argv[])
{
    double Rz;
    int d;

    /*  Set up main parameters */
    if (!read_params(argc, argv))
        exit(1);

    for (d=0; d < 24; d++)
        doblock(d);

    Rz = 0.0;
    for (d=24; d < D; d++)
        Rz += doblock(d);

    Rz /= (D-24);

    printf("Residue = %g\n", Rz);
}

static double doblock(int d)
{
    static int doinit = TRUE;
    static CMPLX rc;
    CMPLX rv, rn, rz, ro;
    int n;

    if (doinit) {
        rc.R = (double *) calloc(N, sizeof(double));
```



```
        rc.I = (double *) calloc(N, sizeof(double));
        doinit = FALSE;
    }

    /* Generate data signal*/
    rv = transmit(N);

    /* Generate AWGN */
    rn = noise(No, N);

    /* Generate IMI */
    rz = imi(V, d, N);

    /* Generate received samples */
    for (n=0; n < N; n++) {
        rc.R[n] = rv.R[n] + rn.R[n] + rz.R[n];
        rc.I[n] = rv.I[n] + rn.I]n] + rz.I[n];
    }

    /* Cancel the interference */
    ro = cancel(rc);

    return getPower(rv, rn, rc, ro);
}

static CMPLX transmit(int N)
{
    static int doinit = TRUE;
    static CMPLX Data;
    double *rptr, *iptr;
    int n;

    if (doinit) {
        Data.R = (double *) calloc(N, sizeof(double));
        Data.I = (double *) calloc(N, sizeof(double));
        doinit = FALSE;
    }

    rptr = Data.R;
    iptr = Data.I;

    for (n=0; n < N; n++) {
        *rptr++ = ((lrand48()>>10)&0x06) - 3;
        *iptr++ = ((lrand48()>>10)&0x06) - 3;
    }

    return Data;
}

static CMPLX noise(double No, int N)
{
    static int doinit = TRUE;
    static CMPLX Noise;
    double *rptr, *iptr;
    double r1, r2;
    int n;

    if (doinit) {
        Noise.R = (double *) calloc(N, sizeof(double));
        Noise.I = (double *) calloc(N, sizeof(double));
        doinit = FALSE;
    }

    /* Apply no noise if SNR is set correctly */
    if (No == 0.0)
        return Noise;

    rptr = Noise.R;
```

```
    iptr = Noise.I;

    /* This creates complex Gaussian noise ~N(0, No) */
    for (n=0; n < N; n++) {
        r1 = sqrt(-No*log(drand48()));
        r2 = 2.0*M_PI*drand48();
        *rptr++ = r1 * cos(r2);
        *iptr++ = r1 * sin(r2);
    }

    return Noise;
}

static CMPLX imi(IMITYPE *V, int d, int N)
{
    static int doinit = TRUE;
    static CMPLX IMI;
    double *rptr, *iptr;
    double t1, theta;
    int n;

    if (doinit) {
        IMI.R = (double *) calloc(N, sizeof(double));
        IMI.I = (double *) calloc(N, sizeof(double));
        doinit = FALSE;
    }

    /* Apply no tone if SIR is set correctly */
    if (V->Ki == 0.0)
        return IMI;

    rptr = IMI.R;
    iptr = IMI.I;

    t1 = 2.0 * M_PI * V->freq / N;
    for (n=0; n < N; n++) {
        theta = t1 * (double) (n+d*N) + V->phi;
        *rptr++ = V->Ki * cos(theta);
        *iptr++ = V->Ki * sin(theta);
    }

    return IMI;
}

static double getPower(CMPLX rv, CMPLX rn, CMPLX rc, CMPLX ro)
{
    double Rz;
    double dzr, dzi;
    int n;

    Rz = 0.0;
    for (n=0; n < N; n++) {
        dzr = rc.R[n] - (rv.R[n] + rn.R[n]);
        dzi = rc.I[n] - (rv.I[n] + rn.I[n]);
        Rz += (dzr*dzr + dzi*dzi);
    }

    return Rz / N;
}

static int read_params(int argc, char *argv[])
{
    char junk[80];
    double SNRdb;
    long Seed = 17L;
    int n;
    FILE *fp;
```



```
    fp = fopen("params", "r");
    if (fp == (FILE *) NULL) {
        fprintf(stderr, "%s:  unable to open parameter file\n", argv[0]);
        return FALSE;
    }

    fscanf(fp, "%d%[^\n]",  &N, junk);
    fscanf(fp, "%d%[^\n]",  &D, junk);
    fscanf(fp, "%d%[^\n]",  &L, junk);
    fscanf(fp, "%lf%[^\n]", &SNRdb, junk);

    V = (IMITYPE *) calloc(1, sizeof(IMITYPE));
    fscanf(fp, "%lf%lf%lf%[^\n]", &V->Ki, &V->freq, &V->phi, junk);

    fclose(fp);

    if (argc >= 2)
        Seed = atol(argv[1]);

    while (argc >= 4 && argv[2][0] == '-') {
        switch (argv[2][1]) {
          case 's':
            N = atoi(argv[3]);
            break;
          case 'D':
            D = atoi(argv[3]);
            break;
          case 'L':
            L = atoi(argv[3]);
            break;
          case 'M':
            M = atoi(argv[3]);
            break;
          case 'N':
            SNRdb = atof(argv[3]);
            break;
          case 'K':
            V->Ki = atof(argv[3]);
            break;
          case 'f':
            V->freq = atof(argv[3]);
            break;
          default:
            fprintf(stderr, "usage: %s [Seed [-# val]]\n", argv[0]);
            return FALSE;
        }
        argc -= 2;
        argv += 2;
    }

    if (SNRdb > 100)
        No = 0.0;
    else
        No = 10.0 / 4.0 * exp10(-SNRdb/10.0);

    if (V->Ki > 100)
        V->Ki = 0.0;
    else
        V->Ki = sqrt(10.0 / 4.0 * exp10(-V->Ki/10.0));

    /* Initialize System */
    srand48(Seed ? Seed : time(0L));

    return TRUE;
}
```

```
#include <stdio.h>
#include <fcntl.h>
#include <sys/stat.h>
#include <math.h>

#define TRUE    1
#define FALSE   0

typedef struct {
    double *R, *I;
} CMPLX;

CMPLX cancel(CMPLX rc);
static void FFT(CMPLX data, int N);
static void IFFT(CMPLX data, int N);
static void FFTNS(CMPLX data, int N);
static void IFFTNS(CMPLX data, int N);
static void swap(CMPLX data, int N);
static void fftshift(CMPLX data, int N);

#define DETECT1(X)      ((X < -2) ? -3 : ((X < 0) ? -1 : ((X < 2) ? 1 : 3)))
#define DETECT(Ras)     (CMPLEX) { DETECT1(Ras.R), DETECT1(Ras.I) }

int Mo[] = { 3, 3, 3, 3, 3, 3, 3, 5, 11, 21, 41, 84, 169, 337, 673 };
double Go[] = { 0.146447,   0.256621,   0.280929,  0.286841,
                0.288309,   0.288676,   0.288767,  0.166299,
                0.0740845,  0.0386535,  0.0197762, 0.00976602,
                0.00479596, 0.00240506, 0.00120431 };

/* Global parameters */
extern int N, L, M;

typedef struct {
    double R, I;
} CMPLEX;

typedef struct {
    double freq, C;
} TONE;

#define PTR_GET(x, n)           (CMPLEX) { (x).R[n], (x).I[n] }
#define PTR_PUT(x, n, y)        { (x).R[n] = (y).R; (x).I[n] = (y).I; }

/* Local function prototypes */
static void getTone(CMPLX R, TONE *tone);

CMPLX cancel(CMPLX rc)
{
    static int doinit = TRUE;
    static TONE tone;
    static CMPLX ro, fb, Ea;
    static CMPLEX Za;
    static double C1, S1, CL, SL;
    static double ofreq;
    static int P;
    CMPLEX Ia, Ra, Rap, Qa;
    double tr, ti;
    int a;

    if (doinit) {
        ro.R = (double *) calloc(N, sizeof(double));
        ro.I = (double *) calloc(N, sizeof(double));
        fb.R = (double *) calloc(N, sizeof(double));
        fb.I = (double *) calloc(N, sizeof(double));
        Ea.R = (double *) calloc(L, sizeof(double));
        Ea.I = (double *) calloc(L, sizeof(double));
        Za = (CMPLEX) { 0.0, 0.0 };
        tone = (TONE) { 0.0, 0.0 };
```



```
        ofreq = 0.0;
        P = 0;
        doinit = FALSE;
    }

    C1 = cos(tone.freq);
    S1 = sin(tone.freq);
    CL = cos(tone.freq*L);
    SL = sin(tone.freq*L);

    for (a=0; a < N; a++) {
        Ra = PTR_GET(rc, a);                    /* Detected symbol */

        Rap.R = Ra.R - Za.R / (L + tone.C);     /* Corrected decision var */
        Rap.I = Ra.I - Za.I / (L + tone.C);
        PTR_PUT(rc, a, Rap);

        Ia = DETECT(Rap);                       /* Detected symbol */
        PTR_PUT(ro, a, Ia);

        Qa.R = Ra.R -  Ia.R;                    /* Sample w/o data */
        Qa.I = Ra.I -  Ia.I;
        PTR_PUT(fb, a, Qa);

        /* Subtract old sample */
        if (a < L) {
            tr = cos(tone.freq*a+ofreq*(L-a));
            ti = sin(tone.freq*a+ofreq*(L-a));
            Za.R -= Ea.R[P]*tr - Ea.I[P]*ti;
            Za.I -= Ea.R]P]*ti + Ea.I[P]*tr;
        }
        else {
            Za.R -= Ea.R[P]*CL - Ea.I[P]*SL;
            Za.I -= Ea.R[P]*SL + Ea.I[P]*CL;
        }

        /* Add new sample */
        Za.R += Qa.R;
        Za.I += Qa.I;

        /* Rotate phase */
        tr = Za.R*C1 - Za.I*S1;
        ti = Za.R*S1 + Za.I*C1;
        Za = (CMPLEX) { tr, ti };

        /* Save new sample */
        Ea.R[P] = Qa.R;
        Ea.I[P] = Qa.I;
        P = (P+1) % L;
    }

    ofreq = tone.freq;

    getTone(fb, &tone);

    return ro;
}

static void getTone(CMPLX R, TONE *tone)
{
    static int doinit = TRUE;
    static double G, GC;
    static double *X;
    static int D;
    double S1, S2, T1, T2;
    double high, low, deltai;
    int k, ki, isleft;
```

```
    if (doinit) {
        int n;
        X = (double *) calloc(N, sizeof(double));
        D = 0;
        n = (int) (log2((double) N) + 0.5) - 2;
        M = (M == 0) ? Mo[n] : M;
        GC = Go[n];
        G = 1.0;
        doinit = FALSE;
    }

    FFT(R, N);

    for (k=0; k < N; k++)
        X[k] += (R.R[k]*R.R[k] + R.I[k]*R.I[k]) / N;

    D++;

    /* Find tone spike and calculate S1 */
    ki = 0;
    S1 = 0.0;
    for (k=0; k < N; k++) {
        S1 += X[k];
        if (X[k] > X[ki])
            ki = k;
    }
    S1 /= (N*D);

    /* Calculate S2 */
    S2 = 0;
    for (k=ki-(M-1)/2; k <= ki+(M-1)/2; k++)
        S2 += X[k];
    S2 /= D;

    isleft = (X[ki-1] > X[ki+1]);
    low = (isleft ? X[ki-1] : X(ki+1]) / D;
    high = X[ki] / D;

    /* Calculate THETA1 */
    T1 = (N*G*S1 - S2) / (N*G-M);
    T1 = (T1 < 0) ? 0.0 : T1;

    /* Subtract data and noise power from AP */
    high -= T1;
    low -= T1;

    /* Interpolate frequency estimate */
    deltai = (low > 0.0) ? 1.0 / (1.0 + sqrt(high/low)) : 0.0;
    tone->freq = 2.0*M_PI*((ki - N/2) + (isleft ? -deltai : deltai)) / N;

    G = 1.0 - GC*deltai;

    /* Calculate T1 and T2 */
    T1 = (N*G*S1 - S2) / (G*N-M);
    T2 = (S2 - M*S1) / (G*N-M);

    T1 = (T1 < 0) ? 0.0 : T1;
    T2 = (T2 < 0) ? 0.0 : T2;

    /* Calculate C */
    tone->C = (T2 > 0) ? (T1 / T2) : 999999;
}

/* Local function prototypes */
static int *InitFlip(int N);
static void Fill(int *flip, int val, int n);

void FFT(CMPLX data, int N)
```



```
{
    FFTNS(data, N);
    swap(data, N);
    fftshift(data, N);
}

void IFFT(CMPLX data, int N)
{
    fftshift(data, N);
    swap(data, N);
    IFFTNS(data, N);
}

void FFTNS(CMPLX data, int N)
{
    int i, m, max, step;
    double *dir, *dii, *djr, *dji;
    double temp, tempr, tempi, theta;
    double W1r, W1i, W2r, W2i;

    for (max = N/2; max >= 1; max >>= 1) [
        step = 2*max;
        theta = M_PI / (double) max;
        temp = sin(0.5*theta);
        W1r = -2.0 * temp * temp;
        W1i = sin(theta);
        W2r = 1.0;
        W2i = 0.0;
        for (m = 0; m < max; m++) {
            dir = &data.R[m];
            dii = &data.I[m];
            djr = &data.R[m+max];
            dji = &data.I[m+max];
            for (i = m; i < N; i += step) {
                tempr = *dir - *djr;
                tempi = *dii - *dji;
                *dir += *djr;
                *dii += *dji;
                *djr = W2r * tempr + W2i * tempi;
                *dji = W2r * tempi - W2i * tempr;
                dir += step;
                dii += step;
                djr += step;
                dji += step;
            }
            tempr = W2r;
            tempi = W2i;
            W2r += tempr * W1r - tempi * W1i;
            W2i += tempr * W1i + tempi * W1r;
        }
    }
}

void IFFTNS(CMPLX data, int N)
{
    int i, m, max, step;
    double *dir, *dii, *djr, *dji;
    double temp, tempr, tempi, theta;
    double W1r, W1i, W2r, W2i;
    double inv;

    for (max = 1; max < N; max <<= 1) {
        step = 2*max;
        theta = M_PI / (double) max;
        temp = sin(0.5*theta);
        W1r = -2.0 * temp * temp;
        W1i = sin(theta);
        W2r = 1.0;
```

```
        W2i = 0.0;
        for (m = 0; m < max; m++)  {
            dir = &data.R[m];
            dii = &data.I[m];
            djr = &data.R[m+max];
            dji = &data.I[m+max];
            for (i = m; i < N; i += step)  {
                tempr = W2r * *djr - W2i * *dji;
                tempi = W2r * *dji + W2i * *djr;
                *djr = *dir - tempr;
                *dji = *dii - tempi;
                *dir += tempr;
                *dii += tempi;
                dir += step;
                dii += step;
                djr += step;
                dji += step;
            }
            tempr = W2r;
            tempi = W2i;
            W2r += tempr * W1r - tempi * W1i;
            W2i += tempr * W1i + tempi * W1r;
        }
    }

    inv = 1.0 / (double) N;
    for (i=0; i < N; i++) {
        data.R[i] *= inv;
        data.I[i] *= inv;
    }
}

void fftshift(CMPLX data, int N)
{
    double *temp;

    temp = (double *) calloc(N/2, sizeof(double));

    memcpy(temp,          &data.R[0],   N/2 * sizeof(double));
    memcpy(&data.R[0],    &data.R[N/2], N/2 * sizeof(double));
    memcpy(&data.R[N/2], temp,          N/2 * sizeof(double));

    memcpy(temp,          &data.I[0],   N/2 * sizeof(double));
    memcpy(&data.I[0],    &data.I[N/2], N/2 * sizeof(double));
    memcpy(&data.I[N/2], temp,          N/2 * sizeof(double));

    free(temp);
}

void swap(CMPLX data, int N)
{
    int i, j, *flip;
    double temp;

    flip = InitFlip(N);

    for (i=0; i < N; i++) {
        j = flip[i];
        if (j > i) {
            temp = data.R[i];
            data.R[i] = data.R[j];
            data.R[j] = temp;
            temp = data.I[i];
            data.I[i] = data.I[j];
            data.I[j] = temp;
        }
    }
}
```



```
static int *InitFlip(int N)
{
    static int oN = 0, *flip = (int *) NULL;
    int val, n;

    if (N == oN)
        return flip;
    else {
        free(flip);
        flip = (int *) calloc(N, sizeof(int));
        oN = N;
    }

    flip[0] = 0;

    n = 1;
    val = N >> 1;
    while (val) {
        Fill(flip, val, n);
        val >>= 1;
        n <<= 1;
    }

    return flip;
}

static void Fill(int *flip, int val, int n)
{
    register int i;

    for (i=0; i < n; i++)
        flip[i+n] = flip[i] + val;
}
```